Feasibility of Liquid Organic Hydrogen Carriers (LOHC)

As Seasonal Energy Storage for the Green Village

by

Spyridon Kotsolakis

to obtain the degree of Master of Science in Sustainable Energy Technology
at the Delft University of Technology,
to be defended publicly on October 30 at 13:00.

Student number:	6074669	
Project duration:	January 2025 – October 2025	
Thesis committee:	Prof. dr. ir. Z. Lukszo,	TU Delft, supervisor
	Dr. M. Cvetkovic,	TU Delft
Daily Supervisor:	Ir. E.S. Van Rheenen.	TU Delft
	Ir. L. Van Trigt.	The Green Village

TU Delft

Preface

This thesis represents the final requirement before acquiring my Master of Science degree in Sustainable Energy Technology at TU Delft. The research investigates a case study on the feasibility of Liquid Organic Hydrogen Carriers (LOHCs) as a seasonal energy storage for the Green Village, reflecting my academic interest in energy systems and hydrogen technologies, as well as my commitment to support the energy transition.

This multiple-month research proved to be equally demanding and fulfilling, as developing the model and assessing the LOHC integration in the Green Village required not only technical skill but also continuous reflection and decision-making to balance detail, feasibility, and scope. During this journey, I gained valuable insights into the practical limits and opportunities of hydrogen-based systems in urban areas. I also learned about the complexity of linking technical design with economic and operational viability.

I wish to express my gratitude to my supervisor, Prof dr ir. Zofia Lukszo and my daily supervisor, Erin van Rheenen, for their invaluable mentorship and constructive feedback, which helped me navigate through the academic challenges of this project and complete my thesis.

Finally, I would like to thank my family and close friends for their support throughout my study period. Their motivation and understanding provided me with the motive and determination necessary to complete this endeavour.

Spyridon Kotsolakis
Delft, October 2025

Abstract

The Green Village (TGV), located at TU Delft, is a regulatory-free field lab where innovative projects relevant to the energy transition are tested in a built environment. In this context, seasonal storage is considered a promising research pathway for TGV, as increasing renewable energy penetration and resulting grid congestion are expected to make seasonal storage a key factor in the energy transition. The objective of this thesis is to assess whether liquid organic hydrogen carriers can provide a feasible seasonal storage solution for the TGV community and to compare it to a compressed hydrogen storage pathway.

A literature review was conducted to shape the research angle of this thesis by gaining insights from relevant studies, identifying the principles and components necessary for the LOHC process, and examining existing safety regulations and measures applicable to this storage pathway. The review identified that economic viability was hindered by the heat supply, carrier selection, and system integration. At the same time, an evident gap was found for community-scaled systems and for studies that model the entire energy system under varying loads. Currently, there is no clear regulatory framework for hydrogen storage, as it is still in development. However, several studies focused on the safety of hydrogen-related components suggest using PGS 35 as a technical guideline. This document outlines the necessary permits, safety measures, and distance requirements for such installations. For the LOHC, there is currently no specific regulatory framework; however, some studies suggest that PGS 29 may be applicable to certain aspects of the process. The system of focus for this study is a community-scale hybrid energy system connected to the grid for TGV. This system comprises a PV system, a $LiFePO_4$ battery for short-term storage, an electrolyser for hydrogen production, seasonal hydrogen storage, and a PEM fuel cell for electricity generation during periods of low PV output. For this system, two separate hydrogen storage pathways were developed. The primary scenario involves an LOHC-based hydrogen storage system (a quick overview of this scenario can be found in Figure 1.2). In this scenario, hydrogen is bonded to the LOHC through hydrogenation during summer for seasonal storage. Then, during winter, when PV availability is scarce, it is converted back through dehydrogenation. In the second scenario, hydrogen is stored in compressed gas cylinders (an overview of this system can be found in 3.4). Both pathways' operation was modelled to follow the energy management system currently applied in TGV Energy Hub 24/7. This prioritises direct PV use, daily battery cycling, and extended operation of the electrolyser during the summer (with one start per day) to produce the seasonally stored hydrogen, as well as dispatch of the Fuel Cell during winter utilising the stored hydrogen. This way, grid exchanges are minimised as they occur only after all internal energy sources have been fully utilised.

To assess the feasibility of these scenarios, a techno-economic model was developed in MATLAB. The model employs a modular approach, creating a module for each component of the system. The overall sizing and cost estimation are conducted by a main script that simulates the entire calendar year 2023 at an hourly resolution. The model preprocesses load and PV inputs, applies three hard constraints that limit annual PV export to 10%, annual grid import to 5% of load, and annual LOHC mass balance deviation to 0.5%, and then runs the EMS, battery, electrolyser, hydrogenation, dehydrogenation, and fuel-cell modules. Peak duties and temperatures are extracted for ASPEN EDR heat-exchanger sizing and costing. Economic results are reported as CAPEX, OPEX, LCOE, NPV, and IRR. The validation of the model is conducted through internal checks of the EMS logic, evaluation of pitch diagrams to ensure thermodynamic consistency, and comparison of results with established manufacturer and literature values.

For the LOHC scenario, the optimal configuration is found for 552 PV modules with a total capacity of 165.6 kWp, a 261 kWh battery, a 116 kW electrolyser, and a 34 kW PEM fuel cell. Annual grid import is 0.88 % of load, and annual PV export is 8.79 %. Summer electrolysis produces about 1,813 kg of hydrogen that is stored in the NEC. Annual hydrogenation produces 30,986 kg of hydrogenated carrier. Dehydrogenation releases 1,610 kg of hydrogen, of which 898 kg is used by the PEM fuel cell and 710 kg is combusted for process heat. The annual requirement of hydrogenated NEC is 30,591 kg, which results in a mass-balance deviation of 0.41 %. Waste-heat recovery covers 88 % of hydrogenation

preheat duty and 11.4 % of dehydrogenation duty. An overall system efficiency of 41.4 % is found, with 49.5 % for the LOHC chain and an electrical round-trip efficiency of 23.4 %. The capital expenditure is €2.36 million, of which €1.64 million is attributed to the LOHC process and about €1.16 million to the initial NEC fill. The operational expenditure is €12,901 per year. The levelised cost of electricity is €1.695 per kWh with an NPV of −€2.67 million and an IRR of −29.5 %. The total footprint of the LOHC system was found at 1,020 m^2 while the space required for the process tanks and reactors is estimated at 66 m^3 when two tanks are used and 36 when a single tank is used.
For the alternate scenario with compressed hydrogen, the same EMS and component models are used, except for hydrogenation and dehydrogenation. This scenario resulted in a PV system consisting of 379 PV modules and totalling 113.70 kWp, the same battery and PEM fuel-cell sizes, and an 80 kW electrolyser. Annual PV export is 10.38 % and annual import is 1 % of load, with an annual hydrogen balance error of 2.09 %. The capital expenditure is €565,306, and the operational expenditure is €6,004 per year. The levelised cost of electricity is €0.79 per kWh with an NPV of −€0.732 million and an IRR of −18.21 %. The total area required for the system is approximately 699 m^2 while the space used for the 1,039 50L tanks required a total of 52 m^3.
Sensitivity analysis indicates that the discount rate is the principal driver of LCOE variation within a range of about −9.8 to +10.3 %. Project lifetime produces a range of about −5.8 to +9.5 %. LOHC process costs, in particular the carrier, produce changes of about ±8 % in LCOE and have notable effects on NPV.
Concluding, the case study shows that a PV–battery–electrolyser–fuel-cell system using LOHCs can deliver near year-round autonomy at The Green Village, but its energy efficiency is constrained by dehydrogenation heat demand (only 12% high-grade heat recovered with PEMFC) and consequent hydrogen combustion, which limits the electrical round-trip efficiency to 24% despite strong waste-heat integration on the hydrogenation side. Economically, LOHCs remain impractical at current prices as CAPEX is dominated by the LOHC chain (including the NEC inventory) and yields an LCOE around €1.70/kWh with strongly negative NPV/IRR, whereas a compressed-hydrogen baseline achieves similar operational adequacy at far lower cost but still fails to reach profitability under base assumptions. The feasibility is primarily influenced by financing conditions and the lifespan of components, with LOHC-specific costs (particularly the price of the carrier) being the next most significant factors. In contrast, the costs associated with PV/batteries are less critical. This suggests that improvement efforts should focus on enhancing high-grade heat integration (such as SOFC fuel cells), reducing capital and operational expenses in the LOHC chain, and implementing financing or policy strategies to lower capital costs. Finally, safety and siting considerations favour LOHC's ambient-condition liquid storage for built environment applications, while the compressed-gas alternative required as high amount of pressure vessels and safety setbacks; taken together, these results suggest LOHCs are technically feasible with a favourable safety profile, but deployment hinges on cost and heat-management breakthroughs or supportive market frameworks before community-scale adoption becomes realistic

Contents

List of Figures

List of Tables

Nomenclature

Abbreviations

Abbreviation	Definition
AEM	Anion Exchange Membrane (electrolyser)
APEA	Aspen Process Economic Analyser
ATEX	EU directive for equipment used in explosive atmospheres
AWE	Alkaline Water Electrolyser
Bal	Besluit Activiteiten Leefomgeving (NL)
Bbl	Besluit Bouwwerken Leefomgeving (NL)
Bkl	Besluit Kwaliteit Leefomgeving (NL)
BRZO	Major Accidents Risks Decree (Seveso)
CAPEX	Capital Expenditure
CE	Conformité Européenne marking
CEPCI	Chemical Engineering Plant Cost Index
CHP	Combined Heat and Power
CSTR	Continuous Stirred-Tank Reactor
DBT	Dibenzyltoluene
EDR	Aspen Exchanger Design & Rating
EMC	Electromagnetic Compatibility (EU directive)
EMS	Energy Management System
EU	European Union
EUT	Eutectic biphenyl/diphenylmethane LOHC
FC	Fuel Cell
HT-PEMFC	High-Temperature Proton Exchange Membrane Fuel Cell
HX	Heat Exchanger
HYSYS	Aspen HYSYS
IRR	Internal Rate of Return
KOH	Potassium hydroxide
LCOE	Levelized Cost of Energy
LCOH	Levelized Cost of Hydrogen
LHV	Lower Heating Value
LH_2	Liquefied hydrogen
LOHC	Liquid Organic Hydrogen Carrier
LT-PEMFC	Low-Temperature Proton Exchange Membrane Fuel Cell
MBP	2-(N-methylbenzyl) pyridine
MCH	Methylcyclohexane
MET	Methanol
NAP	Naphthalene
NEC	N-ethylcarbazole
NEN-EN-IEC	Dutch/EU adoption of IEC standards
NPR	Nederlandse Praktijkrichtlijn
NPV	Net Present Value
ORC	Organic Rankine Cycle
OPEX	Operating Expenditure
Pd/Al_2O_3	Palladium supported on alumina
PEM (EL)	Proton Exchange Membrane Electrolyser
PEMFC	Proton Exchange Membrane Fuel Cell
PGS	Publicatiereeks Gevaarlijke Stoffen

Abbreviation	Definition
PHC	N-phenylcarbazole
Pt	Platinum
PV	Photovoltaic
PVGIS	Photovoltaic Geographical Information System
QRA	Quantitative Risk Assessment
R&D	Research & Development
rSOC	Reversible Solid Oxide Cell
Ru/Al_2O_3	Ruthenium Sumpported on alumina
SEBM	Structured monolith reactor type (as referenced)
SOEC	Solid Oxide Electrolysis Cell
SOFC	Solid Oxide Fuel Cell
SoC	State of Charge
STY	Space Time Yield
TC	Temperature-Cascade
TOL	Toluene
TPI	Toxicity Potential Indicator
TRL	Technology Readiness Level
WHR	Waste Heat Recovery

Symbols

Symbol	Definition	Unit
c_p	Specific heat at constant pressure	kJ kg^{-1} K^{-1}
CF_y	Cash flow in year y	€
E_{daily}	Average daily energy demand	kWh
$E_{dch}(t)$	Battery discharge energy in hour t	kWh
E_{demand}	Annual building electricity demand	kWh
E_{import}	Annual grid-imported electricity	kWh
$E_{PV,y}$	Annual PV energy in year y	kWh
$E_{total,AC}$	Total AC energy required for the autonomy period	kWh
E_{daily}	Average daily energy demand	kWh
$E_{dch}(t)$	Battery discharge energy in hour t	kWh
E_{demand}	Annual building electricity demand	kWh
E_{import}	Annual grid-imported electricity	kWh
$E_{PV,y}$	Annual PV energy in year y	kWh
$E_{total,AC}$	Total AC energy required for the autonomy period	kWh
f_{exp}	Annual grid-export fraction	–
f_{imp}	Annual grid-import fraction	–
$H(t)$, $D(t)$, $M(t)$	Hour, day, month indices	–
H_{12}-NEC	Hydrogenated N-ethylcarbazole	–
H_{18}-DBT	Hydrogenated dibenzyltoluene	–
H_n-LOHC	Generic hydrogenated LOHC notation	–
H_2, O_2, H^+, OH^-	Hydrogen, oxygen, proton, hydroxide	–
kW_{LHV}	Thermal power on LHV basis	kW
$LCOE$	Levelized cost of energy	€/kWh
$\Delta LCOE$	Relative LCOE change vs. baseline	%
NPV	Net present value	€
ΔNPV	Relative NPV change vs. baseline	%
$\dot{m}_{H_2}(t)$	Hydrogen mass flow	kg h^{-1}
$\dot{m}_{L^-}(t)$	Unloaded LOHC (NEC) mass flow	kg h^{-1}
$\dot{m}_{L^+}(t)$	Loaded LOHC (12H-NEC) mass flow	kg h^{-1}
$m_{tot,produced,dehy}$	Annual LOHC$^+$ consumed by dehydrogenation	kg

Symbol	Definition	Unit
$m_{\text{tot,produced,hy}}$	Annual $LOHC^+$ mass from hydrogenation	kg
N_{mod}	Number of EL 2.1 modules	–
N_{stacks}	Number of fuel-cell stacks	–
P_{cap}	Installed electrolyser capacity	kW
$P_{\text{EL}}(t)$	Electrolyser electric power	kW
$P_{\text{export}}(t)$	Grid export power	kW
$P_{\text{FC}}(t)$	Fuel-cell electric power	kW
$P_{\text{FC,cap}}$	Installed fuel-cell capacity	kW
$P_{\text{import}}(t)$	Grid import power	kW
$P_{\text{load}}(t)$	Site electric demand at hour t	kW
$P_{\text{net}}(t)$	Net load after PV/FC/battery	kW
$P_{\text{PV}}(t)$	PV electric power at hour t	kW
$\dot{Q}$	Heat duty	kW
$Q_{\text{cool}}(t)$	Fuel-cell system cooling heat	kW
q_{dehy}	Dehydrogenation reaction enthalpy	$\text{kJ mol}_{\text{H}_2}^{-1}$
q_{hy}	Hydrogenation reaction enthalpy	$\text{kJ mol}_{\text{H}_2}^{-1}$
r, r^*	Discount rate; internal rate of return	%
ρ_{H_2}	Hydrogen density (normal conditions)	kg Nm^{-3}
$s_{\text{elec}}(t)$	Electrolyser specific energy	kWh Nm^{-3}
STY_{De}	Space-time yield (dehydrogenation)	g (L h)^{-1}
STY_{Hy}	Space-time yield (hydrogenation)	g (L h)^{-1}
T, y, t	Project lifetime; year index; hour index	–
$T_{\text{amb}}(t)$	Ambient temperature	K (or °C)
T_{dehy}	Dehydrogenation temperature	K
T_{hy}	Hydrogenation temperature	K
$T_{\text{h,in/out}}$, $T_{\text{c,in/out}}$	Hot/cold stream inlet/outlet temperatures	K (or °C)
ΔT_{min}	Pinch minimum approach temperature	K
η_{dehy}	Dehydrogenation conversion	–
$\eta_{\text{elec}}(t)$	Electrolyser electrical efficiency	%
$\eta_{\text{H}_2\text{ storage}}$	Electrical round-trip (EL→FC)	–
η_{LOHC}	LOHC chain efficiency	–
η_{system}	Overall system efficiency	–
$\dot{V}_{\text{H}_2}(t)$	Hydrogen volumetric flow	$\text{Nm}^3\ \text{h}^{-1}$
HHV_{H_2}, LHV_{H_2}	H_2 heating values (basis noted in text)	kWh kg^{-1} (or MJ kg^{-1})
$\phi(t)$	Electrolyser load fraction	–

1 Introduction

1.1. Background and Context

To mitigate the risk of global temperatures exceeding a 2 °C increase above pre-industrial levels, the Paris Agreement was established to limit the rise to 1.5 °C (United Nations Framework Convention on Climate Change, 2015). Under this agreement, countries around the world pledged to take urgent measures to reduce greenhouse gas (GHG) emissions. Greenhouse emissions from energy production and consumption account for 75% of global GHG emissions (International Energy Agency, 2025), with 2023 recording a new high of 37.4 Gt (International Energy Agency, 2024a). In addition, 2024 was marked as the hottest year ever recorded, with the average global temperature exceeding 1.5 °C compared to the pre-industrial era (Copernicus Climate Change Service, 2025), thus making the energy transition necessary and urgent. In 2023, renewables accounted for 13% of final energy consumption, projected to increase to 20% by 2030 (IEA, 2024).In 2023, solar and wind energy production accounted for 13% of the global electricity generated, with a projected increase of up to 30% by the year 2030, according to IEA (International Energy Agency, 2024b). The intermittency associated with wind and solar energy production has necessitated the development of effective energy storage solutions. Hydrogen serves as a versatile energy carrier that, when integrated with intermittent energy sources, can enhance grid flexibility while contributing to the decarbonization of industries that are difficult to electrify (IRENA, 2025). Hydrogen is the most abundant substance in the universe and has a high energy density, which generates 120 MJ (33.33 kWh) per kg, making it a good alternative as the energy generated is three times higher than that of diesel, four times coking coal, and six times coal (wet basis)(Abe et al., 2019). However, hydrogen's widespread adoption as a storage medium is hindered by its low volumetric energy density and increased safety concerns. In terms of safety, hydrogen is highly flammable with a flammability range of 4-75% vol. in air, has an invisible flame, a very low ignition energy, and can be rapidly dispersed due to high diffusivity (U.S. Department of Energy, Hydrogen and Fuel Cell Technologies Office, 2017). These properties necessitate a wide selection of preventive measures to be safely handled and used in the built environment. Storing hydrogen requires significantly more space compared to other fuels due to its very low volumetric energy density of 0.01 MJ per litre (B.V., 2025); therefore, requiring storage methods that increase its volumetric energy density. The most well-known hydrogen storage methods are compressed hydrogen gas (CHG) and liquefied hydrogen gas (Niermann, Beckendorff, et al., 2019). Both of these methods present increased safety concerns due to the high pressure storage of CHG and low temperatures of LH_2 (Niermann, Beckendorff, et al., 2019). Additionaly, a significant portion of hydrogen energy content is consumed as both energy storage methods are energy intensive(Ali et al., 2023; U.S.DOE, 2022). On the other hand, Liquid organic hydrogen carriers (LOHCs) offer a promising and safer alternative storage method due to their ability to store hydrogen at ambient conditions (Shukla et al., 2012) by reversibly binding hydrogen in liquid media such as dibenzyltoluene (Niermann, Beckendorff, et al., 2019). These processes increase the volumetric and gravimetric capacity of hydrogen (Niermann et al., 2021), while storing it in ambient conditions for extended periods, without risks of leakages, boil-off or other losses, helping to overcome issues faced with other methods (Niermann, Beckendorff, et al., 2019). This research aims to bridge the significant gap between seasonal storage methods and their application within the built environment, thereby facilitating the transition to sustainable energy systems. Our research will integrate various disciplines, focusing on techno-economic modelling for an LOHC system for the Green Village.

1.2. What is the Green Village

The Green Village, located at TU Delft, is an open-field lab where innovative projects and ideas focusing on sustainable building and renovation, future energy systems, and climate-adaptive cities are tested. This campus community comprises several buildings, including offices, labs, and residences, where various conceptual ideas are developed and tested as its premises are considered a regulatory-free

Figure 1.1: The Green Village field lab (Village, 2025)

zone. This regulatory-free zone facilitates testing of projects and technologies in the built environment, that are currently at niche and experimental stages and face technical, regulatory or economic barriers that hinder their widespread application.
One such project is the 24/7 Energy Hub initiative, which implements an autonomous energy system, providing an apartment in the TGV premises with nearly complete self-sufficiency. This system aims to provide the apartment with 2200 kWh of energy annually, using a 5.34kWP PV system for electricity production, a 15.4 $LiFePO_4$ battery for daily storage and hydrogen for seasonal storage. The hydrogen needed for seasonal storage is produced using surplus electricity from the PV system through a 2.4 kW anion exchange membrane (AEM) electrolyser. This hydrogen is then compressed at 270bar and stored seasonally in 53 compressed hydrogen tanks, each with a capacity of 50 litres. At times when the electricity generated by the PV system is insufficient, the stored hydrogen is converted back into electricity using a 6.8 kW Proton Exchange Membrane (PEM) fuel cell, thereby ensuring a consistent power supply(van Trigt & van Praag, n.d.). In this context, TGV is investigating seasonal storage solutions that may currently considered infeasible. However as the share of renewables grow and the grid congestion intensifies, the need for long term storage is expected to grow (Schleifer et al., 2025), thus increasing the willingness to pay for it.
The TGV as the main stakeholder expects to gain a straightforward yet realistic estimate of the system's size and cost from this research, which will provide insight into whether a LOHC seasonal storage solution is feasible in comparison to other hydrogen storage technologies and if it is worth studying further for a potential implementation.

1.3. Problem Statement

Providing an uninterrupted electrical supply during extended low-generation periods for a building's community, such as the Green Village, remains a challenge. Batteries are suitable for covering a system's day-to-day fluctuations, but they are impractical for multi-month deficits due to technical and economic constraints. On the other hand, traditional hydrogen storage methods' safety and efficiency drawbacks make researchers explore other hydrogen storage alternatives, such as LOHC. While LOHC technology has mainly been studied for industrial applications, its potential for stationary energy storage in buildings has not been significantly investigated.

1.4. Research Objective

In this research a techno-economic framework to evaluate the feasibility of LOHC-based seasonal hydrogen storage energy system presented in figure 1.2 for a community such as TGV will be developed. This framework will provide a clear and realistic estimate of the required system size, layout, performance, and cost, and to compare these with compressed hydrogen under the same site restrictions.

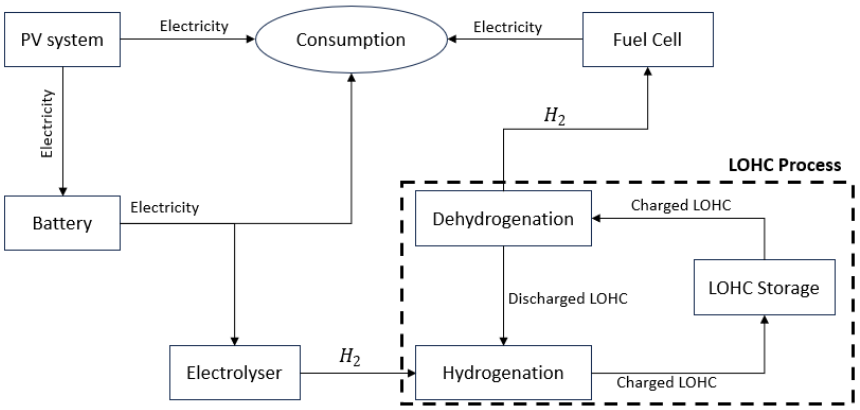

Figure 1.2: Simplified overview of the LOHC based energy system

The objective of this thesis are:

1. To determine an appropriate system sizing that can support uninterrupted supply during extended deficits
2. To identify key barriers to real-world implementation
3. To assess the effectiveness of waste-heat recovery and potential process-heat integration within the LOHC system
4. To formulate practical recommendations for the design and implementation of LOHC-based hybrid storage systems for TGV

1.5. Report Outline

To achieve the objectives set, a literature review will be conducted in chapter 2. This review will enhance our understanding of the components involved and their selection criteria, while also identifying research gaps in the existing literature. The methodology followed and the detailed model development will then be introduced in chapter 3 and 4 and the detailed results will be outlined in chapter 5. Finally a reflection of the work done will be provided in the Discussion chapter 6 and the thesis will be concluded in the Conclusion chapter 7.

2
Literature Review

The scope of this chapter is to provide the foundational background knowledge for this research by analysing and reviewing existing literature.

2.1. Traditional Hydrogen Storage Methods

Currently, there are several hydrogen storage technologies, such as pressurised hydrogen storage, liquefied hydrogen storage, and LOHC hydrogen storage. Each technology presents different challenges that need to be addressed, such as density, efficiency, safety, cost, and compatibility with existing infrastructure. In the paragraphs below, a brief overview of each technology's operation, strengths and weaknesses will be presented.

2.1.1. Compressed Hydrogen Storage

Compressed hydrogen storage is the most widely adopted hydrogen storage technology, which involves storing hydrogen in high-pressure vessels between 350 and 700 bar (Magliano et al., 2024). This storage method is relatively simple and has fast refuelling rates(Ali et al., 2024); thus, it is widely adopted in automotive and industrial applications. Standard cylinder technology and gas handling equipment can be used without the need for new infrastructure, making it a viable option (Ali et al., 2023). However, compressed hydrogen storage has significant safety and efficiency concerns, as storing a large amount of hydrogen at hundreds of bars of pressure induces substantial mechanical stress to the tanks, increasing the risk of leaks or ruptures. In addition, compressing hydrogen requires a significant amount of energy, somewhere between 15-–20% of the total hydrogen energy content (Ali et al., 2023). Another limitation is the relatively low volumetric density of compressed hydrogen, where, at a pressure of 700 bar, it is estimated to be 36 kg/m³ (Yue et al., 2021). This makes storing large amounts challenging, as it requires more space compared to other fuels (Magliano et al., 2024). Despite these challenges, compressed hydrogen is a mature technology and is the most common form of hydrogen storage used.

2.1.2. Liquefied Hydrogen Storage LH_2

Liquefied hydrogen storage (LH_2) involves cooling hydrogen gas to temperatures below 20 K to liquify (U.S.DOE, 2022). This process significantly increases hydrogen's volumetric capacity by approximately 70–71 kg/m³, thus reaching nearly twice that of 700 bar compressed hydrogen (Aziz, 2021). To achieve the liquefaction, multi-step refrigeration cycles are needed as hydrogen cannot be liquefied by pressure at ambient temperature (U.S.DOE, 2022). After liquified hydrogen must be stored in specialised insulated cryogenic tanks, where even with the advanced insulation, boiloff losses are between 0.3 and 0.6% per day (Aziz, 2021). This boil-off not only results in hydrogen loss but also increases safety concerns as the vented hydrogen must be safely handled to avoid fire risks. Another significant disadvantage is the energy consumption. Cooling hydrogen to 20 K is highly energy-intensive. Approximately 30–35% of the hydrogen's energy content is consumed during the liquefaction process (U.S.DOE, 2022), making liquid hydrogen a less efficient storage method compared to compressed gas in terms of energy efficiency.

2.1.3. Liquid Organics Hydrogen Cariers

Another possible storage method for hydrogen is LOHCs, which can be stored at ambient conditions (Niermann, Beckendorff, et al., 2019). They are considered cost efficient, safe, and easy to handle alternatives, as they share similar properties to those of crude oil derivatives(Niermann, Beckendorff, et al., 2019). Hydrogen in LOHCs can be stored for long periods, without boil-off or hydrogen losses, while their transportation is easy, as it can be done using existing infrastructure (Niermann et al., 2021).

Hydrogen is stored in LOHCs using reversible hydrogenation and dehydrogenation reactions, as illustrated in 2.1.

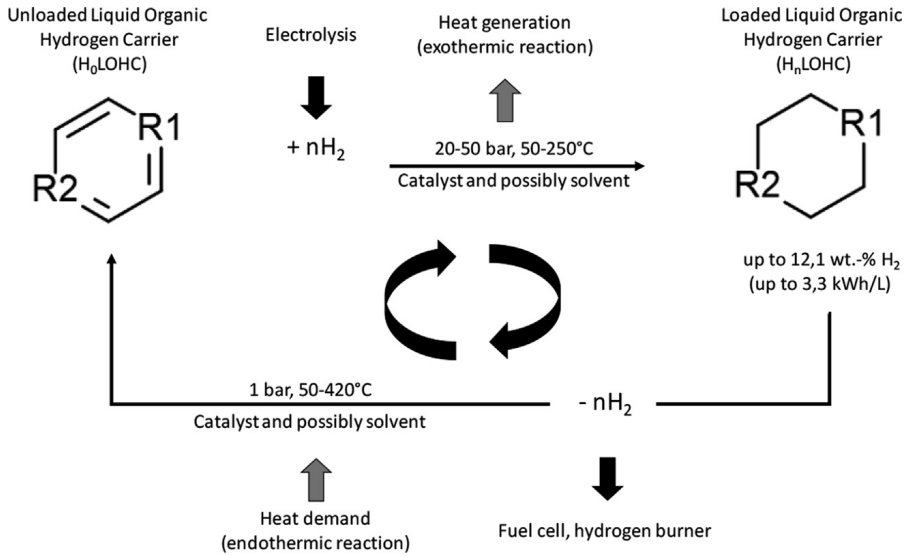

Figure 2.1: LOHC Hydrogenation and dehydrogenation Concept (Niermann, Beckendorff, et al., 2019)

Hydrogenation occurs when double bonds are filled with hydrogen under high temperatures and pressures in an exothermic reaction, while dehydrogenation occurs at near-atmospheric pressures and high temperatures (Niermann, Beckendorff, et al., 2019). In dehydrogenation, hydrogen is released via a catalytic endothermic dehydrogenation reaction (Niermann, Beckendorff, et al., 2019). The advantages of this method are that it increases volumetric energy density and simplifies handling, as its similarities with crude oil derivatives increase LOHCs' public acceptance due to the public's familiarity with these substances (Niermann, Beckendorff, et al., 2019).

2.2. System Components for LOHC Storage

In this section, an overview of the most studied LOHC media will be provided, and the necessary system components required for the proposed system will be identified.

2.2.1. Electrolyser

Electrolysers are electrochemical components that utilise electricity to split water into hydrogen and oxygen through the electrolysis process. They consist of a cell that comprises an anode, a cathode and an ion-conductive separator, which splits water molecules when hydrogen is applied, producing hydrogen and oxygen gas in the cathode and anode.

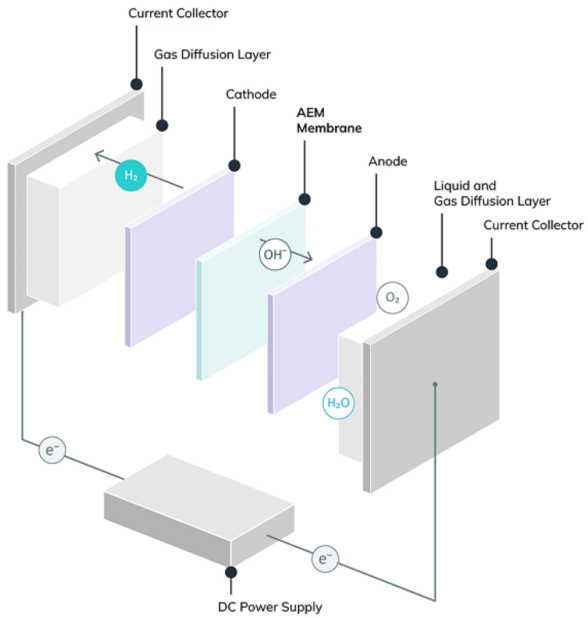

Figure 2.2: AEM Electrolyser Schematic (Enapter, n.d.)

Alkaline Water Electrolyser Alkaline water electrolysis is one of the most well-established and mature hydrogen production technologies that utilises a 20–30% potassium hydroxide (KOH) solution as a liquid alkaline electrolyte for ionic transport. It consists of a porous diaphragm separating the anode and the cathode, allowing the migration of hydroxyl ions, OH. During the reaction, hydrogen and hydroxide ions are produced at the cathode, while oxygen is created at the anode through hydroxide reactions.

AWE typically operates between 65–100°C and pressures of 25 to 30 bar, achieving conversion efficiencies from 60% to 80%. The anode is composed of nickel (Ni), while cobalt oxides are used for the cathode (El-Shafie, 2023).

The operational lifetime of an AWE exceeds $60,000$ hours, thus making it suitable for large-scale hydrogen production. However, AWE's operational limitations under pressure, as well as slow startup times, can affect coupling with variable renewable energy sources (Wei et al., 2024). Furthermore, the relatively large footprint of AWE can reduce its suitability for urban deployment when compared to PEM (Wei et al., 2024).

From an economic perspective, AWE systems have relatively low capital expenditure, estimated at €1,000–€1,200 per kW_{el}, making them an affordable electrolysis option (El-Shafie, 2023). Regarding safety, there are concerns during the handling and maintenance of KOH due to its caustic nature. At the same time, the emission during manufacturing is estimated by the LCA to be around 253.7 kg CO_2-eq per 1 kW electrolyser (Wei et al., 2024).

Proton Exchange Membrane (PEM) Electrolyser Another mature method for hydrogen production is Proton Exchange Membrane (PEM) electrolysis. PEM uses a solid polymer electrolyte, typically Nafion, to conduct the hydrogen ions (H^+), while the anode is made of iridium oxide (IrO_2) and a cathode

of platinum (Pt). During PEM's operation, water is pumped and split at the anode, releasing oxygen and protons and electrons. The protons pass through the membrane to the cathode, while the electrons pass through the anode to an external power circuit, creating the reactions that generate a cell voltage. The electrons then move to the cathode, where they recombine, producing high hydrogen purity (> 99.999%) (Kumar & Himabindu, 2019).
Operating temperatures range between 70–90°C and pressures of 30 to 80 bar, while conversion efficiencies are 48.5% to 65.5%. The acidic nature of electrolyte and metallic electrode surfaces in PEM electrolysers enhances reaction kinetics. These enhanced kinetics increase safety and enable operation at atmospheric pressure on the anode side while allowing higher pressures on the cathode side (El-Shafie, 2023).
From an economic perspective, PEM electrolysers have high capital costs, estimated at €1,860–€2,320 per kW_{el}, mainly due to the noble metals such as iridium and platinum used as catalysts (El-Shafie, 2023), and has an expected lifetime stack of 50,000–80,000 h (Wei et al., 2024). The emission during the manufacturing of the PEM electrolyser was estimated to be around 137.4 kg CO_2-eq per 1 kW, lower than AWE (Wei et al., 2024). Despite these challenges, the compact and modular design of PEM makes it suitable for built-environment applications.

Anion Exchange Membrane (AEM) Electrolysis Anion Exchange Membrane (AEM) is a relatively new electrolyser that is still in the research and development (R&D) phase. AEM aims to merge the advantages of AWE and PEM without using precious metal catalysts, thus reducing the cost (Wei et al., 2024). AEM electrolysers utilise a polymer electrolyte that facilitates the conduction of hydroxide ions. The anode is typically composed of nickel or cobalt oxides, while the cathode consists of non-precious metal catalysts. During operation, hydroxide ions move through the membrane, enabling hydrogen generation at the cathode and oxygen evolution at the anode. The operating temperatures are between 50–70°C and pressures below 30 bar, achieving conversion efficiencies from 39.7% to 65% (El-Shafie, 2023). Even though cost reductions of AEM are possible due to the use of non-noble metals, the challenges related to mechanical stability, degradation, and low ionic conductivity need to be resolved in order not to limit their commercial viability (El-Shafie, 2023). Economically, AEM systems are expected to be more cost-effective than PEM systems, although the exact capital cost estimates vary due to ongoing research and development.

Solid Oxide Electrolysis Cells (SOEC) Solid Oxide electrolysers are considered the most efficient compared to other electrolyser types, with conversion efficiencies ranging from 81 to 86%. SOEC operate at high temperatures of 900–1,000°C and has a solid ceramic electrolyte to facilitate oxygen ion conduction. The anode is composed of a perovskite-type material, while the cathode consists of a nickel-based alloy. During operation, the steam is electrolysed to produce hydrogen and oxygen, with oxygen ions moving through the electrolyte (El-Shafie, 2023). The ability of SOEC to be thermally integrated with industrial heat sources further enhances its efficiency and reduces the cost. Currently, the capital costs are estimated to exceed €2,000 per kW_{el} and the stack lifetime is around 20,000 h. The SOEC lifetime is reduced compared to other systems due to high operating temperatures that accelerate the degradation of ceramic electrolytes and metal interconnects (El-Shafie, 2023; Esposito et al., 2024; Wei et al., 2024). SOEC remains promising for industrial applications but is currently less viable for urban applications due to higher operation temperatures and increased costs.

2.2.2. Fuel Cell

Solid Oxide Fuel Cells (SOFC) Solid Oxide Fuel Cells (SOFCs) are high-temperature fuel cells that operate at temperatures from 600 to 1,000°C. Their average efficiency ranges from 25% to 50%, while their electrical efficiency can reach 60%. The system efficiencies can increase to 85–90% when used in combined heat and power (CHP) systems, due to effective waste heat recovery (Qasem & Abdulrahman, 2024). The robust construction and fuel flexibility of SOFCs make them well-suited for large-scale stationary power generation, remote energy applications, and even hybrid systems where integration with gas turbines can push overall efficiencies up to 70% (Buonomano et al., 2015). The challenges that solid oxide fuel cells (SOFCs) face are related to thermal stress during startup and shutdown, as well as long-term material degradation. Additionally, due to their high operating temperatures, SOFCs cannot quickly respond to load changes because of the warm-up time needed to reach operational

temperatures (Sharaf & Orhan, 2014). The capital cost for a 1 kW SOFC stack was found to be approximately $8,482/kW, while it could be reduced to $1,183/kW at production volumes near 50,000 units per year. Finally, the durability of SOFCs varies considerably, with reported lifetimes ranging from 20,000 to 90,000 hours and degradation rates between 1% and 2.5% per year (Cigolotti et al., 2021).

Proton Exchange Membrane Fuel Cells (PEMFC) Proton Exchange Membrane Fuel Cells (PEMFCs) are one of the most well-established fuel cells due to their simple design, lightweight construction, and high mass power density. There are two types of PEMFC: low temperature (LT-PEMFC) and high temperature (HT-PEMFC). LT-PEMFCs usually operate at temperatures between 60°C and 100°C(Authayanun et al., 2013). In contrast, high temperatures have been developed to run in the range of 120–160°C to improve water management and mitigate catalyst poisoning from CO (Authayanun et al., 2013). The electrical efficiency of the LT-PEMFCs ranges from 30% to 40% and can increase to 70–90% for CHP plants. Due to their simple design, PEMFCs benefit from fast startup times, a modular configuration, and a relatively low maintenance burden, owing to the solid polymer electrolyte and the limited number of moving parts. (Cigolotti et al., 2021) in their research presented that the cost for a PEMFC stack can decrease from about $1,052/kW to roughly $460/kW if the production increases to 50,000 units per year. Finally, the expected lifetime of PEMFC ranges from 40,000 to 80,000 hours (Cigolotti et al., 2021).

2.2.3. LOHC Selection

The following section provides a comprehensive overview of available LOHCs and the selection criteria used for this research. Dibenzyltoluene (DBT), N-ethylcarbazole (NEC), Toluene (TOL), and methanol (MET) are compared, and their key characteristics and suitability for seasonal energy storage in the built environment are highlighted.

Dibenzyltoluene (DBT): Dibenzyltoluene (DBT) is one of the most extensively studied LOHCs. Originally developed as a heat transfer oil for industry, in 2014, Brucker et al introduced it as a hydrogen carrier due to its availability, low toxicity and liquid phase over a wide temperature range. Its fully hydrogenated form, perhydrodibenzyltoluene (H_{18}-DBT), allows for a hydrogen storage capacity of around 6.2% and an energy density of 1.9 kWh/L, making it a viable option for seasonal hydrogen storage. DBT has as high boiling point of 390°C, which is higher than the reaction temperature of dehydrogenation, hydrogen is generated only in a gaseous phase. The catalysts used for the hydrogenation reaction are heterogenic and consist of precious metals like platinum (Pt) and ruthenium (Ru). At 150°C temperature and 50 bar pressure using Ru/Al_2O_3 or Ni-based catalysts, complete hydrogenation can be achieved within 240 minutes (Lang et al., 2020; Niermann, Beckendorff, et al., 2019). Dehydrogenation requires 310°C when using Pd/C catalysts, which achieve 97% hydrogen release in 120 minutes. In contrast, only a 40% release can be completed in the same duration when the temperature is reduced to 270°C, thus highlighting the temperature dependency of the process (Niermann, Beckendorff, et al., 2019). In terms of toxicity, DBT is considered less toxic in comparison to NEC and Toluene and has a toxicity potential indicator (TPI) of 13.8 TPI/mg (Hoecke et al., 2021; Niermann, Beckendorff, et al., 2019). Although not classified as carcinogenic, DBT still poses environmental hazards, particularly for aquatic ecosystems, and should not be released into marine environments. The compound's low vapour pressure of 0.07 Pa at 40°C and relatively high viscosity (44.1 mPa·s at 20°C) increase difficulty when pumping due to increased resistance (Niermann, Beckendorff, et al., 2019). Unlike many LOHC systems, DBT remains in the liquid phase throughout hydrogenation and dehydrogenation, eliminating the need for additional solvents or phase management systems (Lang et al., 2020). The production of DBT is calculated in several thousand-ton capacities per year and has an estimated price of $3000/ton (Hoecke et al., 2021). In conclusion, the combination of DBT's low cost of around 4€/kg , along with its availability, safety, low toxicity, and technology readiness level (9), makes it a viable choice for applications in the built environment (Niermann, Beckendorff, et al., 2019).

N-ethylcarbazole (NEC): Another possible candidate as an LOHC medium is N-ethylcarbazole (NEC). NEC is a nitrogen-substituted heterocycle that can theoretically store up to 5.8% hydrogen and have 99.9% purity of hydrogen released upon dehydrogenation (Niermann, Beckendorff, et al., 2019). NEC

with a high melting point of 69°C, is solid at ambient conditions, limiting its practical applications. To solve this issue (Teichmann, Arlt, & Wasserscheid, 2012) propose to limit dehydrogenation to 90% by reducing the residence time in the reactor, which will result in a reduced storage capacity of 5.3% but a liquid end product(Hoecke et al., 2021; Teichmann, Arlt, & Wasserscheid, 2012). The boiling point ranges from 270°C for NEC to over 280°C for its hydrogenated form perhydro-N-ethyl carbazole (Niermann, Beckendorff, et al., 2019). NEC has a flashpoint of 186°C, thus having relatively low flammability under standard storage conditions. Hydrogenation of NEC occurs at 150°C and 50 bar with a Ru/Al_2O_3 catalyst, and a complete hydrogenation reaction can be achieved within 180 minutes. Dehydrogenation, however, requires temperatures ranging between 180°C and 270°C, depending on the reaction speed, with catalysts like Pd/Al_2O_3 and a full dehydrogenation can be completed in 25 minutes at 270°C or in 250 minutes at 180°C (Niermann, Beckendorff, et al., 2019). While these conditions are feasible, at temperatures above 270°C NEC exhibits thermal instability, which generates by-products, deactivates catalysts and reduces overall system efficiency (Hoecke et al., 2021). In terms of availability and cost, NEC is a chemical with an annual global production of less than 10,000 tons, primarily derived from coal tar distillation. The raw material costs approximately €40/kg, which, combined with its limited production capacity, presents challenges for large-scale deployment (Hoecke et al., 2021; Niermann, Beckendorff, et al., 2019). NEC, as it is solid in ambient temperature, has a high viscosity (121 mPa·s at 20°C), compared to the 44.1 mPa·s of DBT, resulting in an increased pumping resistance (Niermann, Beckendorff, et al., 2019). Regarding its toxicity, NEC has a toxicity potential indicator (TPI) of 5.1 TPI/mg (Niermann, Beckendorff, et al., 2019), suggesting low health risks, while it is considered toxic with long-lasting effects for the aquatic environment (National Center for Biotechnology Information, 2025). NEC is considered safe due to its low vapour pressure, as there is no vapour phase at ambient temperatures, resulting in reduced risks during storage and when handling (Niermann, Beckendorff, et al., 2019; Teichmann, Arlt, & Wasserscheid, 2012). The technology readiness level (TRL) of NEC as an LOHC is currently low, assessed at TRL 3, indicating that the system has been demonstrated at a lab scale but requires further testing and validation in real-world operating environments. Despite these challenges, NEC is a promising LOHC candidate due to its liquid state after partial dehydrogenation, high energy density (2.5 kWh/L), and ability to release hydrogen of exceptional purity without requiring additional purification steps (Niermann, Beckendorff, et al., 2019).

Toluene (TOL): Toluene (C_7H_8) (TOL) is also an aromatic hydrocarbon widely researched as an LOHC due to its simple structure and well-established industrial use, while its hydrogenated form is called cyclohexane. It has a very high capacity for hydrogen storage, which theoretically can store up to 6.2 wt.%, when fully hydrogenated. In reality, when the dehydrogenation is maintained at 95%, the hydrogen capacity reduces to 5.9 wt.%. The temperature under which the dehydrogenation is efficient ranges from 250°C to 450°C when catalysed with Pt or Ni on supports like Al_2O_3. Noble metal catalysts such as Pt, Pd and Ru can be used for the hydrogenation at temperatures ranging from 150–230°C and pressures of 0.5 to 3 bar. While dehydrogenation achieves high yields of up to 95%, the endothermic dehydrogenation process is very energy intensive with a heat demand of 68.3 $kJ/molH_2$ (Lang et al., 2020; Niermann, Beckendorff, et al., 2019). Toluene has a liquid state at ambient conditions, with a boiling point of 111°C and a low viscosity of 0.6 mPa·s, which is practical for pumping and transport. However, during dehydrogenation, Toluene becomes gaseous, requiring additional energy for gas flow handling and hydrogen purification. Toluene's and MCH's slow ignition temperatures of 535°C and 260°C increase fire hazards, as the flammability and volatility of the substances make the handling process more complex. Regarding toxicity, TOL is considered carcinogenic and has a toxicity potential indicator of 19.3 TPI/mg, while MCH is hazardous for the environment with a TPI of 7.3 TPI/mg (Hoecke et al., 2021; Lang et al., 2020; Niermann, Beckendorff, et al., 2019).

Annually, Toluene has a production exceeding millions of tons, and it is mainly created through the catalytic reforming of naphtha and pyrolytic cracking of petroleum. The cost is estimated at $700–800 USD/ton or €0.3/kg, and has a well-established position in the chemical industry, making it an appealing option for large-scale LOHC applications (Hoecke et al., 2021; Lang et al., 2020; Niermann, Beckendorff, et al., 2019). The technology readiness level (TRL) of Toluene is estimated at 8, with demonstrative projects already constructed, such as the Chiyoda Corporation's large-scale hydrogen transport initiative, in which a 99.9% dehydrogenation of MCH was achieved. Despite the high TRL and low cost of TOL, its high toxicity and increased fire hazard make it unsuitable for the built environment.

Methanol (MET): Methanol (CH_3OH) (MET) is a widely produced industrial chemical, with a global production that exceeded 70 million in 2015 (Hoecke et al., 2021). It has a well-established infrastructure network for production, transport, and storage, thus making it a candidate for LOHC systems. Methanol is in a liquid state under standard conditions and has a hydrogen storage capacity of 12.1 wt.% and an energy density of 3.3 kWh/L. This capacity can be reduced to 10 wt.% and 2.7 kWh/L if there are present solvents required for the dehydrogenation (Hoecke et al., 2021; Lin & Bagnato, 2024; Niermann, Beckendorff, et al., 2019). The temperatures and pressures under which hydrogenation occurs range from 220–270°C and 20–80 bar using Cu-based catalysts, while dehydrogenation occurs at higher temperatures (420°C) when using Ir and Pt catalysts. A Low-temperature dehydrogenation (<100°C) is possible and has simpler heat management and reduced energy demand (16.5 kJ/mol H_2), though it reduces storage capacity to 4 wt.% and energy density to 1.1 kWh/L. In addition, methanol has several drawbacks. It is toxic, flammable, and poses health hazards; thus, it requires caution when handling and storing. Its high vapour pressure (35,400 Pa at 40°C) increases storage requirements. Additionally, it can produce carbon monoxide (CO) and carbon dioxide (CO_2) during dehydrogenation, which can enhance the completeness of downstream processes. High-temperature systems are fully mature, with a Technology Readiness Level (TRL) of 9, whereas low-temperature applications are still in development, currently at a TRL of 3 (Niermann, Beckendorff, et al., 2019).

Considering all the aforementioned characteristics, N-Ethylcarbazole is selected as the primary LOHC for our study, over DBT, which is our second choice. NEC has a storage density comparable to DBT (5.8 wt% versus 6.2 wt%), but it requires significantly milder dehydrogenation conditions (180–270 °C compared to 260–310 °C). This allows for the use of low-grade waste heat and simplifies reactor design. NEC also offers enhanced safety due to its low toxicity, high flash point and negligible vapour pressure, making it an excellent choice for the built environment. Additionally, its lower operating temperatures decrease energy requirements and catalyst degradation, ultimately resulting in reduced overall system costs, despite NEC's higher cost compared to DBT.

2.2.4. Catalyst Selection

The efficient operation of LOHC storage systems heavily relies on the performance of the catalysts used for both hydrogenation and dehydrogenation. The literature shows that optimising catalyst composition, support characteristics, and reaction conditions is crucial for achieving high conversion, selectivity, and overall process efficiency.

Hydrogenation Many studies have focused on noble metal catalysts as they demonstrate high activity for NEC reactions. Among these catalysts, ruthenium-based ones perform better for the hydrogenation of NEC, followed by Rh, with Pd being less active (Zhang et al., 2023). In addition, Ru-based catalysts have been found to have an extended lifetime due to their stability over multiple cycles and minimal deactivation. In his research,(Eblagon et al., 2012) reported that Ru catalysts were the most effective among various catalysts (Ru, Rh, Pd), with a 5 wt% Ru/Al_2O_3 catalyst having the highest catalytic performance with a nearly complete conversion and a hydrogen storage density of up to 5.7 wt%, while he also noted that under certain conditions Ru yielded incomplete hydrogenation stalling at octahydro-NEC stage. (Yang et al., 2014b) found that under conditions of 180°C and 80 atm of cyclic hydrogenation using 5 wt% Ru/Al_2O_3 catalyst, a yield of 5.79 wt%, which indicates that ruthenium-based catalysts are capable of complete conversion if high-pressure conditions are achieved. Non-noble metal catalysts have also undergone extensive research. Nickel-based catalysts dominate this research due to lower costs and higher abundance. They can suffer from sintering and carbon deposition at high temperatures, but they show a promising stability over multiple cycles when combined with stable supports. Conventional Ni/Al_2O_3 catalysts have limited activity for aromatic hydrogenation because strong metal-support interactions can immobilise active nickel, forming $NiAl_2O_4$(Zhang et al., 2023). However, optimised Ni catalysts have shown significant improvements. (Ding et al., 2021) developed a Ni/Al_2O_3–SiO_2 composite catalyst with a 1:1 Al:Si ratio, which achieved a complete hydrogenation of NEC in 1.5 hours over multiple cycles. The silica component in the support facilitated the reduction of NiO, while alumina enhanced dispersion and prevented sintering. (Wu et al., 2019) found that mixing rare-earth hydride (YH_3) with Ni/Al_2O_3 boosted hydrogenation efficiency, matching the performance of Ru/Al_2O_3. (Wu et al., 2019) also noted that ruthenium-based catalysts can also benefit from such supports, as a Ru/YH_3 catalyst allowed complete NEC hydrogenation at a low tem-

perature of 90°C and 1 MPa H_2. Ni-based catalysts, such as Ni on Si-Al or Raney Ni, are feasible and low-cost choices, but they typically require higher temperatures and H_2 pressures to achieve high conversion. In conclusion, while Ni catalysts are a promising solution, Ru-based catalysts are preferred as they offer superior hydrogenation performance and selectivity, operating at milder temperatures and with decreased process time.

Dehydrogenation For the dehydrogenation process, extensive research has focused on noble metal catalysts such as Palladium (Pd) and Platinum (Pt) catalysts, as they effectively activate C–H bond scission in cycloalkanes and heterocycles. Through research, the selection of catalysts has shifted from initially favoured Pt to more economically viable Pd-based systems. Under mild conditions for temperature (180–190-textdegreeC and a pressure of 0.1 MPa), both 5 wt% Pd/Al_2O_3 and 5 wt% Pt/Al_2O_3 can achieve a complete conversion of 12H-NEC to NEC with 100% selectivity in 4–5 h (Yang et al., 2014a). (Sotoodeh & Smith, 2011) demonstrated that a 100% conversion of fully hydrogenated N-ethylcarbazole is achieved within 1.6 h at 443 K and 101 kPa, with an optimal Pd nanoparticle size of approximately 9 nm delivering a catalytic activity of 4 wt%. Recent work has focused on nanostructured and bimetallic catalysts to reduce noble metal use. In their research, (Jiang et al., 2019) found that Pt/TiO_2 outperformed Pd/TiO_2 in dehydrogenating 12H-NEC, with a 1 wt% Pt/TiO_2 catalyst achieving about 5.6 wt% hydrogen release in 3 hours at 180°C, with >90% of the reaction product being the desired NEC. For the selection of the dehydrogenation catalyst, even though a 1% Pt/TiO_2 can be considered a great candidate, given recent findings as it offers a high hydrogen release efficiency, a 5 wt% Pd/Al_2O_3 is chosen due to its commercial availability.

2.2.5. Reactor Selection

Choosing the right reactor in the LOHC process is crucial due to the significant heat and mass transfer requirements during dehydrogenation, as well as the need for effective heat removal during hydrogenation.

In the process of hydrogenation, fixed-bed reactors are commonly used because they provide effective liquid–solid contact and facilitate straightforward heat removal through multi-tubular or plate designs. While slurry beds can enhance mass transfer, they may complicate solids handling. Recent continuous flow studies on NEC hydrogenation in a micro-packed bed achieved complete conversion and an impressive 99.41% selectivity for H_{12}–NEC. This is accomplished with a 5.79 wt% storage at 80°C and 4 MPa using a 1 wt% Ru/Al_2O_3 catalyst. The work established a kinetic network where hydrogenation of the octahydro intermediate is rate-limiting, which supports process optimisation under mild conditions (Fan et al., 2024). Overall, the literature suggests that modular multi-structured plates, monoliths, and enhanced membrane variants are promising methods for addressing heat management, phase behaviour, selectivity, and scalability in LOHC applications (Makaryan & Sedov, 2021; Modisha et al., 2019).

For dehydrogenation, various reactor designs have been studied options including fixed-bed reactors operated in horizontal tubular or multi-tubular or plate configurations, 3D structured monolith systems such as SEBM, spray pulsed and pressure swing concepts, and lab-scale CSTR or batch setups, with more recent proposals for radial flow to promote gas disengagement (Modisha et al., 2019). Reactor designs that promote phase separation manage to achieve the very high gas evolution that can exceed 600 mL of H_2 per mL of H_{12}-NEC at ambient conditions (Peters et al., 2015). Horizontal tubular and plate designs effectively separate phases, allowing gas to rise while liquid moves through the bed. The turbulence caused by bubble formation enhances heat transfer from the walls to the liquid (Modisha et al., 2019). Monolith and microstructured reactors increase the surface area-to-volume ratio and shorten diffusion pathways, which improves temperature uniformity under high heat flux conditions (Modisha et al., 2019). Xue et al. conducted a study on a packed bed and discovered that smaller catalyst particles enhance liquid–solid transfer and lead to flatter axial temperature profiles. Within their tested range, at around 183 °C and using 2 mm pellets, they achieved a hydrogen production rate of 9.61 mol H_2 per gram of Pd per hour. In addition, increasing the pressure decreased hydrogen yield but helped prevent evaporation and reduced temperature differences between the wall and bed (Xue et al., 2024).

To further enhance transfer efficiency, Fan et al. utilised a micro-packed bed for H_{12}-NEC, achieving full conversion with a hydrogen release of 5.65 wt% at 180 °C over 1% Pd/Al_2O_3. No carbazole is detected, and the operation remained stable for over 200 hours. At 140 °C and 0.1 MPa, the specific productivity was nearly 1.8 times greater than that of a batch reactor under comparable conditions (Fan et al., 2025).

2.2.6. Waste Heat Recovery Strategies

As mentioned earlier, hydrogenation releases heat during reaction (exothermic reaction), while dehydrogenation requires heat (endothermic reaction), and high temperatures for hydrogen release. With no waste heat integration in place, a significant amount of the heat generated during hydrogenation is wasted, while large amounts of energy need to be provided to the dehydrogenation, usually via auxiliary firing, thus reducing the overall round-trip efficiency of the system. Several studies that have focused on different waste heat recovery strategies of LOHC chains will be presented below and the suitable strategies for this research will be selected.

(Müller et al., 2019) in their study examined two concepts of LOHC-based hydrogen storage that produce electricity using fuel cells. The first concept dehydrogenates LOHC and feeds the released H_2 to a fuel cell. Three different pathways for providing the heat required for dehydrogenation were then adopted. In the first pathway, dehydrogenation was driven by the high-temperature waste heat of a fuel cell, combined with internal recovery, where the hot dehydrogenated stream preheats the cold stream entering the reactor. In the second, the heat required for the process was provided by electric heating, while for the third, the heat required was provided by combusting a fraction of the released hydrogen. The second concept involved an alternative "transfer-hydrogenation + organic fuel cell" that thermally couples an exothermic reaction from acetone to isopropanol step to the LOHC dehydrogenation. Based on their results, the waste-heat-driven dehydrogenation recovered roughly 48% of the electricity, outperforming hydrogen-combustion operation with about 29% and electric heating with about 14%. In the transfer-hydrogenation setup, the heat that must be supplied drops to 28 kJ per mol H_2, giving 36% electricity recovery. The preferred option was waste-heat-driven dehydrogenation, with H_2 burner as an alternative.

(Krieger et al., 2016) coupled the dehydrogenation of dibenzyltoluene (H18-DBT →H0-DBT) with high-temperature exhaust streams from a cement plant, which operates between 200–600 °C. They then utilised this waste heat directly to cover the heat demand, while they also employed a thermal oil storage system to cover for temporal variability. Finally, a hydrogen burner was used to supply any shortfall in energy. In their results, they found that coupling the system directly to high-temperature exhaust streams increased the overall efficiency of the LOHC system to 21.9%, compared to the hydrogen burner average efficiency of about 15-–17%. In addition, when adding 20 cubic meters of thermal storage, all the needed heat for dehydrogenation was provided from waste heat, raising the efficiency to 28.5%, reducing the electricity cost by about €1 million per year in the standard scenario. Finally, when there was not enough waste heat available, auxiliaries were still needed to provide this heat deficit, and an Organic Rankine Cycle (ORC) option was considered only as an alternative.

(Knosala et al., 2021) integrated a reversible solid-oxide cell (rSOC) with an LOHC unit. In their setup, the high-temperature heat generated during the fuel-cell operation of rSOC provided the required heat for the LOHC dehydrogenation. Additionally, hydrogenation heat is reused to preheat/evaporate the water needed for electrolysis. In variations where PEMFC is used, the dehydrogenation heat must be supplied electrically. The thermal integration between rSOC and LOHC reduced the needed hydrogen storage capacity by 25% compared to the PEM system, where dehydrogenation was heated electrically. This integration also eliminated the requirement for high-pressure vessels in the optimal scenario, and resulted in the lowest total annualised cost among the compared self-sufficient options. The heat-integrated configuration increased the round-trip electrical efficiency to about 40%, excluding any use for space-heating, as rSOC's high-temperature output balanced the hydrogenation's and dehydrogenation's heat duties internally.

(Teichmann, Stark, et al., 2012) explored the use of waste heat recovery at the building scale for NEC/12H-NEC, in which the dehydrogenated NEC leaving the reactor is used to preheat the incoming hydrogenated 12H-NEC entering the reactor. In their study, they compared three distinct dehydrogenation heat-supply cases. The first is providing the high-temperature waste heat to cover the reactor's duty from a solid-oxide fuel cell, the second is to use PEMFC and electric heating to supply the reactor's demand by electrical heaters, and finally using a PEMFC and porous hydrogen burner, where

a fraction of the released hydrogen is combusted to provide the needed duty. In their results, they reported that the electricity-to-electricity storage efficiencies of the SOFC case are 38%, 20% for the case with electrical heating, and 28% for the case with the burner. Finally, they emphasised that in the PEM-based cases, the available heat is low-grade, making it suitable for sensible preheats and space heating use, while the SOFC case was the only one able to provide the reactors' heat duty.

Based on this literature, it is evident that several waste heat recovery strategies exist for the LOHC chains. The selected strategies for this research are chosen based on the available waste heat streams. The available waste heat streams for hydrogenation are the heat produced during the reaction, which can be recovered through the reactor coolant, and the waste heat from the reactor outflow. For dehydrogenation, the available waste heat streams are the PEMFC coolant heat and the waste heat from the unloaded LOHC reactor outflow.

2.3. Technical & Economic Feasibility of LOHCs

As mentioned above, LOHCs are considered a promising solution for hydrogen storage and transport, particularly for large-scale applications. The viability of the LOHC system and the comparison of traditional methods, such as compressed and liquefied hydrogen, have been widely explored. In this section, a selection of LOHC studies focused on the technical and economic feasibility of LOHC systems will be evaluated to find their relevance to this research, while also identifying the research gaps of these studies.

In their paper, (Teichmann, Stark, et al., 2012) worked on a decentralised storage system in which buildings stored the excess electrical energy in NEC-based systems. Their methodology approach combined thermodynamic simulations with Aspen Plus and economic assessments to evaluate the overall feasibility of the system. For the simulation of the system, a 15 kW input scenario was introduced where hydrogen was generated by a PEM electrolyser operated at 80°C and 80 bar, which was then fed into a fixed-bed reactor with hydrogen-lean NEC to be hydrogenated. The hydrogen-rich NEC was later dehydrogenated at about 230°C, releasing hydrogen for electricity production through a PEMFC or SOFC. Three different scenarios were considered for supplying the heat required for dehydrogenation:

1. The use of a SOFC that will provide high-temperature heat (650–1000°C) directly, raising the electrical round-trip efficiency to 38%.
2. The use of a PEM fuel cell that relies on electrical heating for dehydrogenation, thus dropping the overall efficiency to 20%.
3. The use of a small fraction of the produced hydrogen of PEMFC in a porous burner to provide the needed heat for dehydrogenation and achieve an efficiency of about 28%.

As (Teichmann, Stark, et al., 2012) suggested, these efficiencies alone are below the efficiencies of some other storage methods, but when capturing and reusing the thermal outputs from all steps (electrolyser, hydrogenation, fuel cell) for space heating and absorption cooling, total annual average efficiencies that approach 95% can be achieved if waste heat is optimally utilised. The economic analysis showed that residential or commercial use of LOHC storage can be profitable if building owners are utilising the fluctuating electricity prices, providing negative balancing power for regional grids, while reducing the reliance on conventional fuels due to the reuse of the process heat. The researchers assumed that a capital expenditure of 40,000 euros is needed for a mass-produced 15 kW LOHC system, about 30,000 euros more than a typical gas- or oil-heating installation. They therefore suggest that converting 1.8 million oil-heated households in Bavaria alone to LOHC storage systems could collectively store up to 5.8 TWh of renewable energy and offer 27 GW of negative balancing capacity. Finally, (Teichmann, Stark, et al., 2012) suggested that system dynamics during startup and partial load, exploration of community-scale LOHC storage systems, and the potential integration of LOHC fueling for hydrogen vehicles to link stationary storage and zero-emission mobility should be explored. In 2017, (Eypasch et al., 2017) conducted a study regarding the techno-economic evaluation of an electricity storage system that utilised dibenzyltoluene (DBT) for an industrial energy supply system. In this study, the focused system included electricity being generated from wind turbines and photovoltaic panels, converting the renewable electricity into hydrogen via electrolysis, storing the hydrogen in LOHC through hydrogenation, and then reconverting it into electricity when needed. The research aimed to

determine the feasibility and cost-effectiveness of such a system in comparison to conventional electricity storage and energy consumption strategies. The results showed that while the LOHC-based storage system has technical viability, it is not economically competitive under current market conditions. A self-sufficient energy storage system, using LOHC to store and supply all electricity demand, was found to be significantly more expensive than purchasing electricity from the grid, with a calculated electricity cost of 225.7 €/MWh, which had a 47% higher electricity price than the industrial grid electricity price of 153.7 €/MWh. The study suggested that at present, the conversion of the excess renewable electricity into heat through power-to-heat applications is a more cost-effective option than storing it in LOHC. However, energy storage became more viable, with a self-sufficiency level of 77% and an electricity cost of 122.8 €/MWh, where the cost was 20% lower than the grid electricity price. After conducting a sensitivity analysis, (Eypasch et al., 2017) identified that the most critical factors that can affect the economic feasibility of the LOHC storage system are the cost of wind and PV electricity, and the capital expenditure of electrolysers and CHP units. When it came to the total cost, the LOHC system accounted for only 11.6% of the total cost, thus indicating that even though it plays a role in system economics, other factors, such as RE production costs and storage efficiency, are the ones that matter. In addition, the study projected future economic viability by estimating cost reductions of key system components by 2030 where they assumed that with a 30% price drop in electrolyser and reactor costs, a 50% reduction in CHP costs, and a PV electricity price dropping from 110 €/MWh to 70 €/MWh, a self-sufficient system would be economically viable as the estimated electricity cost was calculated at 158.3 €/MWh compared to projected 2030 grid electricity price of 157 €/MWh. Finally, (Eypasch et al., 2017) concluded that while such a system is not yet a cost-effective solution for large-scale electricity supply, it holds potential for future applications such as seasonal energy storage scenarios. Their suggestion for further research mentioned that it should focus on energy subsidies, evolving energy price structures, and the integration of LOHC storage with heat-intensive industrial processes to enhance its cost-effectiveness.
In their research, (Abdin et al., 2021) examined the feasibility of LOHCs for large-scale, long-term hydrogen storage, where they compared these with compressed gas, liquid hydrogen, and circular carriers such as ammonia and methanol. The system was designed to store 500 tonnes of hydrogen per day and store it for 30 days. Their methodology approach involved an assessment of technical requirements, energy consumption, and capital costs for primary system components for each storage type. For the LOHC system, the research focused on DBT, which operated at ambient conditions, had no boil-off, and required 0.016 kWh/kgH_2 of electricity for the hydrogenation process, compared to the approximate 10–15 kWh/kgH_2 consumed during liquefaction and 2–7 kWh/kgH_2 needed for compression. The cost analysis showed that a cost of around 350 million USD is required when storing 500 tonnes per day at 200 bar steel pressure vessels, whereas the cost for a liquefied hydrogen system can exceed 935 million USD. Compared to that, the DBT-based hydrogenation solution of 693 MW (lower heating value basis) had an estimated 67 million USD cost for the reactor and a cost of 5 USD per liter for the LOHC material. Ammonia and methanol are compatible with existing fuel infrastructures; however, the additional processes required to obtain pure hydrogen led to significantly higher capital expenditures. They noted that although ammonia and methanol benefit from established global markets, the capital expenditure of producing equivalent ammonia to 500 tonnes of hydrogen per day will increase due to the reactor loop, nitrogen separation, and compression. While for methanol, capturing of CO_2 from flue gas or directly from the air would be the responsible factor for the cost increase. In conclusion, (Abdin et al., 2021) suggested that further research should be focused on LOHC alternatives with higher storage capacity and lower melting points, the development of non-noble metal catalysts to reduce the cost, and the integration of LOHC technology with other industrial processes at scale to optimise capital and operating costs.

Another study by (Brigljević et al., 2020) provided a detailed techno-economic analysis of five dehydrogenation processes sized to supply approximately 82 kgH_2/h. In their study, four specific reversible LOHCs were examined: an eutectic biphenyl/diphenylmethane mixture (EUT), 2-(N-methylbenzyl) pyridine (MBP), (c) N-phenylcarbazole (PHC), and (d) N-ethylcarbazole (NEC). In addition, the fifth process studied was a temperature-cascade (TC) configuration that combined all of the above. Each of the abovementioned systems utilised a part of the released hydrogen to provide the required heat for dehydrogenation via a burner. This allowed a large part of the process to be CO_2-free at the point of hydrogen delivery. The components of each of the processes included a fired reformer furnace, a cat-

alytic plug-flow reactor, a product-separation stage, pumping units, a multi-stage compression system (up to 51 bar), and storage tanks for both hydrogenated ($LOHC^+$) and dehydrogenated ($LOHC^-$) forms. In the base scenario, flue gas entering the furnace is set to about 300°C above the LOHC reaction temperature ($T_{fg} - T_r$ = 300°C). To estimate energy balances, equipment sizes, and operating conditions, the process was simulated in Aspen Plus. The temperature-cascade (TC) configuration integrates all four LOHCs in a multi-stage process, where the high-temperature flue gas leaving the LOHC reactor heats one or more reactors that require lower dehydrogenation temperatures. With this method, (Brigljević et al., 2020) aimed to reduce the total hydrogen consumption for heat supply and shrink the volume of each reactor. A significant factor that determined the overall capital expenses was LOHC logistics. The initial monthly supply and shipping costs were higher than those associated with typical unit operations. Depending on the selected LOHC candidate, the total capital investments (TCI) ranged from $24 million to $44 million. The economic evaluations revealed that, under the specified conditions, MBP achieved the lowest minimum hydrogen selling price among the single carriers, at $7.25 per kg. In contrast, the prices for PHC and NEC exceeded 10 USD per kg. While the implementation of a cascade system increases the number of reactor units and auxiliary components, this approach can effectively reduce shipping volumes by enhancing the overall gravimetric efficiency of LOHCs. Furthermore, a market-uncertainty analysis conducted using the Monte Carlo method, which assessed LOHC prices ranging from $5 to $80 USD per kg, illustrated that the temperature cascade was cost-effective as LOHC prices rose, frequently surpassing the performance of single-carrier systems. (Brigljević et al., 2020) concluded that their findings highlight the importance of accurately assessing LOHC prices and shipping distances when evaluating large-scale hydrogen supply chains. It is recommended to investigate further the hydrogenation (charging) process of these LOHCs, conduct more in-depth comparisons between ”one-way” and ”recyclable” LOHCs, and explore temperature-cascade methods for additional applications, including LOHC-based maritime transport.

(Tsogt et al., 2024) in their research, presented a comprehensive techno-economic and energy analysis of LOHC systems for efficient hydrogen storage and transport. The study utilised Aspen HYSYS to simulate an integrated, large-scale plant that includes both the hydrogenation (charging) and dehydrogenation (discharging) processes for four different LOHC candidates: Methylcyclohexane (MCH), Dibenzyltoluene (DBT), N-ethylcarbazole (NEC), and Naphthalene (NAP). The simulation utilised the Peng-Robinson equation of state, along with property data and kinetic equations derived from experimental studies, to accurately represent the physicochemical characteristics and reaction kinetics of each carrier. The process design first modelled the hydrogenation process, in which a hydrogen-lean LOHC is converted into its hydrogen-rich form under exothermic conditions. Next, the dehydrogenation process is carried out, releasing hydrogen under endothermic conditions at temperatures ranging from 200 to 360°C. The sizing and estimation of the cost of the needed equipment was carried out by the Aspen Process Economic Analyser (APEA), with adjustments based on the Chemical Engineering's Plant Cost Index (CEPCI) and the Marshall and Swift Equipment Cost Index. The resulting capital expenditure (CAPEX) and operating expenditure (OPEX) were calculated for each of the LOHC options, thus allowing (Tsogt et al., 2024) to compute key economic indicators such as the levelized cost of hydrogen (LCOH), breakeven point, net present value (NPV), and internal rate of return (IRR). Among the studied LOHCs, DBT and MCH exhibited the best economic performance, with DBT achieving a breakeven point in approximately three years and providing an IRR of 33.43%, alongside the highest NPV. In contrast, NEC exhibited the highest costs and had a breakeven point of 5.9 years. The study also incorporated heat integration via pinch analysis, which shows that the DBT process achieved a reduction of up to 80% in utility consumption, significantly enhancing the overall energy efficiency of the system. They used a spiderweb diagram as a decision-making tool to compare LOHCs across multiple criteria, such as storage capacity, energy density, dehydrogenation temperature, toxicity, price, energy demand, and material handling, with DBT emerging as the most appealing option. The authors ' discussion emphasised the impact of multiscale approaches, from atomistic simulations to macro-scale modelling, on the deployment of LOHCs. The authors argued that these methods provide valuable insights for catalyst design and process optimisation, improving the efficiency and economic viability of LOHC for hydrogen storage and transport. In summary, (Tsogt et al., 2024) found that LOHC systems, especially when using dibenzyl-toluene (DBT) and methylcyclohexane (MCH), are competitive alternatives to traditional hydrogen storage methods. In addition, they highlighted the need for detailed techno-economic analyses, heat integration, and multiscale modelling to guide future research. Finally,

(Tsogt et al., 2024) recommended that future work focus on integrating these systems with power generation, enhancing catalyst performance, and evaluating long-term stability under changing electricity prices. In summary, prior studies suggested LOHC systems can be technically viable, but their economic viability depends heavily on the heat supply, carrier selection, and system integration. However, most of the literature studies found were conducted for industrial-scale systems, sizes much larger compared to this research, which is focused on a community-level stationary system for the Green Village, presenting a gap. The most relevant study identified for comparing the final results of this research is that of (Teichmann, Stark, et al., 2012), which focused on a built environment application but on a smaller scale.

2.3.1. Research Gaps

While extensive research has been conducted on individual components and process segments for hydrogen storage and transport using LOHCs, several critical gaps remain:

1. **End-to-End System Integration:**
   The insight from prior studies (Abdin et al., 2021; Brigljević et al., 2020; Eypasch et al., 2017; Teichmann, Stark, et al., 2012) have provided us with detailed techno-economic assessments focused on the hydrogenation/dehydrogenation processes, equipment sizing, and heat integration. However, these studies typically researched upstream hydrogen production (e.g., via water electrolysis) and downstream conversion (e.g., via fuel cells) as separate or pre-assumed stages rather than modelling them as parts of a single, integrated system. Thus, there is a shortage of comprehensive models integrating water electrolysis, LOHC-based storage, and fuel cell conversion for stationary applications.

2. **Dynamic Electricity Pricing and Operational Flexibility:**
   Although some studies incorporate economic assessments comparing LOHC storage with traditional methods under static market conditions, there is limited analysis that integrates dynamic, time-resolved electricity pricing into the overall system model (Eypasch et al., 2017; Teichmann, Stark, et al., 2012). The fluctuating nature of renewable electricity prices significantly influences the economics of hydrogen production and storage, and a detailed model that incorporates these market variations and optimises operational strategies is currently not available (Abdin et al., 2021; Teichmann, Stark, et al., 2012).

3. **Process Dynamics and Transient Operation:**
   Most models of the abovementioned studies (Brigljević et al., 2020; Eypasch et al., 2017; Teichmann, Stark, et al., 2012) assume steady-state conditions and overlook the dynamic behaviour, such as start-up, partial load operation, or temporary responses to variable renewable energy inputs. These dynamic factors can significantly affect overall efficiency and economic performance, particularly when coupled with fluctuating electricity prices.

4. **Waste Heat Recovery Integration:**
   While pinch analysis has been utilised in industrial LOHC studies, additional research is essential to assess how waste heat can be effectively recovered throughout the entire hydrogen chain within a building environment. In these systems, the recovered heat can serve a dual purpose: it can either provide the energy required for dehydrogenation or be used directly for space heating. This dual strategy is largely overlooked in existing models.

Table 2.1: Gap Summary Table

Gap Category	Description	Implications	Proposed Focus
End-to-End Integration	Current studies model electrolyser, LOHC storage, and fuel cell conversion separately, primarily for industrial systems.	Overlooks interdependencies critical for optimising performance in the built environment.	Develop an integrated model combining water electrolysis, LOHC storage, and fuel cell conversion for a stationary application.
Dynamic Electricity Pricing	Analyses typically assume static electricity prices, not reflecting real-time fluctuations.	Static models fail to capture the impact of variable electricity costs on system operation and cost allocation between dehydrogenation and building heating.	It will not be addressed
Process Dynamics and Transients	Models often assume steady state operation, neglecting startup, shutdown, and partial load conditions.	This may lead to inaccurate predictions of system efficiency and cost in environments with variable loads.	The developed model will operate under varying loads to accurately represent the built environment operating conditions.
Holistic Waste Heat Recovery Integration	Current work examines heat integration only in parts of the LOHC process and does not fully explore the dual use of recovered heat (for dehydrogenation and building heating).	Incomplete waste heat utilisation may reduce overall energy efficiency and economic viability.	Integrate comprehensive waste heat recovery to either power the dehydrogenation process or provide heat to the building, optimising overall energy use.

2.4. Safety and Regulatory Framework of Hydrogen Storage

In the following section, an overview of the applicable regulations and standard practices for hydrogen systems will be presented.

2.4.1. Overview of National and EU Regulations and Standards

In the EU, all equipment installed and sold must carry a CE marking. The relevant directives for this system include the Pressure Equipment Directive (2014/68/EU) (European Commission, 2014d) for pressure parts, the ATEX Product Directive (2014/34/EU) (European Commission, 2014a) for equipment intended for use in explosive atmospheres, the Low Voltage Directive (2014/35/EU) (European Commission, 2014c) and the Electromagnetic Compatibility (EMC) Directive (2014/30/EU) (European Commission, 2014b).

From January 1st, 2024, permitting applications must be submitted under the Omgevingsloket. Activities that can harm the environment, such as hydrogen installations, may require a permit in accordance with Chapter 3 of the Besluit Activiteiten Leefomgeving (Bal) (Seveso-Omgevingsdiensten, 2024). This also includes adherence to the relevant regulations outlined in the Besluit Bouwwerken Leefomgeving (Bbl) and the Besluit Kwaliteit Leefomgeving (Bkl). In Bbl, the general fire safety obligations are outlined, including specific responsibilities for safety and control measures, fire safety practices, and construction activities that may require a building permit. Bkl sets the standards for external safety assessments, including designated safety zones and individual risk contours, which authorities follow when making siting decisions.

Dutch regulations rely on the Publicatiereeks Gevaarlijke Stoffen (PGS). The most relevant PGS issue for hydrogen applications is PGS 35 (PGS, 2021), which refers to installations of hydrogen delivery to road vehicles and is used by authorities for similar stationary hydrogen equipment. Currently, there is no other applicable PGS for the production and use of LOHC in existence. For LOHC, PGS 29 (PGS, 2023) could be relevant to the storage part of the process, as it regulates above-ground tanks that store flammable liquids. This regulation may apply to LOHCs as they have similar properties to crude oil (Seveso-Omgevingsdiensten, 2024).

In the Netherlands, the Major Accidents Risks Decree (SEVESO, formerly BRZO) requires companies that handle significant quantities of hazardous substances, such as hydrogen, which is classified as a flammable gas, to take measures to prevent major accidents and minimise their impact on people and the environment. The lower threshold is set at 10 tons, and the higher threshold is at 50 tons (Collignon, 2019). Small installations usually operate below these thresholds, but it may be required to show proof of compliance with external safety standards through a proportional quantitative risk assessment (QRA).

2.4.2. Safety Requirements

Even small-scale hydrogen energy systems can cause significant hazards that must be carefully handled. In the following paragraphs, the specific safety requirements and considerations that may apply to our setup will be analysed:

Explosion Safety (ATEX Compliance)

Hydrogen is a highly flammable gas, and strict measures are required to prevent explosions. Under the ATEX, the hazardous areas must be classified, explosion-proof equipment must be used, and ATEX zoning analysis must be conducted to identify potential leak areas. There are typically two categories used: Zone 1 (characterised by frequent gas presence) and Zone 2 (characterised by infrequent leaks). In these zones, all electrical components must be certified to NEN-EN-IEC 60079 for hydrogen (Group IIC). Non-electrical ignition sources must also be carefully controlled, including the use of ATEX-rated equipment, avoiding hot surfaces, and implementing maintenance protocols such as hot work permits. The safety measures must be clearly documented in the Explosion Safety Document as part of the risk assessment, to demonstrate that the system design minimises explosive atmospheres and mitigates ignition risks (European Commission, 2014a).

Separation Distances

During installation, safety distances must be kept between the hydrogen system components and other equipment or buildings. These distances aim to minimise domino effects and to protect people and buildings in case of a fire or explosion. PGS 35 specifies that internal spacing should be based on heat radiation and overpressure calculations for worst-case scenarios.

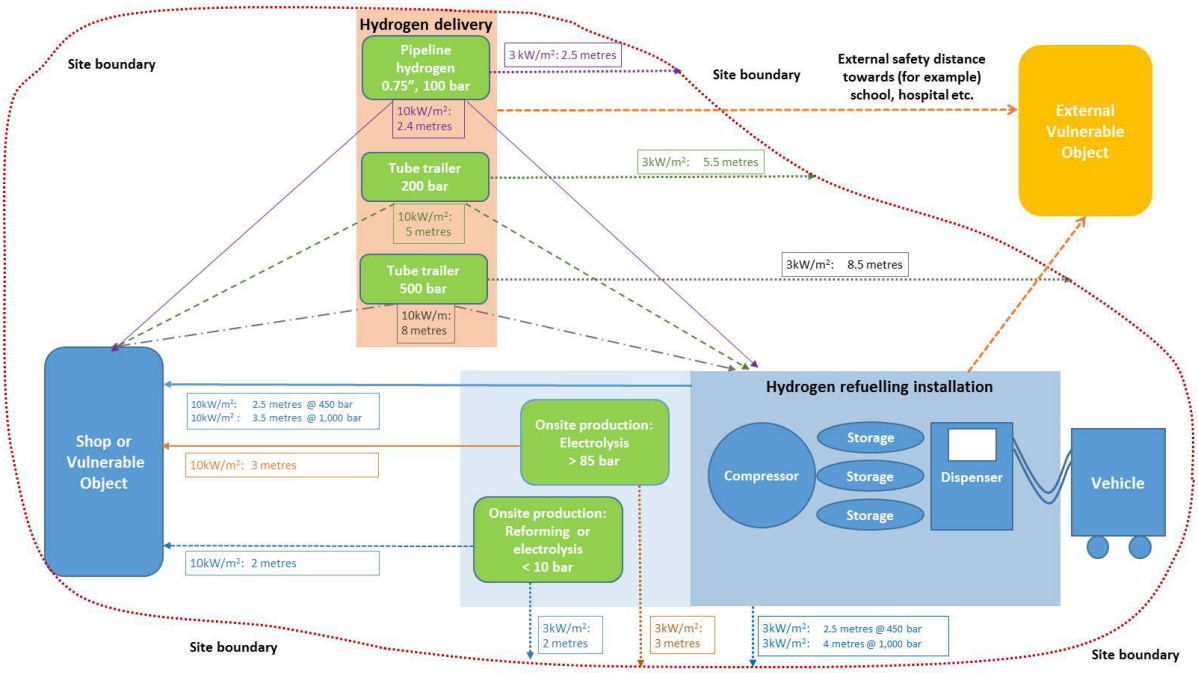

Figure 2.3: Separation Distances of Hydrogen Refueling Stations (Büthker et al., 2015)

If a hydrogen storage ignites, the heat flux at ground level should remain below about 3 kW/m² at the site boundary and below 1 kW/m² outside the establishment based on (PGS, 2021). The system components should therefore have the needed separation distances between them so that, in the event of an incident, they do not influence each other. PGS 35 suggests determining such internal distances via engineering analysis of thermal radiation and explosion effects (PGS, 2021). In addition, any ignition sources should be located outside the hazardous gas zones and at a safe distance from hydrogen release points (PGS, 2021). Components enclosed in a container, as specified in the Building Decree (Bouwbesluit), also require fire-resistant construction and possibly blast-resistant panels between compartments to prevent a fire in one part from rapidly spreading or affecting the building (PGS, 2021).

Ventilation and Leak Detection

Another safety aspect that needs to be considered is the implementation of adequate ventilation and gas detection measures (ANSI/AIAA, 2017). These measures are critical, as hydrogen is odourless and disperses quickly upward. Enclosed system components must have sufficient ventilation and gas detection measures to prevent hydrogen gas accumulation, to keep hydrogen concentrations well below the lower explosive limit, which is 4% in air. For outdoor installations, natural ventilation is typically considered sufficient. For components such as electrolysers and fuel cells, located inside cabinets or containers, the same rules apply. NEN-EN-IEC 60079-10-1 and PGS 35 provide guidance on the required ventilation rates, while placing hydrogen leak detectors in strategic locations is considered a best practice (PGS, 2021). In the event of a leak detection, automatic safety actions, such as closing hydrogen supply valves and shutting down the electrolyser/fuel cell, should be taken to prevent an incident (PGS, 2021). Similar measures should be considered for oxygen in areas where pure oxygen could accumulate, thereby reducing the risk of fire hazards.

Fire Safety Measures
For the studied system, fire safety measures should also be considered both for hydrogen and conventional fires. The design of the system should first focus on preventing such incidents by installing the proper signage, minimising ignition sources, and using materials that reduce fire spread. It should also be equipped with flame detectors and appropriate fire suppression measures, such as emergency shut-off valves (PGS, 2021). PGS 35 explicitly requires that a hydrogen production system have a remote-safe shutdown capability in the event of an emergency. For the LOHC part of the system, traditional fire protection measures are necessary, including fire detectors (smoke/heat) near the LOHC storage and reactor, as well as portable fire extinguishers.

Risk Classification and Hazard Zoning
If such a project were to be realised, a two-dimensional risk assessment (of internal and external) to classify hazards and define suitable zones and controls should be conducted. In internal hazardous area zoning, each part of the system is categorised based on the severity of the hazard (ICM, 2023). This ATEX zone classification must be documented with zone drawings and used to guide equipment selection and installation practices, which for the Netherlands follow the NPR 7910 standard for gas explosion hazard zoning based on IEC 60079-10-1. The risks surrounding the facility in terms of external safety should be defined in the external area hazard zoning. For small installations, the individual risks at the site boundary should be demonstrated to be below the regulatory limit of 1×10^{-6} per year (Spoelstra, 2025). If such a system is installed near a public area or residences, a Quantitative Risk Assessment (QRA) might also be required by the permitting authority to quantify scenarios such as a hydrogen release and ignition or an LOHC tank fire (Hydrogen Safety Innovation Programme (WVIP), 2020).

Permitting Requirements
Environmental permits or official clearances may be required in the Netherlands for small-scale hydrogen system applications, such as the one studied for the Green Village. These permits are needed to ensure that the authorities supervise safety and environmental factors. The permits and approvals that may be required include:

Environmental Permit (Omgevingsvergunning) Milieu) Covering environmental and safety aspects of an installation. The full permit obligations depend on the activity categories as defined in the Bor (Environmental Licensing Decree). Hydrogen fueling stations are always required to obtain an environmental permit, as they are classified as Type C under the Activities Decree. For smaller applications, such as on-site research or energy supply, such a permit may not be required as the project is considered a Type B. However, the local authorities need to be notified. The safest course for any community deployment is to consult the local environmental service (Omgevingsdienst) early(PGS, 2021). If a formal permit is not strictly required, the authorities may request one or an equivalent safety report due to project-associated risks.

Building Permit (Omgevingsvergunning Bouw): If the project involves constructing a new structure (such as a housing system or a concrete foundation), a building permit is likely required. For hydrogen installations at existing facilities, building permits may be required for structures.

Consultation with the Safety Region and Fire Brigade: For such projects, it is common practice for the Fire Brigade to review the plans as part of the environmental permit process (WVIP, 2021) and evaluate emergency access, firefighting water supply, explosion venting, etc. For small systems, the Fire Brigade's input is necessary to ensure that an emergency response plan is in place and that first responders are informed of potential hazards.

2.4.3. Conclusions of Safety Requirements

In summary, the current regulatory landscape for hydrogen in the built environment still has gaps, especially when it comes to LOHC-based hydrogen storage. The Green Village is a regulatory-free community where innovative projects are tested. Under Bal, such installations may not require a full environmental permit (notification can suffice), but Bbl (building/fire safety) and Bkl (external safety/siting) still apply via the Omgevingsloket. Guidelines regarding the safe handling of hydrogen and the required

measures can be referenced in PGS 35 for stationary hydrogen equipment and PGS 29 for LOHC storage tanks. The system's components require CE marking under PED, ATEX Product, LVD, and EMC, while for hydrogen-related components, ATEX area classification must be conducted, and ventilation and leak detection, ignition-source control, and separation distances must be documented in an Explosion Safety Document. Although an environmental permit may not be necessary, the permitting authority (Omgevingsdienst) or Fire Brigade may request a proportional QRA to ensure compliance with the boundary individual-risk criterion.
Finally, Table 2.2 is created to establish a clear overview of the regulation and preventive measures that need to be applied in each system component.

Table 2.2: System components and their applicable regulation and safety measures.

Component	EU directives	NL regulations	Safety measures
PV array & inverter	Low Voltage (2014/35/EU); EMC (2014/30/EU).	Bbl (building/fire safety if in building works).	Treat as potential ignition sources; locate outside hazardous gas zones defined by ATEX classification.
Battery	Low Voltage; EMC.	Bbl.	Keep outside classified zones; general fire-safety practices and clear egress as per building/fire provisions.
Electrolyser	Pressure Equipment (2014/68/EU); ATEX Product (2014/34/EU); Low Voltage; EMC.	Omgevingsloket process; Bal (environmental permit); Bbl (housing/container fire safety); Bkl (external safety contours); PGS 35.	ATEX zoning with Explosion Safety Document; ventilation and H_2/O_2 leak detection with automatic shutdown; separation distances based on (PGS 35); ignition sources outside zones; remote shutdown for hydrogen production (PGS 35).
Fuel cell	Low Voltage; EMC (PED where pressurised).	Bbl; PGS 35	Zone classification; ventilation and H_2 detection; ignition sources outside zones; emergency shutdown.
Compressors	Pressure Equipment; ATEX (if installed in classified zones); Low Voltage/EMC for controls.	Bal; Bbl; PGS 35.	Identify/classify leak points; ventilation and hydrogen detection.
Compressed H_2 tanks	Pressure Equipment; ATEX vicinity for surrounding equipment.	Bal/Bbl/Bkl; PGS 35; SEVESO threshold check; proportional QRA may be requested.	Internal spacing and separation distances according to PGS 35; natural or forced ventilation; ignition sources outside zones; emergency shutdown; containerised enclosures with fire-resistant separations.
LOHC reactors (de/hydrogenation)	Pressure Equipment; ATEX Product; Low Voltage; EMC.	Bal/Bbl/Bkl; PGS 35 (H_2 elements) and PGS 29 (flammable liquid handling/storage).	ATEX zoning; ventilation; hydrogen detectors; automatic shutdown.
LOHC storage tank(s)	-	Bal/Bbl/Bkl; PGS 29 (above-ground tanks storing flammable liquids).	Separation distances based on PGS 29; smoke/heat detectors; fire extinguishers.
Hydrogen burner (aux heat)	ATEX area compliance for installation location; Low Voltage/EMC for controls.	Bal; Bbl; PGS 35.	Treat as an ignition source: position outside hazardous gas zones; gas detection & automatic shutdown.
Pumps / valves / piping (LOHC & H_2)	Pressure Equipment; ATEX ; Low Voltage/EMC for drives/controls.	Bal; Bbl; PGS 35 (hydrogen) / PGS 29 (LOHC).	ATEX zone classification; ventilation and leak detection; ignition sources located outside zones; leak control measures.
Container/housing	—	Bbl (fire-resistant construc-tion/compartmentation); PGS 35/PGS 29 .	Fire-resistant construction; blast-resistant panels between (if needed); natural/forced ventilation; gas-tight separations.

2.5. Literature Review Conclusion

Based on the literature research conducted above and the identified gaps, an integrated, end-to-end techno-economic model tailored for a stationary LOHC-based hydrogen storage system at Green Village will be developed. The system components modelled include Enapter EL2.1 AEM electrolyser, NEDSTACK FCS 7-XXL PEM, and BYD LVL 15.4 $LiFePO_4$ battery, components already familiar to the Green Village due to their installation in the energy hub. NEC is the LOHC of choice, as it is considered safer and more practical compared to other LOHCs for a stationary application, such as the one considered in this study. The selected catalysts are $RuAl_2O_3$ for hydrogenation and $PdAl_2O_3$ for dehydrogenation due to their increased performance and commercial availability. Although literature indicates that fixed-bed reactors are a promising option for both hydrogenation and dehydrogenation processes, this study will model the reactors as batch systems for the sake of simplicity.
The developed model will:

- **Couple Key Processes:** Seamlessly integrate water electrolysis, LOHC-based hydrogen storage (via hydrogenation and dehydrogenation), and fuel cell conversion into one unified system designed for Green Village.
- **Address Process Dynamics:** Model the system under partial load conditions, to represent the variable energy demands typical in built environments.
- **Integrate Waste Heat Recovery:** Develop a strategy that utilises the waste heat from both the LOHC process and the fuel cell. This recovered heat can then be used to provide the heat required for the dehydrogenation process by reducing the need for external heating.

Following this comprehensive research approach aims to fill the current literature gap by providing deeper insights into the economic viability and operational performance of LOHC-based hydrogen storage systems under realistic, dynamic conditions prevalent in the built environment.

2.6. Research Question

The main research question that this thesis will be called to address is:

How feasible is a LOHC-based system for seasonal energy storage in The Green Village, considering its technical, economic, and operational aspects?

2.6.1. Sub Questions

In order to sufficiently answer the research question, the following sub-questions are created:

1. How does a hybrid energy system consisting of PV, battery, electrolyser, and fuel cell, which stores hydrogen via LOHC, compare to compressed hydrogen under identical operating conditions in terms of component sizing, performance,safety, and cost?
2. Which techno-economic factors most significantly influence the economic feasibility of the project?
3. What percentage of the required process heat for hydrogenation and dehydrogenation can be recovered through waste heat recovery, and how does this affect round-trip efficiency and hydrogen consumption?

3
Methodology

3.1. Overview of the Approach

To answer the research questions identified in the previous chapter, a modular approach is employed to size and evaluate the feasibility of the energy system. As previously mentioned, the hybrid system comprises a PV-Battery-Electrolyser-LOHC-Fuel Cell system that is connected to the grid. The system's primary goal is to minimise grid exchange by implementing a hydrogen seasonal storage. This can be achieved by storing the surplus energy of PV, which cannot be stored in batteries during summer, in LOHC. The stored energy will then be used in winter to meet energy demand when batteries or the PV are insufficient, thereby reducing Green Village's grid dependency. The model architecture begins with a main script created in MATLAB, operating at an hourly resolution over a full year and consists of the following modules.

1. Preprocess Inputs Module: This module structures the given data for solar production and building demand.
2. Battery-EMS: This module sizes the battery, updates the state of charge and implements the dispatch logic for daily balancing based on the already existing EMS of the Green village.
3. Electrolyser Module: This module sizes the electrolyser and calculates the amount of hydrogen that is produced by the electrolyser.
4. Fuel Cell Module: This module aims to size the fuel cell and estimate the hydrogen demand that is needed for the fuel cell to cover the building's electrical demand.
5. LOHC Dehydrogenation/ Hydrogenation Modules: In these modules, the amount of LOHC required for seasonal storage is calculated by applying mass and energy balances, and utilising WHR strategies and a hydrogen burner to supply the energy needed for the processes. Additionally, the space time yield of each process, reactor size, catalyst mass, and tank size are estimated.
6. Economic Simulation module: This module converts all the sizes found in the previous modules and converts them into economic metrics.

The system component capacities are then estimated iteratively, as shown in 4.1, adjusting the PV size to find the PV size that satisfies the grid exchange and LOHC balance constraints introduced at **??**. When a feasible solution is obtained, the economic module converts the sizes into actual cost (CAPEX & OPEX) and the financial indicators introduced in 3.5.2. A verification of the system will be conducted to ensure that the system operates as intended, while a sensitivity analysis for different economic parameters will be performed to provide insights into the factors that affect the system's economic output the most. Finally, an alternative scenario of CHG hydrogen storage with adjusted capacities will be introduced, using the same time resolution and operational logic, to provide a one-to-one economic comparison with our system.

3.2. System Description and Boundaries

The system studied consists of a PV-Battery-Electrolyser-LOHC-Fuel Cell hybrid energy system that is connected to the grid as presented in figure 3.1 below.
The system boundaries encompass an on-site mindset for all of the system components, where PV generation, battery energy storage, hydrogen production, seasonal storage in a liquid organic hydrogen carrier (LOHC), hydrogen release, and conversion back to electricity all occur within the Green Village premises.

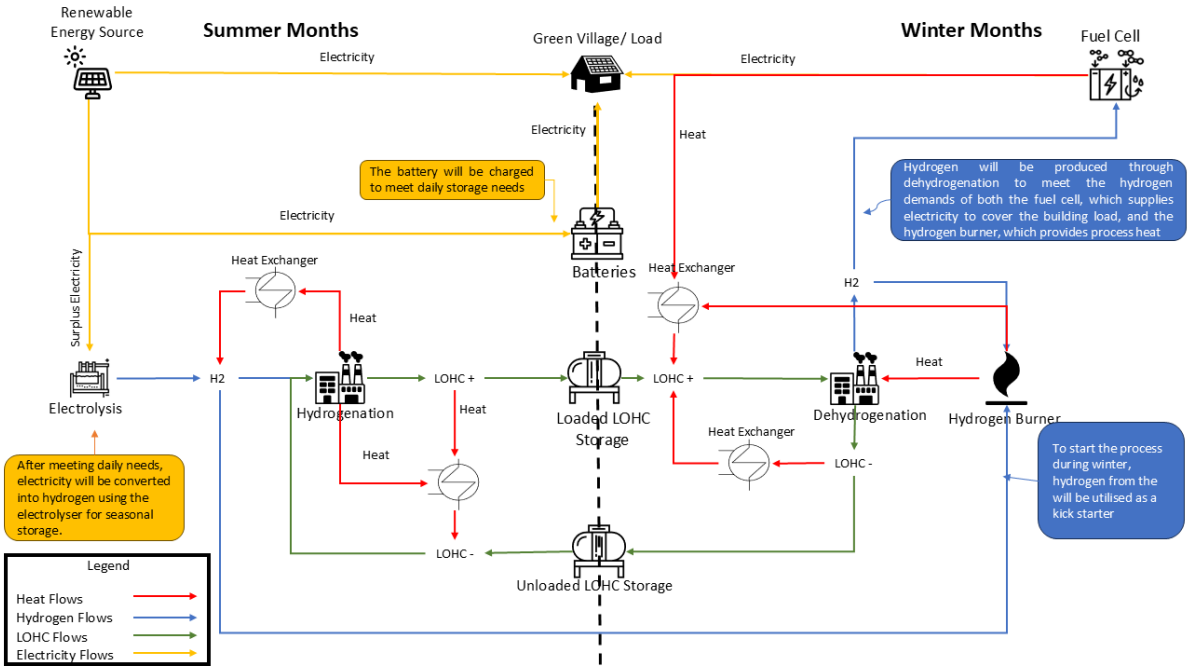

Figure 3.1: Process diagram

The boundary when it comes to operation will be defined by seasonality, as the system will operate in two distinct time periods Summer Months (March 1st to October 15th) and Winter Months (October 16st to February 28/29th).
During the summer months, the electricity produced from photovoltaics will first be channelled to cover the electrical load of the Green Village, while the surplus will be used to charge the battery that handles daily fluctuations. The remaining surplus will be converted into hydrogen using an AEM electrolyser. This hydrogen will then be stored in a tank after being hydrogenated with a Liquid Organic Hydrogen Carrier (LOHC) to create a hydrogen-rich N-ethylcarbazole (NEC) compound, dodecahydro-N-ethylcarbazole (12H-NEC). Three heat exchangers will recover iste heat from the reactors' coolant and outflow, reducing the heat needed to preheat both the hydrogen and N-ethylcarbazole (NEC) that enter the hydrogenation reactor. This heat will be recovered from the reactor's outflow and the heat released during hydrogenation
During the winter months, and at times of prolonged limited solar availability, where solar production and the battery cannot meet electrical demand, a PEM fuel cell will be used to satisfy the building's energy requirements. The hydrogen used in the fuel cell will be released from the 12H-NEC via a dehydrogenation reaction, while the hydrogen-lean LOHC (NEC) will be stored and reused.
The necessary heat for preheating the 12H-NEC feed before entering the dehydrogenation reactor will be supplied through a heat exchanger utilising the iste heat from the fuel cell and the iste heat from the reactor's outflow. The rest of the heat required for preheating the 12H-NEC, as well as the dehydrogenation reaction heat, will be provided by a hydrogen burner. The hydrogen needed for the burner will be provided by the dehydrogenation process. For kick-starting the processes, the required heat is assumed to be provided by the hydrogen burner. The size of all components will be determined based on a full calendar year operation at an hourly time step. Grid connection serves both as a safeguard against power outage and as a sink for surplus generation. This is ensured by supplying the load dur-

ing periods when the battery and fuel cell together are insufficient, thus increasing the security against outages, and it absorbs excess PV when the battery is full and the electrolyser cannot operate under its required conditions. To minimise these interactions, exchange and LOHC balance constraints needed to be introduced. These include: an annual exchange export constraint of 10% of the annual PV production, an import constraint of 5% of the annual building demand, and the LOHC seasonal balance constraint that must be less than 1%.

Summarizing, the boundaries of the above-mentioned system are:

1. Operational: one full calendar year at an hourly timestep.Two seasons Summer: 1 Mar–15 Oct & Winter: 16 Oct–28/29 Feb.
2. System: PV, Batteries, AEM Electrolyser, LOHC hydrogenation & dehydrogenation units, Heat-exchanger network, Liquid tanks, Fuel cell, Hydrogen burner
3. Flows modelled: Electricity, Hydrogen, LOHC (loaded/unloaded), Heat.
4. Grid interaction: Grid interaction at times on need with maximal annual exchange values.
5. Seasonal closure: LOHC hydrogen balance error.

3.3. Data Sources & Processing

The following section documents the data retrieved from the Green Village and manufacturers' datasheets and literature, as well as the processing steps required to obtain a consistent hourly time series for use in our model.

3.3.1. Green Village Electricity Demand

To develop an accurate load profile, the electricity consumption of the buildings from the Green Village monitoring system is requested. A provided dataset for the calendar year 2023 is given. This dataset comprised the aggregated consumption of eight houses, the Co-Creation Centre, and the Office Lab, all located in the Green Village premises. The data is reported as electrical energy per 15 minutes (kWh/15-min) in Amsterdam time. The 15-minute intervals were summed for every four quarter-hours to compose the annual hourly consumption. The total annual electrical demand for the Green village is estimated at 60.86 MWh.

3.3.2. Photovoltaic Generation

Hourly PV generation and ambient temperature were estimated using PVGIS (2025) which assumed crystalline silicon PV panel technology and system loss of 14% for the following coordinates:

Latitude	51.996°
Longitude	4.376°

To estimate the maximum possible installed capacity in the Green Village premises, the PV Scan for the Green Village created by Zhou (2022) is utilised. The PV Scan identified all feasible PV mounting installations, including dual tilt, portrait, landscape, and facades, which totalled a capacity of 312.8 kWp using a 300 Wp panel. All roof and open area installations as seen in 3.2 were considered a possible choice, while facade installations were excluded from this study. The maximum installed capacity, excluding the facades, is estimated to be 257.4 kWp. This includes the installation of 701 PV panels of 300 Wp in dual tilt and an additional 157 panels that can be mounted in both landscape and portrait orientations.

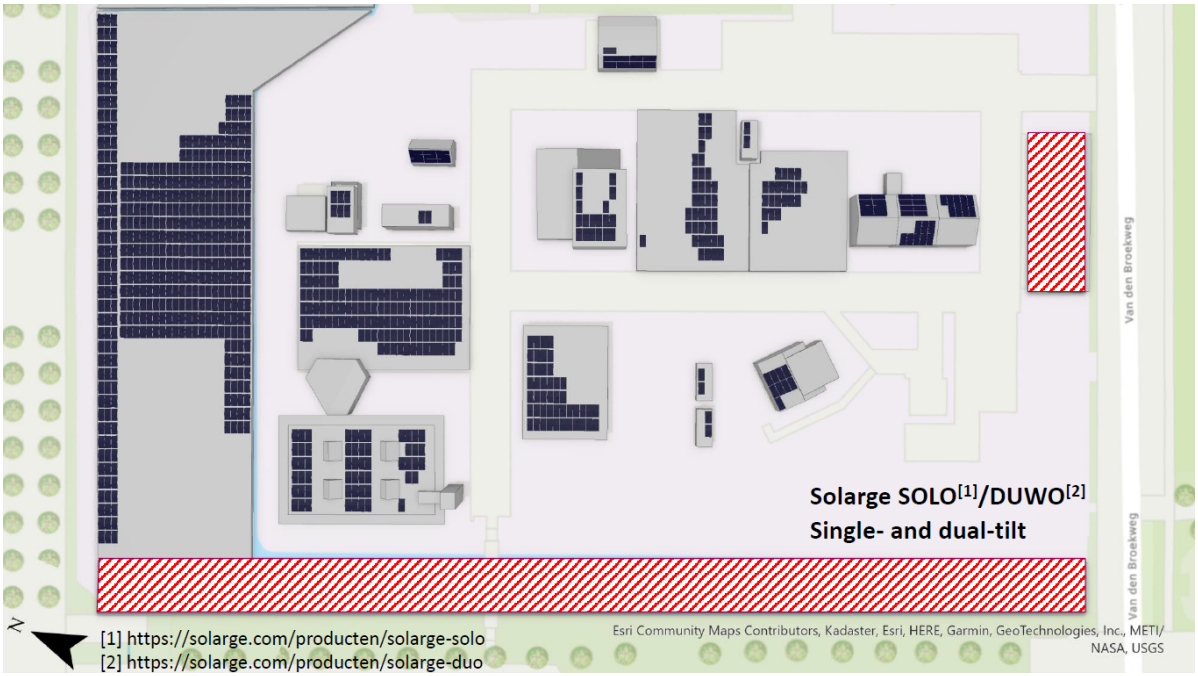

Figure 3.2: Roof and Open area installation Zhou, 2022

To represent the diversity of orientation for the different mounting types, the maximum installed capacity of each type is divided in half. This division is taken to preserve the total possible installed capacity by estimating a more realistic aggregate generation profile and avoiding an undersized/oversized system due to a single orientation. The two extreme cases are examined, using the convention of ”relative to true south,” where 0° represents south as defined by the scan. These extreme cases are characterised by the following:

Table 3.1: Extreme cases used to construct the PV profile (2023).

Mounting type	Tilt (°)	Azimuth (°)†	Capacity (kWp)
Dual-tilt	12	-90	105.15
Dual-tilt	12	$+90$	105.15
Single-tilt (landscape/portrait)	15	-45	23.55
Single-tilt (landscape/portrait)	15	$+45$	23.55
		Total	**257.40**

† Azimuth is measured relative to due south ($0°$): $-90°$ east-facing, $+90°$ west-facing.

These extreme cases are then introduced to PVGIS to retrieve the hourly PV profiles for each orientation and are summed to create the hourly PV profile, which is later introduced to our model.

3.3.3. Battery Data

The battery selected is the BYD LVL 15.4, the specifications used for the modelling are presented in table 3.2, while more details can be found in the datasheet E.1 in the appendices:

Table 3.2: Technical parameters of BYD Battery-Box Premium LVL 15.4 (BYD Company Limited, 2025)

Parameter	Value
Battery	BYD Battery-Box Premium LVL15.4
Usable Energy	15.36 kWh
Rated Power	12.8 kW
Round-trip Efficiency (η)	$\geq$ 95%
Battery Technology	$LiFePO_4$

3.3.4. Electrolyser Data

The selected electrolyser for our system is the AEM electrolyser Enapter EL2.1, with the specifications taken from its datasheet found in the appendices in E.2 and reports provided by the Green Village and are:

Table 3.3: Technical parameters of the Electrolyser (Enapter, 2025)

Parameter	Value
Production Rate	500 NL/h
Maximum Output Pressure	35 barg
Nominal Power Consumption per Nm^3 H_2	4.8 kWh/Nm^3
Power Consumption	2400 W

In addition to the datasheets' specifications data, a report is provided from the Green Village, where Schat, 2025 in his study calculated the mean power levels of the components based on the steady-state test data, and the results were:

Table 3.4: Mean values of the electrolyser tests (Schat, 2025)

Electrolyser testing rate	60%	70%	80%	90%	100%
Mean stack power [W]	1267.8	1477.4	1701.7	1922.6	2178.4
Mean compressor power [W]	412.3	459.9	494.7	536.5	582.5
Mean hydrogen flow rate [NL/h]	305.9	356.9	407.9	458.7	509.8

This data will be later used when simulating the hourly electrolyser operation.

3.3.5. Fuel Cell Data

The fuel cell selected for this study is the PEMFC Nedstack FCS 7-XXL, the data used were taken from the datasheet that can be found in the appendices in E.3 and are:

Table 3.5: Fuel Cell Specifications (Nedstack Fuel Cell Technology B.V., 2019)

Parameter	Value
Rated Power	6.8 kWe
Stack Temperature	62 °C
Cell Count	48

The fuel cell's hourly operation under different operating points is simulated using the data provided in the datasheet I–V curves, as shown in Table 3.6.

Table 3.6: Fuel Cell IV Curve Data (Nedstack Fuel Cell Technology B.V., 2019)

Current (A)	Stack Voltage (V)	Stack Power (kW)
0	46.6	0.0
40	38.7	1.5
80	36.6	2.9
120	34.7	4.2
160	32.7	5.2
200	31.0	6.2
230	29.5	6.8

3.4. Operational Logic

The system will operate using an Energy Management System (EMS), which will control how the power is distributed throughout the year. Such an EMS already exists in the Green Village energy hub project, as seen in figure 3.3 below.

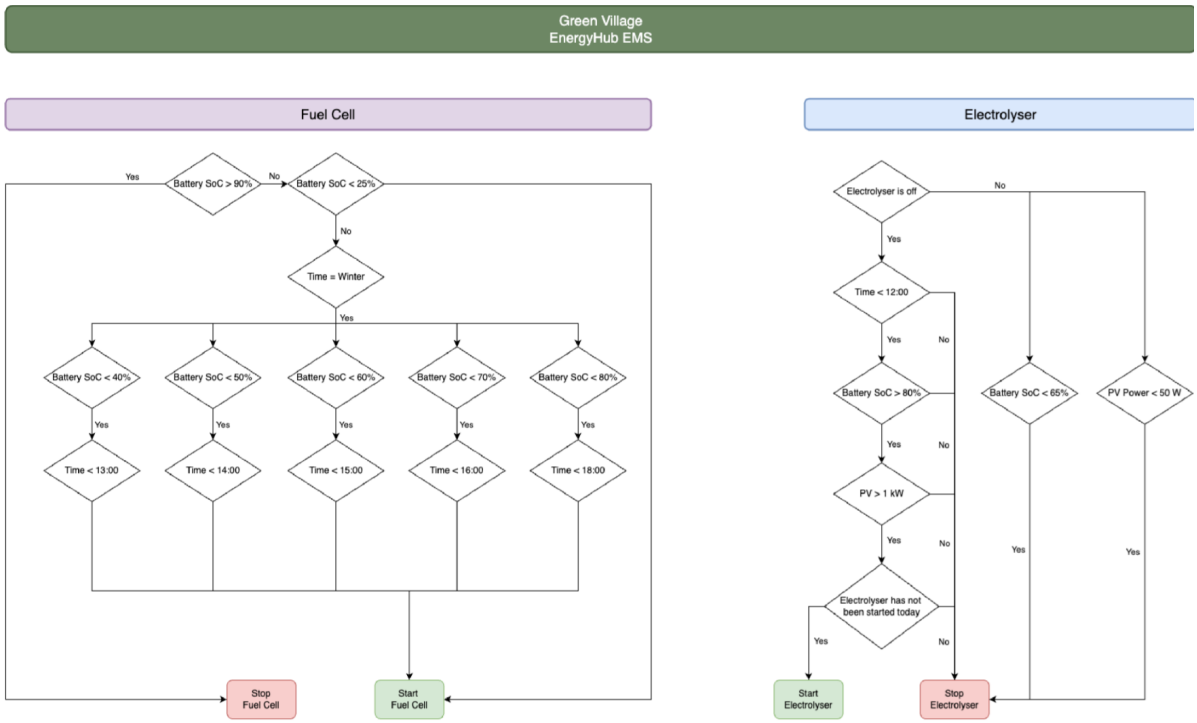

Figure 3.3: Energy Management System of Green Villages' Energy Hub (Schat, 2025)

The operational logic will thus be controlled by rules based on which the energy will be dispatched. To apply this logic, this simulation starts by estimating the difference between the building load and PV production at the current hour. Based on this difference, along with the battery's state of charge (SoC), season, and time of the day, the EMS rules will control the operation of the fuel cell and the electrolyser. The aim of this operational logic is that PV production will be used to cover the buildings' demand. Then the remaining surplus, if any, will be controlled via EMS to charge the battery and satisfy daily storage needs, while any residual energy after the battery is charged will be channelled to the electrolyser to store it seasonally through hydrogenation. During winter, when there are deficit periods, the EMS will determine when hydrogen is released through dehydrogenation and converted into electricity by the fuel cell to supply the load. By implementing this logic, the profile of the fuel cell and electrolyser will be created, based on which the components will be sized.

3.5. Key Performance Indicators (KPIs)

A technoeconomic analysis has two distinct parts: the technical part, which includes sizing, and the economic part, where the cost of the system is estimated. This section defines the technical and economic indicators used to evaluate the technical feasibility of the system. Additionally, performance indicators are introduced to assess the system's performance.

3.5.1. Technical Indicators

The technical indicators are used to size the system effectively and reduce reliance on the grid. For our system, this is achieved by sizing each component in separate modules, starting with the location's maximum PV capacity and reducing it until these technical indicators are met and the sizing loop is terminated. Three indicators were selected to assist in system sizing: two for grid interaction that ensure that import and export stay between the desired bounds, and an LOHC indicator that ensures that there is enough stored energy in summer to be used during winter. As the aim of our system is to minimise grid exchange, annual acceptable import and export thresholds were agreed with the stakeholders.

For import, the indicator introduced is f_{imp} with a maximum import limit of 5%, and is calculated by dividing the annual energy import by the annual demand

$$f_{\text{imp}} = \frac{\sum_{t=1}^{8760} P_{\text{import}}(t)}{\sum_{t=1}^{8760} P_{\text{load}}(t)} \tag{3.1}$$

where P_{import} is the hourly import from the grid and P_{load} is the hourly power demand.

For export, the indicator introduced is f_{exp} with a maximum export limit of 10% and is calculated by dividing the annual energy export by the annual PV production,

$$f_{\text{exp}} = \frac{\sum_{t=1}^{8760} P_{\text{export}}(t)}{\sum_{t=1}^{8760} P_{\text{PV}}(t)} \tag{3.2}$$

where P_{export} is the hourly export to the grid and P_{PV} is the hourly PV production.

The LOHC indicator δ_{LOHC} is a seasonal mass–balance closure indicator, which is introduced to help manage the mismatch between the 12H-NEC produced in the hydrogenation module and the 12H-NEC consumed in dehydrogenation. This indicator ensures the 12H-NEC required for dehydrogenation is available while limiting the excess production of both processes to the necessary amount, and is calculated by dividing the difference between the total hydrogenated LOHC produced via hydrogenation in a year and the total LOHC needed to be consumed by dehydrogenation by the total hydrogenated LOHC produced via hydrogenation.

$$\delta_{\text{LOHC}} = \frac{\left| m_{tot,produced,hy} - m_{tot,produced,dehy} \right|}{m_{tot,produced,hy}} \tag{3.3}$$

where $m_{tot,produced,hy}$ is the total hydrogenated LOHC produced in hydrogenation and $m_{tot,produced,dehy}$ the total consumed in dehydrogenation. Finally, a feasible design is identified when all of the indicators mentioned previously are satisfied.

3.5.2. Economic Indicators

To address the main research question about the feasibility of the system, economic indicators that will define the financial viability of the LOHC project in comparison to a compressed hydrogen alternative

need to be introduced. A common practice for comparing renewable energy systems is to calculate the Levelized Cost of Energy (Marcy, 2017). It is calculated based on the price at which the renewable energy produced needs to be sold for the investment to break even, expressed in €/kWh of energy produced (Papapetrou et al., 2017). The calculation of LCOE is done based on 3.4 where (CAPEX) are capital expenditures and (OPEX) operational expenditures for all components.

$$\mathrm{LCOE} = \frac{\sum_{y=0}^{T} \frac{\mathrm{CAPEX}_y + \mathrm{OPEX}_y}{(1+r)^y}}{\sum_{y=0}^{T} \frac{E_{\mathrm{PV},y}}{(1+r)^y}} \tag{3.4}$$

where CAPEX_y contains the year–zero CAPEX and dated replacements, OPEX_y is the constant annual OPEX with $\mathrm{OPEX}_0 = 0$,y is the lifetime of the project, r is the discount rate, and $E_{\mathrm{PV},y} = \sum_{t=0}^{8760} P_{PV}$ is e annual electricity output produced by the PV. Another economic indicator is the net present value (NPV), the internal rate of return IRR. The net present value measures the total cash flows of a project over its lifetime, discounted to the present.

$$\mathrm{NPV}(r) \;=\; \sum_{y=0}^{T} \frac{\mathrm{CF}_y}{(1+r)^y}, \tag{3.5}$$

IRR is the estimated annual rate at which a project returns its investment.

$$\sum_{y=0}^{T} \frac{\mathrm{CF}_y}{(1+IRR)^y} \;=\; 0. \tag{3.6}$$

Performance Indicators

In addition to the technical and economic indicators, performance indicators were introduced to help us assess the overall system performance. The indicators that were introduced are described below:

1.Overall system efficiency: Assesses the overall system performance by estimating the PV generation that actually serves the building loads, capturing the effects of EMS, the battery, and the seasonal hydrogen pathway. This is estimated by dividing the annual energy served to the load (load demand minus the energy imported from the grid) by the annual PV energy.

$$\eta_{system} = \frac{\sum_{t=1}^{8760} (P_{load}(t) - P_{import}(t))}{\sum_{t=1}^{8760} P_{PV}(t)} \tag{3.7}$$

2.Hydrogen storage efficiency: Estimates the electrical round-trip efficiency across the hydrogen storage by comparing the electricity delivered by the fuel cell with the electricity consumed by the electrolyser over the year, and is estimated as:

$$\eta_{\mathrm{H_2\ storage}} = \frac{\sum_{t=1}^{8760} P_{\mathrm{FC}}(t)}{\sum_{t=1}^{8760} P_{\mathrm{EL}}(t)} \tag{3.8}$$

3.LOHC chain efficiency: Measures the efficiency of the LOHC chain by comparing the annual hydrogen mass used by the fuel cell after dehydrogenation with the hydrogen mass produced from the electrolyser, capturing the hydrogenation and dehydrogenation losses and the hydrogen diverted for process heat within the LOHC system.

$$\eta_{\mathrm{LOHC}} = \frac{\sum_{t=1}^{8760} \dot{m}_{H_2,\mathrm{FC}}(t)}{\sum_{t=1}^{8760} \dot{m}_{H_2,\mathrm{EL}}(t)} \tag{3.9}$$

4. WHR efficiency To estimate the efficiency of each process (hydrogenation and dehydrogenation) in the implemented WHR strategies, the total heat demand for each is divided by the heat recovered. Thus, for hydrogenation, it is estimated as:

$$\eta_{WHR_{hy}} = \frac{\sum_{t=1}^{8760} \left(Q_1(t) + Q_2(t) + Q_H(t)\right)}{\sum_{t=1}^{8760} \left(Q_{pre,L^-}(t) + Q_{pre,H}(t)\right)} \tag{3.10}$$

where Q_1 represent the heat that the NEC inlet recovered from the 12H-NEC reactor outflow, Q_2 is the heat that the NEC inlet recovered from the hydrogenation reactor coolant, and Q_H is the heat that the hydrogen reactor inlet recovered from reactor coolant.
Similarly, for dehydrogenation, it is estimated as:

$$\eta_{WHR_{dehy}} = \frac{\sum_{t=1}^{8760} \left(Q_1(t) + Q_2(t)\right)}{\sum_{t=1}^{8760} \left(Q_{pre,L^+}(t) + Q_{dehy}(t)\right)} \tag{3.11}$$

where Q_1 represent the heat that the 12H-NEC inlet recovered from the PEMFC coolant, while Q_2 the heat recover from the NEC reactor outflow.

3.6. Heat Exchanger Sizing

The sizing of the heat exchangers is conducted using Aspen EDR, employing steady-state design points derived from the hourly energy balances of hydrogenation and dehydrogenation simulations in MATLAB, which are described in 4.6.2 and 4.7.2. The inputs required for EDR include stream properties, mass flows, heat duty, inlet and outlet temperatures, and pressure. The data required for the NEC and 12H-NEC streams, such as heat capacity, density, viscosity, and surface tension, are calculated using linear correlation equations as described in (Stark et al., 2015). The properties of hydrogen and water are obtained using Aspen libraries. For the coolant of the hydrogenation reactor, the heat transfer fluid THERMINOL 55 is assumed, and the data are obtained from the manufacturer's datasheet located in the Appendices E.4.
The sizing of each heat exchanger is carried out at the timestep corresponding to the maximum identified thermal duty, $Q_i(t)$, as observed throughout the annual profile.

$$Q_{i,\mathrm{peak}} = \max_{1 \le t \le 8760} Q_i(t), \qquad i \in \{\mathrm{HX1}, \mathrm{HX2}, \ldots\}. \tag{3.12}$$

After the peak timestep is identified, the inlet and outlet temperatures ($T_{h,(in/out)}$, $T_{c,(in/out)}$), mass flow rates $\dot{m}_h$ and $\dot{m}_c$ of hot and cold streams are inserted in ASPEN and the sizing simulation is executed.

3.7. Model Validation

To ensure the credibility of the model, a validation of the model is necessary. The validation of the model determines whether the model's outputs are plausible for the real system by evaluating whether the model's outputs are consistent with physical principles and external evidence. To verify that the model runs as intended, the following methods are followed.

Validation of the Operational Logic: The validation of the operational logic is performed using yearly plots that present the hourly state of operation for the electrolyser and the fuel cell. For the electrolyser, where only one start is allowed per day, the operating hours and the number of starts per day are also plotted.

Thermodynamic Consistency: To validate that our model is thermodynamically correct, the pinch diagram of each designed heat exchanger is constructed using the adopted $\Delta T_{\min}$ exchangers, where the simulated duties must not exceed the limit and cross paths, thus confirming that the energy balances are valid and that the thermodynamic limits are not crossed.

Performance Realism To validate the realism of the assumptions used to develop the model, the hourly efficiency profiles for the fuel cell and electrolyser are plotted and compared with those in the literature. For the hydrogen storage, the electricity-to-electricity efficiency performance indicator, as introduced in 3.5.2, is compared with literature values.

The model is considered validated only when all heat exchanger duties comply with pinch constraints, the operational plots perform as intended, and the component/chain efficiencies remain within literature bands across the relevant load range.

3.8. Sensitivity Analysis

Following the methodology described above produces a single definitive proposed system design and its associated costs. However, the values used to obtain this estimated cost, such as the components' capital and operating costs, financing conditions and material prices, are subject to uncertainty.
The aim of the sensitivity analysis is to test how changes in key economic parameters affect the overall economic feasibility of the system. By changing one parameter at a time while keeping the rest fixed, it is possible to identify which parameters have the most significant impact on the results. This approach does not re-size the system for each scenario, but instead isolates the effect of economic changes on the overall economic performance of the optimal baseline design.
The sensitivity is carried out by varying each parameter within a ±20% range from its baseline value, with the size of PV, batteries, electrolyser, LOHC reactors, and fuel cell remaining unchanged in all cases. These parameters are presented in Table ref below.

Table 3.7: Parameters tested in the LCOE sensitivity ($\pm 20\%$)

Parameter tested	Variation	Subsystem
Discount rate	±20%	Financial assumption
Project life	±20%	Financial assumption
NEC cost	±20%	LOHC medium
Electrolyzer CAPEX	±20%	Electrolyzer
Reactors CAPEX	±20%	LOHC reactors
Fuel cell CAPEX	±20%	Fuel cell
Battery CAPEX	±20%	Battery
Reactors/Tanks O&M	±20%	LOHC reactors & storage
Electrolyzer O&M	±20%	Electrolyzer
PV CAPEX	±20%	Photovoltaics
Battery O&M	±20%	Battery
Tank cost	±20%	LOHC storage
Fuel cell O&M	±20%	Fuel cell
PV O&M	±20%	Photovoltaics
Catalyst cost	±20%	LOHC catalyst
Import price	±20%	Grid electricity price

In practice, this means that two additional simulations are performed for each parameter: a "low" case, where the parameter is reduced by 20%, and a "high" case, where it is increased by 20%. The economic indicators evaluated for each case are the LCOE and NPV, which are described in section 3.5.2. Each of the aforementioned parameters influences economic indicators in a specific way. Capital-cost variations change the initial investment and the dated replacements. Material costs such as NEC and catalyst prices affect both the one-time purchase for the initial fill and the annual make-up quantities. O&M fractions directly modify the annual operating costs. The electricity import price affects the avoided-cost term in the cash flow and therefore impacts NPV but not the LCOE, while changes in the discount rate or lifetime alter the way all future costs and benefits are discounted to the present. The results of the sensitivity analysis are presented as relative percentage changes compared to the baseline scenario, where for LCOE, the percentage change is expressed relative to the baseline LCOE.

$$\Delta LCOE\ (\%) = \frac{LCOE_{\text{case}} - LCOE_0}{LCOE_0} \times 100 \tag{3.13}$$

and for NPV is expressed relative to the absolute value of the baseline NPV to ensure that percentage changes remain meaningful even if a negative NPV is found

$$\Delta NPV\ (\%) = \frac{NPV_{\text{case}} - NPV_0}{|NPV_0|} \times 100 \tag{3.14}$$

The parameter results are ranked according to their influence on LCOE and NPV. This ranking highlights which assumptions have the most significant impact on the project's economics and provides a valuable

insight into where cost reductions, favourable financing, or market conditions could most effectively enhance the feasibility of the LOHC-based seasonal storage system.

3.9. Alternate Scenario: Compressed Hydrogen Storage

An alternate scenario is introduced, where the seasonal storage pathway is implemented with compressed hydrogen instead of LOHC.

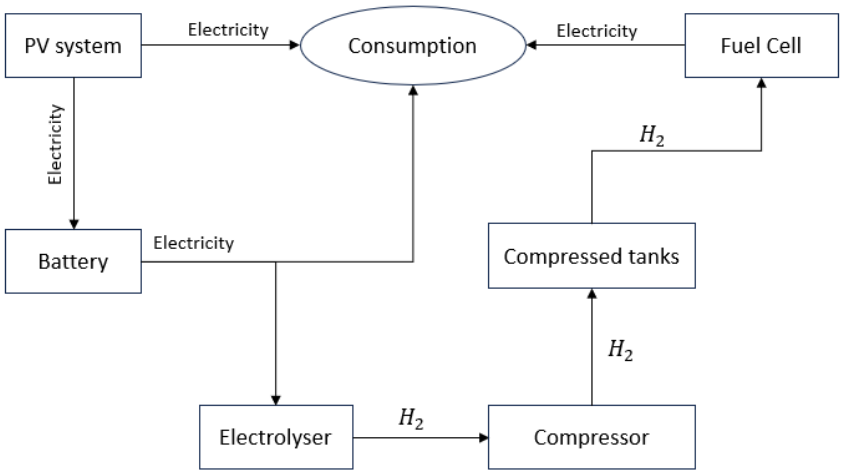

Figure 3.4: CH_2G Process flow Diagram

This model is developed to compare the results of the LOHC storage with those of the compressed hydrogen under the same modelling framework, time resolution, and EMS rules as the main case. Battery dispatch, electrolyser operation, and fuel-cell dispatch use the same equations and thresholds introduced earlier in this chapter. This model's objective remains to minimise grid exchange while adhering to the import, export, and seasonal-closure constraints. For this model, the seasonal-closure constraints are based on the annual hydrogen produced from the electrolyser and the hydrogen consumed by the fuel cell.

The operational sequence follows the same logic. During summer, PV production first serves the building load and then charges the battery for daily balancing. Any remaining surplus powers the electrolyser. The key difference lies downstream of the electrolyser: rather than hydrogenating a liquid carrier, the produced hydrogen is routed to a compression stage and stored as compressed gas. In winter, when PV and the battery cannot satisfy demand, hydrogen is withdrawn from storage and supplied to the PEM fuel cell to generate electricity under the same EMS controls.

Model changes are intentionally minimal. The LOHC hydrogenation and dehydrogenation modules, together with their heat-exchange network and burner integration, are removed. A compressor component is added and sized against the electrolyser outflow. The compressor is sized against the peak daily electrolyser production so that storage can accept the highest daily hydrogen outflow observed during the year.

$$P_{comp} = \max_{1 \le day < 365} \sum_{t=1}^{24} P_{EL}(t) \quad [kg/day] \tag{3.15}$$

The compressor electricity consumption is neglected to ensure a clean comparison focused on the storage pathway rather than auxiliaries. By keeping the EMS and dispatch logic unchanged, this scenario aims to isolate the effect of the storage pathway itself, as any difference in the results between the main and alternate scenarios is therefore attributable to replacing the LOHC chain with compressed storage.

3.10. System Space Use

Once the component sizes and number of modules required in each scenario are defined, the estimate of the space used is conducted.
To make a rough estimate of the area required for the PV system, the value of A_{kWp}=6 m^2/kWp based on a ground-mounted system provided by (Richardson, 2025) is used.
Thus, the area of PV is estimated as:

$$A_{PV} = N_{panel}\, P_{panel}\, A_{kWp} \tag{3.16}$$

where N_{panel} is the total number of panels of each scenario, and P_{panel} is the rated power per panel. To estimate the area required for the fuel cell, electrolyser and batteries, the area per stack/module as mentioned in the appendices datasheets E.1,E.2,E.3, multiplied by the number of modules found by the model. For the LOHC process components, such as reactors and tanks, the volume found using equations introduced in 4.8 is used, while the dimensions of ASPEN results are used for heat exchangers.

Currently, as mentioned in §1.2, the ENERGY HUB 24/7 uses 50 L cylinders for compressed hydrogen storage. To estimate the total spatial requirements in the alternative scenario, the number of 50 L cylinders is determined by first estimating the hydrogen per cylinder using the real-gas relation with a fixed compressibility factor Z=1.2 (Hydrogen Tools, 2025). To estimate the standard (normal) volume of gas in Nm^3 that can be stored in a cylinder of water capacity V_{cyl}=50L pressurised at P=270 bar and temperature of T=273.15 K, the following equation is used,

$$V_{N,\mathrm{cyl}} = \frac{P\,V_{\mathrm{cyl}}}{Z}\,\frac{T_0}{T}\,\frac{1}{P_0} \;\rightarrow\; V_{N,\mathrm{cyl}} = \frac{P\,V_{\mathrm{cyl}}}{Z}\,. \tag{3.17}$$

where P_0 and T_0 are the pressure and temperature at the normal-reference conditions. Using the hydrogen density at normal conditions ρ_N=0.08988kg/Nm^3, the mass per cylinder is

$$m_{\mathrm{cyl}} = \rho_N\, V_{N,\mathrm{cyl}} = \rho_N\, \frac{P\,V_{\mathrm{cyl}}}{Z} \tag{3.18}$$

Finally, the required number of cylinders for a total hydrogen produced in the electrolyser over a year $\dot{m}_{H_2,ELtot}$ is:

$$N_{\mathrm{cyl}} = \frac{m_{\mathrm{req}}}{m_{\mathrm{cyl}}} = \frac{m_{\mathrm{req}}\,Z}{\rho_N\,P\,V_{\mathrm{cyl}}} \tag{3.19}$$

and the total required volume for storing these tanks is:

$$V_{tot} = N_{\mathrm{cyl}}\, V_{cyl} \tag{3.20}$$

4

Model Development

4.1. Detailed Model Overview

The model developed for this research is sized and simulated for a full calendar year (2023) at an hourly resolution, serving as the basis for the economic analysis. As mentioned in 3.1, the model follows a modular approach where each component is a separate module controlled by a single controller script. The simulation begins by calling the preprocess_inputs module, which aggregates the 15-minute intervals of the building's energy consumption into hourly values. Along with the photovoltaic (PV) production and ambient temperature, a time series for the year 2023 is created. This module returns the hourly building demand $P_{load}(t)$, the reference PV production $P_{PV,\,ref}(t)$ corresponding to the maximum number of panels, the ambient temperature $T_{amb}(t)$, and a time vector t that spans the entire calendar year. The maximum photovoltaic (PV) configuration is defined as having $N_{panel,\,ref}$ = 858 panels, each with a power output of $W_{p,\,panel}$ = 300, W_p. The maximum photovoltaic (PV) configuration is defined as having $N_{panel,\,ref}$ = 858 panels, with each panel producing W_{panel} = 300 W_p. After preprocessing the data, the main controller starts with the maximum PV production and conducts a PV search that reduces the PV size to resize the system, based on the technical indicators introduced in 3.5.1. The PV search decreases the number of panels in each iteration by one from the reference value $N_{panel,ref}$ down to a minimum limit of $N_{panel,min}$ = 10, until a solution that meets all three constraints is achieved. For each candidate N_{panel}, the reference PV series is scaled linearly,

$$P_{\mathrm{PV}}(t) \;=\; P_{\mathrm{PV,ref}}(t)\,\frac{N_{\mathrm{panel}}}{N_{\mathrm{panel,ref}}}. \tag{4.1}$$

After PV production is scaled, the modules are sequentially executed as shown in the detailed main script process flow diagram below 4.1.

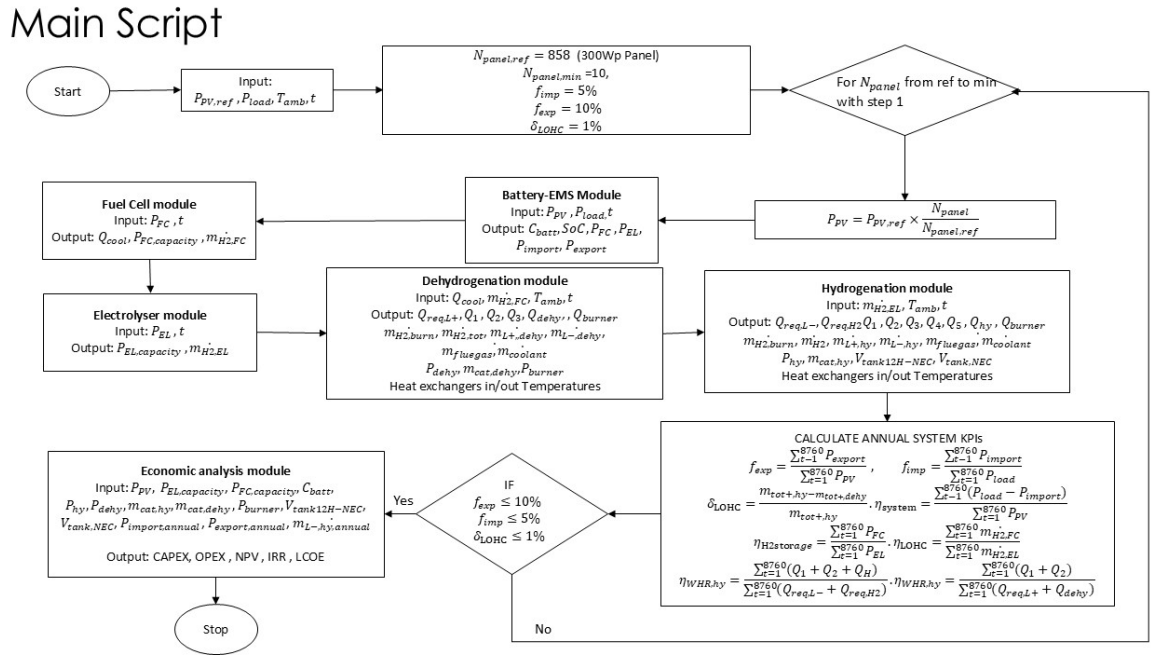

Figure 4.1: Main Script Process Flow Diagram

The first module executed is the Battery–EMS module, which sizes the battery and performs the energy dispatch throughout the entire year as described in §4.3, using the scaled PV production P_{PV} and the building's hourly demand P_{load} along with the time vector (t) data as inputs.
The Fuel Cell module is then executed, using as input the fuel cell profile $P_{FC}(t)$ obtained from the Battery-EMS module, along with the time vector t. This module sizes the fuel cell and estimates the hourly hydrogen consumption $\dot{m}_{\mathrm{H_2,FC}}(t)$ and waste heat being released $Q_{cool}(t)$ during its operation, following the procedure described in §4.5.

Next, the electrolyser module is executed using the electrolyser profile P_{EL} estimated by the Battery-EMS module and the time vector (t) as inputs. This module sizes the electrolyser and estimates the hourly hydrogen production $(\dot{V}_{\mathrm{H_2}}, \dot{m}_{\mathrm{H_2}})(t)$ as described in §4.4.

After Battery-EMS, fuel cell and electrolyser modules dehydrogenation and hydrogenation modules are executed where:
Dehydrogenation module, has as inputs: the time vector (t), the fuel cell's burned hydrogen $\dot{m}_{\mathrm{H_2,FC}}(t)$, the waste heat from the fuel cell $Q_{cool}(t)$, and the ambient temperature $T_{amb}(t)$ and performs the hourly mass and energy balances, including waste-heat recovery from the fuel cell and reactor outflow. This module returns as outputs the hydrogen & LOHC mass flows, stream temperatures, heat exchanger duties, reactor and tank sizes and the required mass of the catalyst.

Hydrogenation module inputs are the hydrogen produced from the electrolyser $\dot{m}_{\mathrm{H_2}}(t)$, the time vector (t) and the ambient temperature $T_{amb}(t)$. Upon execution, the module calculates the hourly mass and energy balances, including the recovery of waste from the reactor's outflow and the reactor coolant as described in §4.6. Additionally, the hydrogen & LOHC mass flows, stream temperatures, heat exchanger duties, reactor & tank sizes and the required mass of the catalyst are returned as outputs.

From the two LOHC modules, the main script calculates the annual produced and consumed 12H-NEC masses,

$$m_{tot,produced,hy} = \sum_{t=1}^{8760} \dot{m}_{L^+}^{\mathrm{hy}}(t) \quad m_{tot,consumed,dehy} = \sum_{t=1}^{8760} \dot{m}_{L^+}^{\mathrm{dehy}}(t) \tag{4.2}$$

When the aforementioned steps are completed, the technical and performance KPIs introduced in §3.5 are computed, and the first N_{panel} candidate that meets all three technical constraints (see 3.5.1) is selected as the optimal PV sizing for the modelled system. Once the optimal PV size is determined, the economic analysis and sensitivity analysis modules are executed, calculating the economic metrics outlined in §4.9 as well as the economic factors that influence these metrics.

4.2. Assumptions

This subsection presents all quantitative and procedural assumptions that made the model executable and are held constant across the simulation. They are presented in a distinct manner below:

4.2.1. General Assumptions

The system of focus is sized based on a full calendar year (2023) and runs at an hourly time step. All energy and mass balances are operated on an hourly basis, while monthly and annual KPIs are accumulated from the hourly results.

4.2.2. Input Data & Scaling Assumptions

The input data of the model is the 15-minute electrical demand for the eight buildings as mentioned in 3.3.1, which is aggregated by summing to produce the demand profile. PV production is obtained as hourly PV production in kWh, as mentioned in 3.3.2. The PV scaling in the model is done linearly by reducing the number of panels, starting from 858 panels of 300Wp.

4.2.3. Grid interaction Assumptions
The grid is assumed to have unconstrained availability, while the model aims to minimise the exchanges and maintain the LOHC balance constraints imposed in Section 3.5.1. The Grid interaction for every hour is estimated after the internal sources are dispatched. The residual load (if any) after the dispatch of the battery, fuel cell/electrolyser is the grid interaction. If positive for those hours, it is considered import; if negative, it is considered export. This way, import and export cannot be done simultaneously.

4.2.4. Battery Assumptions
The battery system is sized to cover the daily fluctuations, and the autonomy, based on which the system is sized, was set to 1 day. The starting state of charge is assumed to be 50% while the state of charge/discharge limits are set to 20% and 90%.

4.2.5. Fuel Cell Assumptions
Operation is modelled at steady state on an hourly basis, with part-load efficiency obtained by piece-wise linear interpolation of the I–P–V data. Start-up and shut-down behaviour and intra-hour ramping are not modelled, while stack degradation is also neglected.
The fuel cell consumption of hydrogen is calculated based on a lower heating value (LHV) basis by converting the electric output using the interpolated efficiency to determine consumption. To compute the waste heat produced by the fuel cell, the difference between the hydrogen chemical power (on an LHV basis) and the electrical output is estimated.

4.2.6. Electrolyser Assumptions
An electrolyser outlet temperature of T_{EL}=55°C is used, while to convert hydrogen gas Nm^{-3} H_2 to kg a density of 0.0899 kg Nm^{-3} H_2 was assumed. The electrolyser is considered to operate within the admissible range with a minimum of 20% per stack of the load enforced by the EMS. The efficiency is time varying based on the load level, and its value is interpolated based on the test data provided in section 3.3.4. Start-up and shut-down behaviour, intra-hour ramping, water treatment, purification, compression, and degradation are neglected. Regarding electrolysers' dispatch, it is assumed that they operate only during summer and it is limited to a single start per day to avoid cycling and reduce degradation.

4.2.7. LOHC Process Assumptions
A molar mass of 195 g/mol for NEC, 207 g/mol for 12H-NEC, and a reaction stoichiometry of 6 moles of H_2 per mole of carrier is used. The hydrogenation and dehydrogenation conditions used in our model are taken from the study by (Brückner et al., 2014).
Hydrogenation is simulated for complete conversion in a batch reactor with a residence time of 3 hours, under a temperature of 150 °C and a pressure of 50 bar, using a 0.25% mol catalyst of 5% wt $Ru/A1_2O_3$ (Brückner et al., 2014).
As mentioned in §2.5, dehydrogenation is also simulated in a batch reactor, but for a 90% conversion using a 0.1 mol% catalyst of 0.5% wt $Pd/A1_2O_3$. To achieve this conversion, a temperature of 230°C, pressure of 1 bar, and residence time of 1 hour were required as seen in 4.2.

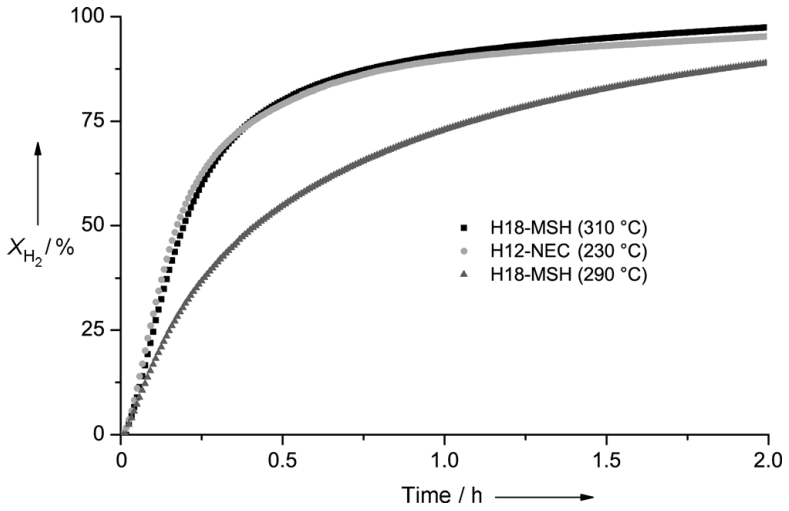

Figure 4.2: H2 release for different LOHCs under similar reaction conditions by temperature variation (Brückner et al., 2014).

The reaction enthalpy used is fixed at $53\mathrm{kJ\ mol}_{\mathrm{H_2}}^{-1}$ both for hydrogenation and dehydrogenation, while heat capacities are considered to be temperature-dependent.
Counter-currents are assumed as the heat exchangers of choice, as they provide a larger log-mean temperature difference (LMTD) than parallel flow for the same terminal temperatures, enabling the same duty with less surface area (Cartaxo & Fernandes, 2011). In addition, counterflow achieves the highest thermal effectiveness for a given NTU and capacity-rate ratio, allowing the cold-stream outlet to approach the hot-stream inlet, which enables tighter temperature approaches in integration (Shah & Sekulic, 2003). Finally, pinch analysis explicitly treats heat recovery in a counter-current picture, separated by a minimum approach temperature ΔTmin, which is exactly the matching that counterflow provides in practice (March, 1998). To model the heat exchangers, a fixed effectiveness of 0.85 and a minimum approach temperature ΔT_{min} of 10 K is assumed, while pressure drops, heat losses to ambient, and fouling are neglected. Any residual sensible-heat deficit and the dehydrogenation endothermic reaction enthalpy are met by a hydrogen burner operating at fixed efficiency. The burners' flue-gas heat capacity is considered constant. A "cold-start" hour is flagged when the immediately preceding hour has no hydrogen production (for hydrogenation) or no hydrogen demand (for dehydrogenation). During these hours, the Burner is assumed to supply the full sensible and reaction duty to reach the reactor inlet temperature.

4.2.8. Economic Analysis Assumptions

To conduct the economic analysis for the project, several assumptions need to be made. A project lifetime of $T_{project}$ = 25 years is assumed and a discount rate of r = 7% is applied, which is typical for renewable energy projects (Thornton, 2019).
A steady price for electricity is assumed, using the average energy price for consumers in the Netherlands of p_{el}=0.28 €/kWh (StatLine, 2025). The only revenues considered are the avoided import benefits. Remuneration for exports, as well as feed-in or other costs, is not considered.
To estimate the capital expenditures (CAPEX) for the photovoltaic (PV) system, batteries, fuel cell, and electrolyser, the following costs were considered:

$$c_{\mathrm{PV}} = 240\ €/\mathrm{kWp}, \quad c_{\mathrm{bat}} = 500\ €/\mathrm{kWh}, \quad c_{\mathrm{EL}} = 3750\ €/\mathrm{kW}, \quad c_{\mathrm{FC}} = 3044\ €/\mathrm{kW}.$$

These values represent the costs associated with purchasing components for the Green Village, as referenced in a similar study conducted by (N. Li et al., 2023).

As there are limited studies estimating the costs for the dehydrogenation and hydrogenation reactors of NEC without modelling the process in ASPEN. The methodology outlined in (Niermann, Drünert, et al., 2019) is followed, where the costs are determined based on correlations related to LHV throughput and space-time yield (STY). This method involves applying the specific cost equations for DBT provided by (Eypasch et al., 2017), which have been curve-fitted for various sizes and adjusted for NEC by multiply-

ing them by the ratio of the space-time yield of DBT to the space-time yield of NEC. These costs have been updated using the Chemical Engineering Plant Cost Index (CEPCI), where $CECPI_{2017} = 567.5$ corresponds to the year of the original study by (Eypasch et al., 2017), and $CECPI_{2023} = 800.8$ refers to the year of this study (The University of Manchester, 2025). To calculate the installed costs, the updated purchase costs are multiplied by a factor of 4.6, which accounts for indirect expenses. The Total Capital Investment (TCI) is then computed by applying a factor of 1.25 to cover additional project-related indirect costs and contingency expenses, as noted by (Niermann, Drünert, et al., 2019).

For the necessary energy carrier (NEC), a cost of c_{NEC}=40€/kg is utilised according to (Niermann, Beckendorff, et al., 2019), the catalyst is assumed to cost c_{cat}=150€/kg (Niermann, Drünert, et al., 2019), while for the tank, a cost of c_{tank}=192€/m^3 is assumed (Niermann, Beckendorff, et al., 2019). The costs associated with the hydrogen burner are estimated using the factsheet for hydrogen boilers by (TNO, 2024) where the initial investment cost is c_{burner}=120€/kW$_t h$ isand the operational cost is 4€/kW$_t h$ based.
For the alternate scenario components, a capital cost of $300\frac{€}{kg/day}$ and an operational cost of c_{commp}= $0.5\frac{€}{kg}$ for the of compressor is used based on the costs provided by (HyETHydrogen, 2025), while for the pressurised tanks the cost of $c_{press,tank}$=200€/kg was used based on (N. Li et al., 2023).

For the components that the operational expenditure (OPEX) could not be retrieved, its cost is estimated as a percentage of capital expenditure (CAPEX) using the following values:

For liquid organic hydrogen carriers (LOHC), the annual operations and maintenance (O&M) cost is calculated as α_{LOHC} = 1%of the total installed investment, which includes the hydrogenation reactor, dehydrogenation reactor, and storage tanks. Additional costs for annual necessary equipment maintenance and catalyst make-up are also included. The annual losses of NEC are estimated at 0.1% of the circulating NEC mass per year, and the catalyst activity of A_{cat}=5×10^5 (kg$_{mat}$/(kg$_{cat}$/year) for annual replenishment of the catalyst is assumed.

For the other components, the annual O&M fractions used are: α_{PV} = 0.5% of CAPEX for the PV, and $\alpha_{bat} = \alpha_{EL} = \alpha_{FC}$ = 1% of their respective CAPEX for the rest.

The lifetime of the PV, Batteries, Fuel cells and Electrolyser used is found by (N. Li et al., 2023),

$$T_{\mathrm{PV}} = 25\ \mathrm{yr}, \quad T_{\mathrm{bat}} = 12\ \mathrm{yr}, \quad T_{\mathrm{EL}} = 12\ \mathrm{yr}, \quad T_{\mathrm{FC}} = 8\ \mathrm{yr}, \quad T_{\mathrm{Burner}} = 25\ \mathrm{yr}.$$

while for the LOHC process, a lifetime of T_{LOHC}=20 years is assumed. Finally, Replacements are assumed at full cost.

4.3. Battery-EMS Module

The Battery and Energy Management System module has two primary objectives. The first is to size the batteries according to PV generation and load demand data. The second is to ensure intra-day balancing by utilising the Energy Management System (EMS) rules that govern the operation of the batteries. These rules are designed to regulate the charging and discharging of batteries, determine when the fuel cell will be activated to meet demand that cannot be satisfied by the Battery and PV system, specify when the electrolyser will operate to utilise surplus energy, and establish the duration of that operation. Additionally, they outline the amount of energy that needs to be imported from or exported to the grid on an hourly basis. The operation of the module will be explained step by step below and can be visualised in the process flow diagram A.4 available in the appendices.

4.3.1. Battery Sizing

To determine the size of the battery, the average daily energy demand, denoted as E_{daily}, needs to be quantified. This calculation involved summing the hourly energy demand, P_{load}, over the entire year and then dividing that total by the number of days in the year, as presented in 4.3.

$$E_{\mathrm{daily}} = \frac{\sum_{t=1}^{8760} \mathrm{P_{load}}(t)}{365} \tag{4.3}$$

Next, the total AC energy $E_{total,AC}$ that the batteries must provide needs to be estimated. To do this, the average daily demand is multiplied by the number of days of autonomy selected for our model, as

mentioned in 4.2.4.

$$E_{\text{total,AC}} = E_{\text{daily}} \times \text{days}_{\text{autonomy}} \tag{4.4}$$

To estimate the required battery capacity before any losses are applied, the total AC energy $E_{total,AC}$ is divided by the round-trip efficiency of the Battery η_{rt} and the inverter efficiency η_{inv}.

$$C_{\text{required}} = \frac{E_{\text{total,AC}}}{\eta_{\text{rt}} \times \eta_{\text{inv}}} \tag{4.5}$$

Our batteries will operate within the fixed state-of-charge (SoC) thresholds mentioned in 4.2.4 to extend their lifespan. To calculate the nominal capacity of our batteries $C_{nominal}$, the required energy is divided by the difference between SoC_{max} and SoC_{min}.

$$C_{\text{nominal}} = \frac{C_{\text{required}}}{\text{SoC}_{\text{max}} - \text{SoC}_{\text{min}}} \tag{4.6}$$

To estimate the total number of battery modules required, the nominal energy is divided by the energy per module (C_{module}=15.36 kWh) and rounded.

$$N_{modules} = \text{round}\left(\frac{C_{\text{nominal}}}{C_{\text{module}}}\right) \tag{4.7}$$

Finally, the total energy capacity is estimated by multiplying the number of modules by the energy produced per module.

$$C_{\text{batt}} = N_{modules} \times C_{\text{module}} \tag{4.8}$$

4.3.2. EMS Dispatch Loop

At the beginning of each hourly iteration t, the model extracts the current hour, day of the month, and month number from the timeseries.

$$H(t) = \text{hour}(\text{time}(t)), \quad d(t) = \text{day}(\text{time}(t)), \quad m(t) = \text{month}(\text{time}(t))$$

where:

- $H(t) \in \{0, \dots, 23\}$ is the current hour,
- $D(t) \in \{1, \dots, 31\}$ is the day of the month,
- $M(t) \in \{1, \dots, 12\}$ is the month number.

Once the day and month are determined, the model identifies the operating season (summer or winter). At the transition from one day to the next ($H(t) = 0$), the daily start permission for the electrolyser is cleared, and the following resets occur:

- $\text{Electrolyser\_started\_today} \leftarrow \text{false}$,
- $\text{Electrolyser\_on} \leftarrow \text{false}$.

By extracting $H(t)$, $D(t)$, and $M(t)$ and applying the specified rules at each hour, the dispatch logic described below is effectively tailored to the time of day and the season. This ensures that daily operations, such as starting the electrolyser, are managed effectively while dispatch decisions consider temporal and seasonal constraints.

At the start of each hour t, and before dispatching any power to conversion devices, the model quantifies two fundamental variables.

The first variable is the net electrical load P_{net}, which represents the mismatch between building demand and PV generation. This variable indicates whether the system draws energy from storage or the grid, or if there is excess energy that needs to be absorbed and is defined as:

$$P_{net}(t) = \underbrace{\text{P}_{\text{load}}(t)}_{\substack{\text{building} \\ \text{demand}}} - \underbrace{\text{P}_{\text{PV}}(t)}_{\substack{\text{PV} \\ \text{output}}} \tag{4.9}$$

- When $\mathrm{P}_{\mathrm{net}}(t) > 0$, demand exceeds solar generation and the deficit must be supplied by the Battery, fuel cell (in winter), or the grid.
- When $\mathrm{P}_{\mathrm{net}}(t) < 0$, PV generation exceeds demand and the surplus can be used to charge the Battery, run an electrolyser (in summer), or export to the grid.
- When $\mathrm{P}_{\mathrm{net}}(t) = 0$ then perfect balance for that hour is achieved .

The second variable to quantify is the state-of-charge fraction SoC_{frac}. The model uses the state-of-charge fraction to make dispatch decisions independent of battery size and is calculated as seen in 4.10. These decisions govern the eligibility for fuel cell startup (in winter) and electrolyser operation (in summer), preventing over–discharge or overcharge.

$$\mathrm{SoC\_frac}(t) \;=\; \frac{\mathrm{SoC}(t)}{C_{\mathrm{batt}}}, \tag{4.10}$$

where

- $\mathrm{SoC}(t)$ is the Battery's stored energy at the beginning of hour t (in kWh).
- $C_{\mathrm{bat,nom}}$ is the total nominal battery capacity (in kWh), as determined in the sizing step.

By expressing SoC as a fraction between 0 and 1, all subsequent dispatch thresholds (e.g. "turn on the fuel cell if $\mathrm{SoC\_frac} < 0.20$") remain valid regardless of the actual battery capacity. So by calculating $\mathrm{P}_{\mathrm{net}}(t)$ and $\mathrm{SoC\_frac}(t)$ upfront, a clear and consistent foundation is ensured for the detailed rules described below.

Fuel Cell Dispatch Strategy

In the winter season, when photovoltaic generation is often insufficient to meet building demand, the on-site fuel cell is dispatched to assist the Battery once the net electrical load becomes positive. The decision to turn on the fuel cell depends on the Battery's state of charge (SoC) and the time of day, ensuring that there are both adequate battery reserves and fuel cell reserves.

When $\mathrm{P}_{\mathrm{net}}(t) > 0$, the fuel cell output $\mathrm{P}_{\mathrm{FC}}(t)$ is set according to the following piecewise logic:

$$\mathrm{P}_{\mathrm{FC}}(t) = \begin{cases} 0, & \text{if } \mathrm{SoC\_frac}(t) \geq 0.90, \\ \mathrm{P}_{\mathrm{net}}(t), & \text{if } \mathrm{SoC\_frac}(t) \leq 0.20, \\ \mathrm{P}_{\mathrm{net}}(t), & \text{if season = winter and } H<13 \\ & \quad \text{and } \mathrm{SoC\_frac}(t)<0.40, \\ \mathrm{P}_{\mathrm{net}}(t), & \text{if season = winter and } H<14 \\ & \quad \text{and } \mathrm{SoC\_frac}(t)<0.50, \\ \mathrm{P}_{\mathrm{net}}(t), & \text{if season = winter and } H<15 \\ & \quad \text{and } \mathrm{SoC\_frac}(t)<0.60, \\ \mathrm{P}_{\mathrm{net}}(t), & \text{if season = winter and } H<16 \\ & \quad \text{and } \mathrm{SoC\_frac}(t)<0.70, \\ \mathrm{P}_{\mathrm{net}}(t), & \text{if season = winter and } H<18 \\ & \quad \text{and } \mathrm{SoC\_frac}(t)<0.80, \\ 0, & \text{otherwise.} \end{cases}$$

Here, $H \in \{0, \ldots, 23\}$ represents the current hour of the day, and the season flag equals "winter". After fuel cell dispatch, net load is calculated again by reducing its original value by the power given by the fuel cell (P_{FC} for winter, otherwise 0), as seen in 4.11,

$$\mathrm{P}_{\mathrm{net}}(t) = \mathrm{P}_{\mathrm{net}}(t) \;-\; \mathrm{P}_{\mathrm{FC}}(t) \tag{4.11}$$

Battery Dispatch Strategy

Throughout every season, the Battery handles any remaining net electrical load after accounting for photovoltaic (PV) generation and, in the winter, fuel cell operation. During the summer months, any excess PV energy may also be sent to an electrolyser, following daily and state-of-charge limits.

As mentioned before, for each hour t, the residual net load is defined based on equation 4.11 for winter months, or based on 4.9 for summer months. Based on the found P_{net}, the battery responds in the 3 ways described below

- A. Discharge ($\mathrm{P}_{\mathrm{net}}(t) > 0$)
  This happens when demand exceeds generation and the battery discharges based on the smallest of the following factors:

1. The unmet load: $\mathrm{P}_{\mathrm{net}}(t)$.
2. Maximum battery discharge power of the battery: $P_{\mathrm{bat,max}}$.
3. Energy above minimum SoC: $\left(\mathrm{SoC}(t) - \mathrm{SoC}_{\mathrm{min}}\right)\eta_{\mathrm{dis}}$.

Thus, the dispatched energy for that hour is calculated based on:

$$P_{\mathrm{dis}}(t) = \min\left[\mathrm{P}_{\mathrm{net}}(t),\ P_{\mathrm{bat,max}},\ (\mathrm{SoC}(t) - \mathrm{SoC}_{\mathrm{min}})\,\eta_{\mathrm{dis}}\right].$$

After the discharge is calculated for that hour, the Battery's state of charge for the next hour and the net load are updated, based on the following equations:

$$\mathrm{SoC}(t+1) = \mathrm{SoC}(t)\ -\ \frac{E_{\mathrm{dch}}(t)}{\eta_{\mathrm{dis}}}, \qquad \mathrm{P}_{\mathrm{net}}(t)\ = \mathrm{P}_{\mathrm{net}}(t) - P_{\mathrm{dis}}(t).$$

- B. Charge ($\mathrm{P}_{\mathrm{net}}(t) < 0$) When generation exceeds demand, the Battery charges up to the smallest of:

  1. The surplus magnitude: $-\mathrm{P}_{\mathrm{net}}(t)$.
  2. Maximum battery charging power: $P_{\mathrm{bat,max}}$.
  3. Available capacity to maximum SoC: $\left(\frac{\mathrm{SoC}_{\mathrm{max}} - \mathrm{SoC}(t)}{\eta_{\mathrm{ch}}}\right)$

  Thus, the absorbed energy for that hour is calculated based on:

$$P_{\mathrm{ch}}(t) = \min\left[-\mathrm{P}_{\mathrm{net}}(t),\ P_{\mathrm{bat,max}}, \left(\frac{\mathrm{SoC}_{\mathrm{max}} - \mathrm{SoC}(t)}{\eta_{\mathrm{ch}}}\right)\right]$$

  After the provided power for charging is calculated, the Battery's state of charge for the next hour and the net load are updated, based on the following equations:

$$\mathrm{SoC}(t+1) = \mathrm{SoC}(t)\ +\ P_{\mathrm{ch}}(t)\,\eta_{\mathrm{ch}}, \qquad \mathrm{P}_{\mathrm{net}}(t) = \mathrm{P}_{\mathrm{net}}(t) + P_{\mathrm{ch}}(t).$$

- C. Idle ($\mathrm{P}_{\mathrm{net}}(t) = 0$) If there is no residual load or surplus, the Battery SoC remains unchanged:

$$\mathrm{SoC}(t+1) = \mathrm{SoC}(t).$$

Electrolyser Dispatch Strategy
The surplus energy generated by the photovoltaic (PV) system can only be directed to the electrolyser during the summer months, specifically from March 1 to October 15. This can occur only after the Battery is sufficiently charged or once certain parameters are met. After the season is identified, the following variable is defined:

$$\mathrm{P}_{\mathrm{surplus}}(t) = \max\left[-\mathrm{P}_{\mathrm{net}}(t),\ 0\right].$$

As indicated by its name, $P_{surplus}(t)$ represents the PV surplus remaining after the energy demands of the buildings have been met, and the Battery has been charged. The purpose of this variable is to manage the operation of the electrolyser along with the two flags introduced below.

- $\mathrm{Electrolyser\_started\_today} \leftarrow \mathrm{false}$,
- $\mathrm{Electrolyser\_on} \leftarrow \mathrm{false}$.

The $Electrolyser\_started\_today$ flag is designed to limit the operation of the electrolyser to once per, helping to extend its lifespan. The $Electrolyser\_on$ flag indicates whether the electrolyser was operating during the previous hour. The operation is then governed by the following conditions

- **A. Start Condition (OFF → ON)**
  For the electrolyser to start when it is off and has not yet started that day, the following conditions must be met:
  - The Hour of the day must be before: $H < 12$

– The battery state of charge (SoC+1) fraction must be: $\frac{\mathrm{SoC}(t+1)}{C_{\mathrm{batt}}} > 80\%$

– The PV surplus must be: $\mathrm{P}_{\mathrm{surplus}}(t) > 1$ kW

If all the conditions are met, then the following updates occur:

$$\mathrm{electrolyser\_on} = \mathrm{true}, \quad \mathrm{electrolyser\_started\_today} = \mathrm{true}.$$

- **B. Stop Condition (ON → OFF)**
  To stop the electrolyser's operation when running, one of the following conditions must be met:

  – The battery state of charge (SoC+1) fraction must be: $\frac{\mathrm{SoC}(t+1)}{C_{\mathrm{batt}}} < 65\%$

  – The PV surplus must be: $\mathrm{P}_{\mathrm{surplus}}(t) < 0.5$ kW

  In that case, the $electrolyser\_on$ flag status change to:

$$\mathrm{electrolyser\_on} = \mathrm{false}.$$

- **C. Surplus Diversion**
  When the electrolyser is on, all PV surplus should be diverted to hydrogen production:

$$\mathrm{P}_{\mathrm{el}}(t) = \mathrm{P}_{\mathrm{surplus}}(t), \quad \mathrm{P}_{\mathrm{net}}(t) \leftarrow \mathrm{P}_{\mathrm{net}}(t) + \mathrm{P}_{\mathrm{surplus}}(t).$$

  When the electrolyser is off, then:

$$\mathrm{P}_{\mathrm{el}}(t) = 0.$$

Grid Dispatch Strategy

To fully characterise the system's interaction with the utility grid, the instantaneous power exchange is recorded on an hourly basis. This is represented by the net building load, which accounts for the contributions from solar photovoltaic (PV) systems, fuel cells, batteries, and electrolysers.

When P_{net} is positive, it indicates that power needs to be supplied to the grid. Conversely, when P_{net} is negative, it signifies that power needs to be exported from the building.

The hourly import and export of the grid can be calculated as follows:

$$\mathrm{P}_{\mathrm{import}}(t) = \max\big(P_{\mathrm{net}}(t), 0\big), \tag{4.12}$$

$$\mathrm{P}_{\mathrm{export}}(t) = \max\big(-P_{\mathrm{net}}(t), 0\big). \tag{4.13}$$

Here, $\mathrm{P}_{\mathrm{import}}(t)$ captures the power drawn from the grid, while $\mathrm{P}_{\mathrm{export}}(t)$ reflects the power sent back to the grid.

4.4. Electrolyser Module

The electrolyser uses the hourly data of $P_{\mathrm{EL}}(t)$ [kW] provided by the Battery–EMS (§4.3) to convert the power given to the electrolyser and convert it into hydrogen production. The model estimates the number of EL2.1 modules N_{mod} needed to meet the annual peak request, then it converts electrical power to hydrogen volume $\dot{V}_{\mathrm{H_2}}(t)$ [Nm^3 / h)] and mass $\dot{m}_{\mathrm{H_2}}(t)$ [kg / h)] using a load-dependent specific energy from steady-state data provided mentioned in 3.3.4, and computes electrical efficiency $\eta_{\mathrm{elec}}(t)$ [%] using the obtained mass flow on an LHV basis. The operation of the module will be explained step by step below.

To size the electrolyser, the peak power supplied to it for the year must be identified from the electrolyser profile $P_{el}(t)$ calculated in the EMS.

$$P_{\mathrm{EL,peak}} = \max_{1 \le t \le 8760} P_{\mathrm{EL}}(t), \tag{4.14}$$

To estimate the number of modules, equation 4.15 is used. The peak power found is divided by the rated power per module $P_{\mathrm{mod}} = 2.426$ kW, and the result is rounded.

$$N_{\mathrm{mod}} = \frac{P_{\mathrm{EL,peak}}}{P_{\mathrm{mod}}} \tag{4.15}$$

Then, the total electrolyser capacity is estimated by multiplying the number of modules by the rated power per module.

$$P_{\text{cap}} = N_{\text{mod}} \times P_{\text{mod}} \tag{4.16}$$

The actual power given to the electrolyser for that hour is then limited by the naming capacity found,

$$P_{\text{act}}(t) = \min\big(P_{\text{EL}}(t),\, P_{\text{cap}}\big). \tag{4.17}$$

To reflect a realistic performance over a changing load, the steady–state data of hydrogen flow (Nm³/h) and electrical input (kW) per module for operating points from (60%-100%) are used. These data are used to estimate the *specific energy* consumption (electricity per produced volume),

$$s_{\text{elec},i} = \frac{E_{\text{elec},i}}{\dot{V}_i} \tag{4.18}$$

where $\dot{V}_i$ $[\text{Nm}^3/\text{h}]$is hydrogen flow and $E_{\text{elec},i}[\text{kW}]$ is the total module electrical input (stack + auxiliaries).
Then, for each hour, a system load fraction is computed based on equation 4.19.

$$\phi(t) = \frac{P_{\text{act}}(t)}{P_{\text{cap}}} \in [0, 1], \tag{4.19}$$

To find the specific energy at our current load fraction, an interpolation for fractions between (60%-100%) and extrapolation for fractions below 60% is used.

$$s_{\text{elec}}(t) = \text{pchip}\big(f,\, s_{\text{elec}},\, \phi(t)\big), \tag{4.20}$$

With $s_{\text{elec}}(t)$ calculated kWh/Nm^3 and the electrical input in kWh given, the volumetric production is found directly:

$$\dot{V}_{\text{H}_2}(t) = \frac{P_{\text{act}}(t)}{s_{\text{elec}}(t)} \quad [\text{Nm}^3/\text{h}]. \tag{4.21}$$

Mass flow is then computed by multiplying the volumetric production by hydrogen density.

$$\dot{m}_{\text{H}_2}(t) = \rho_{\text{H}_2} \times \dot{V}_{\text{H}_2}(t). \tag{4.22}$$

Finally, efficiency is computed by multiplying the mass flow of hydrogen by the lower heating value of hydrogen divided by the actual load.

$$\eta_{\text{elec}}(t) = \frac{\dot{m}_{\text{H}_2}(t) \times \text{LHV}}{P_{\text{act}}(t)} \tag{4.23}$$

4.5. Fuel Cell Module

The Fuel Cell module loads the hourly power demand profile P_{Fc} generated by the 4.3, which represents the electrical power request that the fuel cell must meet for each hour throughout the year. This module aims to quantify the hydrogen flow rates needed for the fuel cell to meet electrical demand and the waste heat generated during operation.
To achieve this, the model first calculates the number of stacks needed to meet the annual peak demand. It then determines the efficiency by interpolating manufacturer data and converts the power requirement into hydrogen consumption. Finally, the model evaluates the heat rejection based on an electrochemical enthalpy balance. The outputs from this module are subsequently fed into the dehydrogenation module. The detailed operation of the module will be thoroughly discussed in the coming paragraphs.
Sizing is done based on the annual peak of the requested profile, as seen below:

$$P_{FC\max} = \max_{1 \le t \le 8760} P_{\text{FC}}(t) \tag{4.24}$$

The required number of stacks is calculated by dividing the annual peak by the maximum power that a single stack can provide, as specified in its datasheet, and rounding the result.

$$N_{\text{stacks}} = \frac{P_{\text{FC,max}}}{P_{\text{stack,max}}}, \tag{4.25}$$

Then the rated system capacity is computed.

$$\mathrm{P}_{\mathrm{FC}_{\mathrm{cap}}} = N_{\mathrm{stacks}}\, P_{\mathrm{stack,max}}. \tag{4.26}$$

After sizing is finished, the per-stack datasheet powers $\mathrm{P}_{\mathrm{stack,\,(i)}}$ are scaled based on the number of stacks found, to form a fixed look-up grid.

$$\mathrm{P}_{\mathrm{FC}_{\mathrm{system}}(i)} = N_{\mathrm{stacks}}\, P_{\mathrm{stack}(i)} \tag{4.27}$$

The hourly power request is then mapped to efficiency by interpolation on this grid. Nedstack 7-XXL fuel cell stack comprises $\mathrm{N}_{\mathrm{Cell}}$=48 cells in series, so the per-cell voltage is:

$$V_{\mathrm{cell},i} = \frac{V_{\mathrm{stack},i}}{N_{cell}}. \tag{4.28}$$

To approximate the fuel cell stack efficiency, equation 4.29 is used, where the operating voltage is divided by the thermodynamic voltage (Harrison et al., 2010).

$$\eta_{\mathrm{cell},i} = \frac{V_{\mathrm{cell},i}}{1.229} \times 100\%, \tag{4.29}$$

where 1.229 V is the Nernst potential for the hydrogen–oxygen reaction.
Then, for each hour t, the fuel cell efficiency is calculated based on the varying load by interpolating the needed power with the known points. ($\mathrm{P}_{\mathrm{sys,i}}$,$\eta_{\mathrm{cell,i}}$):

$$\eta_{\mathrm{sys}}(t) = \mathrm{pchip}\big(P_{\mathrm{sys}},\, \eta_{\mathrm{cell}},\, P_{\mathrm{req}}(t)\big). \tag{4.30}$$

Where the result is clamped within [$\min_i(\eta_{\mathrm{cell,i}})$,$\max_i(\eta_{\mathrm{cell,i}})$] to avoid unphysical values.
After calculating the system efficiency, the volumetric consumption is calculated based on the following equation 4.31

$$\dot{V}_{\mathrm{H_2}}(t) = \frac{P_{FC}(t)}{(\frac{\eta_{sys}(t)}{100}) \times HHV_{H_2}} \tag{4.31}$$

and then mass flow via equation 4.32.

$$\dot{m}_{\mathrm{H_2}}(t) = \dot{V}_{\mathrm{H_2}}(t) \times \rho_{\mathrm{H_2}} \tag{4.32}$$

To calculate the heat recoverable from each fuel cell stack cooling system, (Yu et al., 2024) utilised equation 4.33, which is based on the lower heating value (LHV) of hydrogen.

$$Q_{cool_{stack}}(t) = N_{Cell} \times I(t)\left(\frac{H_{LHV}}{2F} - V_{\mathrm{cell}}(t)\right), \quad [\mathrm{W}]. \tag{4.33}$$

where the per-stack current is calculated as in 4.34.

$$I(t) = \frac{P_{\mathrm{FC}}(t)}{N_{\mathrm{stacks}} \times N_{\mathrm{cell}} \times V_{\mathrm{cell}}(t)} \tag{4.34}$$

Finally, for calculating the whole fuel cell system's waste heat, equation 4.35 is used.

$$Q_{\mathrm{cool}}(t) = \frac{Q_{cool_{stack}}(t) \times N_{\mathrm{stacks}}}{1000}, \quad [\mathrm{kW}]. \tag{4.35}$$

4.6. LOHC Hydrogenation Module

The hydrogenation module is designed to convert the hourly hydrogen feed from the electrolyser, $\dot{m}_{H_2}(t)$ [kg/h], into dodecahydro-N-ethylcarbazole (12H-NEC) by hydrogenating N-ethylcarbazole under isothermal conditions T_{hy}, while conducting a dynamic mass-energy balance with heat integration. To achieve this, the model requires two inputs: the hourly hydrogen feed rate, denoted as $\dot{m}_{H_2}(t)$, and the ambient air temperature, $T_{amb}(t)$ (provided in degrees Celsius and converted internally to Kelvin). The fixed thermophysical constants—such as hydrogenation temperature T_{hy}, reaction heat, heat capacities, exchanger effectiveness η_{hx}, minimum temperature approach ΔT_{min}, burner efficiency η_{burn}, and electrolyzer outlet temperature T_{EL} are defined in Section §4.2. The detailed model structure will be thoroughly presented below.

4.6.1. Mass Balances

To estimate the hourly mass balance for our model, unloaded NEC is named as L^- (0H–NEC) and loaded NEC as L^+ (12H–NEC). The molar masses used will be named as M_{H_2}, M_{L^-}, M_{L^+} accordingly and a stoichiometry of $\nu = 6$ mol H_2/mol NEC will be used. The mass flow of the unloaded NEC is first estimated based on equation 4.36.

$$\dot{m}_{L^-}(t) = \dot{m}_{H_2}(t)\,\frac{M_{L^-}}{\nu\, M_{H_2}} \tag{4.36}$$

As mentioned in Section 4.2.7, the conversion efficiency selected for hydrogenation is 100%. Therefore, the mass flow of the loaded NEC (12-NEC) is calculated by adding the unloaded NEC mass flow to the hydrogen mass flow.

$$\dot{m}_{L^+}(t) = \dot{m}_{L^-}(t) + \dot{m}_{H_2}(t). \tag{4.37}$$

To estimate the specific heat capacity of NEC and 12H-NEC, at T_{amb} and T_{hy} temperatures, the linear correlation provided by (Stark et al., 2015) is used, while equation A-6 by (L. Li et al., 2023) is utilised to estimate the average mass heat capacity of the unloaded LOHC over that range. The detailed methodology for calculating the heat capacities is presented in Appendices B.

4.6.2. Energy Balances

For the reaction to occur, the two streams entering the hydrogenation reactor (NEC and H_2) must reach the reaction temperature T_{Hy}. The heat supplied to the NEC stream Q_{req,L^-} is calculated using equation 4.38 for a temperature difference from T_{Hy} to T_{amb}. Similarly the energy required for the hydrogen stream Q_{req,H_2} is estimated using the same equattion for a difference T_{Hy} to T_{EL}

$$Q = \dot{m} \times C_p \times \Delta T \tag{4.38}$$

The heat produced during the hydrogenation process, due to the reaction's exothermic nature, is calculated by multiplying the reaction enthalpy (q_{hy}) by the number of moles of hydrogen that react.

$$Q_{\mathrm{hy}} = \dot{n}_{H_2}\, q_{\mathrm{hy}} = \frac{\dot{m}_{H_2}}{M_{H_2}}\, q_{\mathrm{hy}} \tag{4.39}$$

The heat exchanger network depicted in Figure 4.3 represents the heat exchangers required to deliver heat to two separate streams.

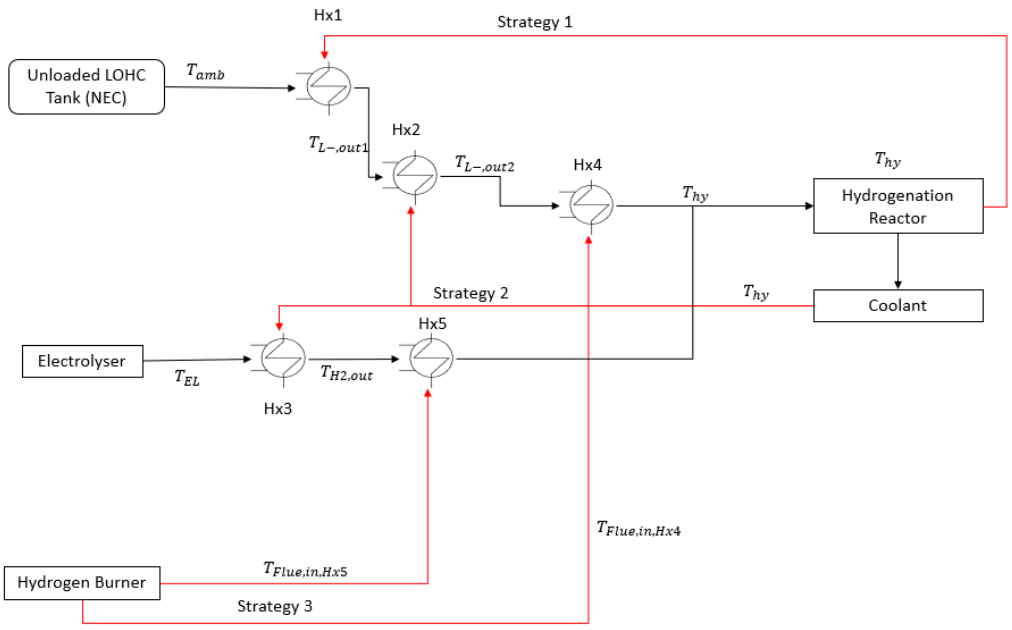

Figure 4.3: Hydrogenation Heat Exchanger Network

Heat exchangers 1 to 3 utilise the waste heat of the process, with HX1 recovering heat from the hot loaded 12H-NEC stream (L^+) exiting the reactor and preheating the incoming cold NEC stream (L^-). While HX2 & HX3 recover the heat from the hydrogenation reactor coolant to preheat the unloaded NEC and hydrogen before entering the reactor. On the contrary, heat exchangers 4 & 5 provide the required heat by an external source (hydrogen burner). The heat exchangers are assumed to operate in a counter-current configuration and have a fixed efficiency, along with a minimum temperature difference ΔT_{min}, as mentioned in 4.2.7.
To estimate the heat exchanged in each heat exchanger, two distinct methodologies are followed:
The first methodology provided by (L. Li et al., 2023) is adopted when both sides of the exchanger are process streams aiming to recover the maximum thermodynamically possible heat. In this methodology, the pinch is applied to the cold stream outlet, which is the limiting factor between the counter-current streams, and the energy balance is solved to estimate the heat that the heat exchanger requires, as shown in equations 4.40 to 4.43 below.

$$T_{hot,\text{out}} = T_{cold,\text{out}} + \Delta T_{\min} \tag{4.40}$$

Where $T_{hot,\,out}$ is the hot stream outlet temperature limited by the pinch. Then the energy balance for the heat exchanger is calculated:

$$\dot{m}_{cold}\, c_{p,cold}\, (T_{cold,out} - T_{cold,in}) = \dot{m}_{hot}\, c_{p,hot}\, (T_{hot,in} - T_{hot,\text{out}})\eta_{hx}. \tag{4.41}$$

and the outlet temperature of the cold stream as :

$$T_{cold,\text{out}} = \frac{\eta_{hx}\, \dot{m}_{hot} c_{p,hot}\, (T_{hot,in} - \Delta T_{\min}) + \dot{m}_{cold} c_{p,cold}\, T_{cold,in}}{\dot{m}_{cold} c_{p,cold} + \eta_{hx}\, \dot{m}_{hot} c_{p,hot}}. \tag{4.42}$$

where η_{hx} is the effectiveness of the heat exchanger.
The provided heat duty to the cold stream from the heat exchanger is calculated as :

$$Q = \dot{m}_{cold}\, c_{p,cold}\, (T_{cold,\text{out}} - T_{cold,in}) \tag{4.43}$$

The second methodology is applied when the hot side is an external utility with a large mass flow, such as the reactor coolant. Here, the exchanger duty is capped by the available utility rather than by process–process balancing. First, a target cold-side outlet is set using the pinch at the hot inlet.

$$T^*_{cold,\text{out}} = T_{hot,\text{in}} - \Delta T_{\min}, \tag{4.44}$$

Then the recovered heat exchanger duty is limited by the available external utility Q_{avail},

$$Q = \min\left(\dot{m}_{cold}\, c_{p,cold}\, \left(T^*_{cold,\text{out}} - T_{cold,\text{in}}\right),\, Q_{\text{avail}}\right), \tag{4.45}$$

and the actual cold-side outlet is calculated from the recovered duty,

$$T_{cold,\text{out}} = T_{cold,\text{in}} + \frac{Q}{\dot{m}_{cold}\, c_{p,cold}} \tag{4.46}$$

The hot outlet is also limited by the pinch so:

$$T_{hot,\text{out}} = T_{cold,\text{in}} + \Delta T_{\min}. \tag{4.47}$$

Then the temperature difference in the hot side is calculated as:

$$\Delta T_{hot} = T_{hot,\text{in}} - \left(T_{cold,\text{in}} + \Delta T_{\min}\right) \tag{4.48}$$

and the hot-side mass flow required to deliver the achieved heat Q is:

$$\dot{m}_{hot} = \frac{Q}{c_{p,hot}\, \Delta T_{hot}\, \eta_{hx}} \tag{4.49}$$

To utilise the waste heat, the hydrogenation process should be running. For this reason, two distinct stages of operation have been set:

A. Cold Start Operation
In this operation, no internal heat recovery is available, and the hydrogen burner needs to supply the heat duties required to increase the temperature of the NEC from T_{amb} and hydrogen from T_{EL} to T_{hy} via heat exchangers (HX4 & HX5). To estimate the heat duty that needs to be provided by the burner, the required heat duty of each stream (Q_{pre,L^-} or Q_{pre,H_2}) is divided by the heat exchanger efficiency.

$$Q_{\mathrm{burn},(\mathrm{L}^-/\mathrm{H}_2)} = \frac{Q_{\mathrm{pre},(\mathrm{L}^-/\mathrm{H}_2)}}{\eta_{hx}} \tag{4.50}$$

The hydrogen consumption of the Burner is then calculated as:

$$\dot{m}_{H_2,\mathrm{burn},(\mathrm{L}^-/\mathrm{H}_2)} = \frac{Q_{\mathrm{burn},(L^-/H_2)}}{\eta_{\mathrm{burn}}\,\mathrm{HHV}_{H_2}}, \qquad , \tag{4.51}$$

To estimate the mass flow rate of the flue gas, an excess air $\lambda = 2.2$ is used (air–fuel ratio $\mathrm{AFR} = \lambda\,\mathrm{AFR}_{\mathrm{stoich}}$), the mass flow of flue gas is calculated as:

$$\dot{m}_{\mathrm{flue},(L^-/H_2)} = \dot{m}_{H_2,\mathrm{burn},(L^-/H_2)}\,(1 + \mathrm{AFR}), \tag{4.52}$$

The inlet temperatures of the flue gas for HX4/HX5 are then estimated by a simple energy balance and the pinch limit:

$$T_{\mathrm{flue,in}} = T_{\mathrm{flue,out}} + \frac{Q_{\mathrm{burn}}}{\dot{m}_{\mathrm{flue}}\,c_{p,\mathrm{flue}}}, \qquad T_{\mathrm{flue,out}} = T_{amb} + \Delta T_{\mathrm{min}}, \tag{4.53}$$

Once the flue gas inlet temperatures are estimated, a Carnot sanity check is applied to each cold stream inlet temperature to indicate if the selected η_{burn} suggests unrealistic performance. The sanity check is:

$$\eta_{\mathrm{Carnot}} = 1 - \frac{T_{\mathrm{cold,in}}}{T_{\mathrm{flue,in}}} \tag{4.54}$$

After some trial and error, a hydrogen burner efficiency of $\eta_{\mathrm{burn}} = 60\%$ is set.

B. Continuous Operation
During continuous operation, waste heat is recovered through heat exchangers 1 to 3. To estimate the heat exchange, mass flow and inlet/outlet temperatures for HX1, the first methodology is adopted, as described in equations 4.40 to 4.43. While for HX2 & HX3 the second methodology (equation 4.44 to 4.49). If the required heat duty is not met through recovery, external heat must be provided by the hydrogen burner via heat exchangers (HX4 & HX5) using the same approach as in equations 4.50 to 4.53.

4.6.3. Iteration for net hydrogen calculation

When mass and energy balances are implemented, the amount of hydrogen consumed by the Burner is successfully determined. However, the challenge that then arises is that the consumed hydrogen is part of the hydrogen produced by the electrolyser. To address this issue, the iteration process presented in Figure **??** is introduced. This iteration method calculates the net hydrogen on an hourly basis by continuing the iterations until the maximum number of iterations is achieved or the difference between the initial value and the calculated value from the energy and mass balance reaches the tolerance $\epsilon = 10^{-8}$.

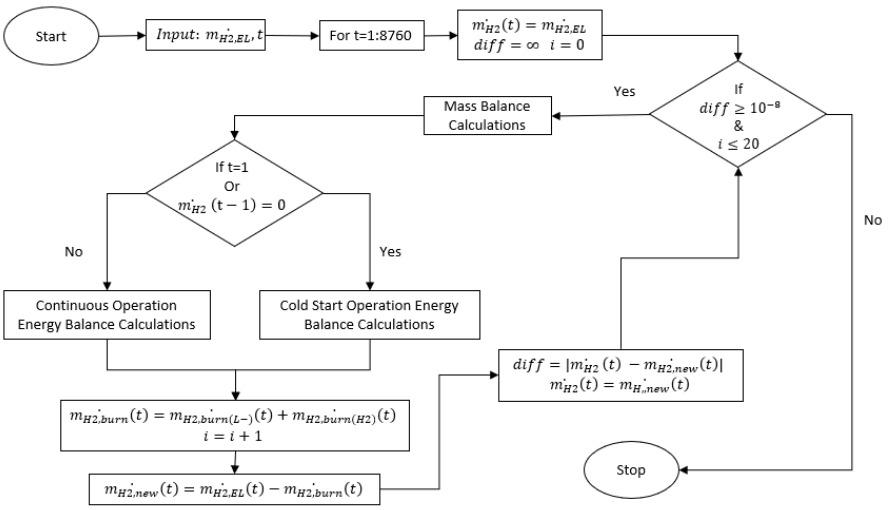

Figure 4.4: Net Hydrogen Iteration Process Flow Diagram

4.7. LOHC Dehydrogenation Module

The dehydrogenation module calculates the hourly mass of 12H-NEC that needs to be dehydrogenated to meet the fuel-cell hydrogen demand $\dot{m}_{H2,FC}(t)$. The inputs for this modules are the hourly values of $\dot{m}_{H2,FC}(t)$, the fuel-cell waste heat $Q_{cool}(t)$, and ambient temperature $T_{amb}(t)$. The fixed thermophysical constants required for the dehydrogenation module (e.g., T_{dehy},q_{de}, heat-capacity data, η_{dehy}, η_{hx}, ΔT_{min}, $T_{coolant}$) are introduced in §4.2.
The detailed model structure will be thoroughly presented below.

4.7.1. Mass Balances

The mass balance for the dehydrogenation module is calculated using the same methodology followed in §4.6.1 for a dehydrogenation conversion efficiency of η_{dehy} = 90%. The total hydrogen that needs to be produced ($\dot{m}_{H2,tot}(t)$) is equal to the sum of the hydrogen supplied to the fuel cell and the hydrogen required from the burner for process heating.

$$\dot{m}_{H_{2,tot}}(t) = \dot{m}_{H_{2,FC}}(t) + \dot{m}_{H_{2,burn}}(t). \tag{4.55}$$

Heat capacities used in this module employ the same methodology as in hydrogenation, utilising the temperature-dependent equation by (Stark et al., 2015) and the average heat capacities equation by (L. Li et al., 2023), as described in Appendices B.

4.7.2. Energy Balances

The enthalpy of the endothermic reaction duty consumed during dehydrogenation (Q_{dehy}) is estimated using equation 4.39 adjusted for q_{dehy} and $\dot{m}_{H2,\,tot}(t)$.
The preheat duty (Q_{req,L^+}) required to increase the temperature of the 12-NEC stream entering the reactor from ambient T_{amb} to reaction temperature T_{dehy} is calculated using equation 4.38.
To provide the required heat duties mentioned above, the heat exchanger network illustrated in Figure 4.5 is modelled.

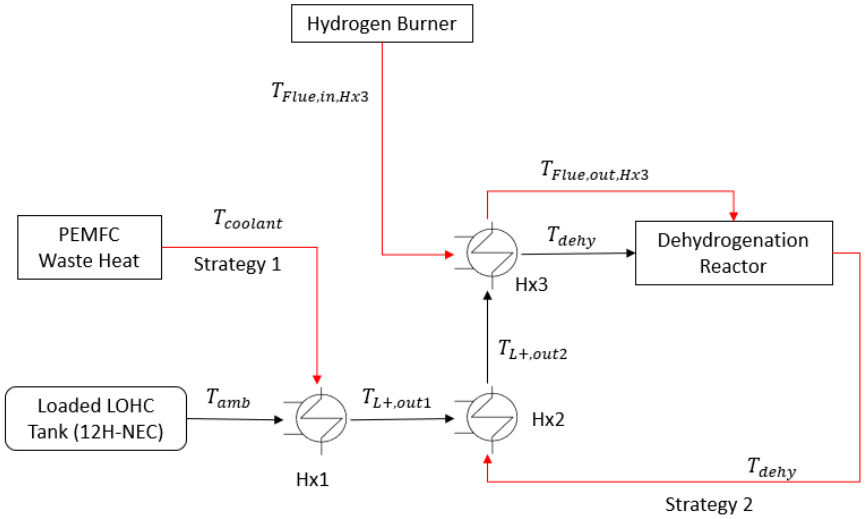

Figure 4.5: Heat Exchanger Network Dehydrogenation

This network utilises the waste heat strategies described in 4.7.2, where HX1 recovers heat from the fuel cell's low-quality waste heat, and HX2 recovers heat from the outflow of the reactor. At times when the heat needed to preheat the stream cannot be supplied by waste heat or when no waste heat is available, this heat is obtained from the burner through heat exchanger HX3. Finally, the endothermic heat duty required is provided by the outflow of HX3, as shown above.

Similarly, to hydrogenation, due to the absence of waste heat when the system is not operational, two separate stages (Cold Start Operation - Continuous Operation) are modelled. Therefore, two distinct stages of operation have been established:

A. Cold Start Operation
In a cold start operation, no internal heat recovery is available, and the burner provides both the reaction duty Q_{dehy} and the preheat duty for 12H-NEC Q_{pre,L^+}. To estimate the heat exchange in HX3, first, the heat that needs to be provided by the burner (Q_{burner}) is calculated 4.50, where Q_{burner} is the sum of the required preheat and reaction heat duty divided by the heat exchanger effectiveness. Equations 4.51 and 4.52 are then used to estimate the mass flow of hydrogen burned and flue gas produced by the hydrogen burner.
After the mass flow of the flue gas is found, the temperature of the flue gas exiting the reactor is calculated, limited by ΔT_{min}.

$$T_{\text{flue,out,reactor}}(t) = T_{dehy} + \Delta T_{min} \tag{4.56}$$

A single energy balance, from the burner outlet to the reactor jacket outlet, is then used to estimate the flue-gas inlet temperature to HX3, where ($c_{p,\,flue}$represents the mean heat capacity of the flue gas..

$$T_{\text{flue,in,3}}(t) = T_{\text{flue,out,reactor}}(t) + \frac{Q_{\text{burner}}(t)}{\dot{m}_{\text{flue}}(t)\, c_{p,\text{flue}}}, \tag{4.57}$$

In the heat exchanger, the flue gas precisely transfers the heat required for the LOHC to reach T_{dehy}, resulting in its outlet temperature from the preheater being:

$$T_{\text{flue,out,3}}(t) = T_{\text{flue,in,3}}(t) - \frac{Q_{\text{pre,L}^+}(t)}{\dot{m}_{\text{flue}}(t)\, c_{p,\text{flue}}\, \eta_{hx}}, \tag{4.58}$$

and the remaining flue-side temperature drop from $T_{flue,out,3}$ to $T_{flue,out,reactor}$ supplies the reaction duty through the jacket contact. The cold-side outlet temperature (loaded LOHC) leaves the preheater HX3 at the reactor setpoint, T_{dehy}. Finally, as in hydrogenation, to ensure thermodynamic plausibility of the hydrogen burner, a Carnot efficiency check is conducted. This check ensures that the burner efficiency η_{burner} does not exceed Carnot efficiency. η_{carnot} and was found after trial and error for dehydrogenation at 58%.

B.Continuous Operation
In continuous operation, the waste heat of the PEMFC and the outflow from the reactor are utilised to preheat the 12H-NEC entering the reactor. The required reaction enthalpy duty, as well as any remaining preheat duty not covered by the waste heat strategies, is provided by the hydrogen burner via HX3 and the reactor jacket. The recovered heat duty, coolant mass flow and inlet/outlet temperatures for heat exchanger 1 are found using the second methodology presented in equations 4.44 to 4.49. Conversely, for estimating the heat duty, coolant mass flow, and inlet/outlet temperatures for heat exchanger 2, the first methodology is adopted, using the equations 4.40 to 4.43. Finally, to estimate the heat duty exchanged in heat exchanger 3 to increase the temperature from $T_{L^+,out2}$ (12H-NEC temperature) to T_{dehy}, the same methodology and equation as in the cold start operation section above are adopted.

4.7.3. Iteration for hydrogen burned calculation

As mentioned above, the hydrogen mass flow produced by the dehydrogenation reaction is found based on equation 4.55. To estimate the hydrogen burner for every hour, the process presented in Figure 4.6 is followed. The iteration starts with an initial guess of $\dot{m}_{H_2,Burner} = 0$. The burned hydrogen estimate is then updated with a new $\dot{m}_{H_2,Burner}$ using the energy balances, regardless of whether it is a cold start or continuous operation, by using the current guess. This process is repeated until the change between successive guesses is below the tolerance $\epsilon = 10^{-8}$ or the maximum number of iterations is reached.

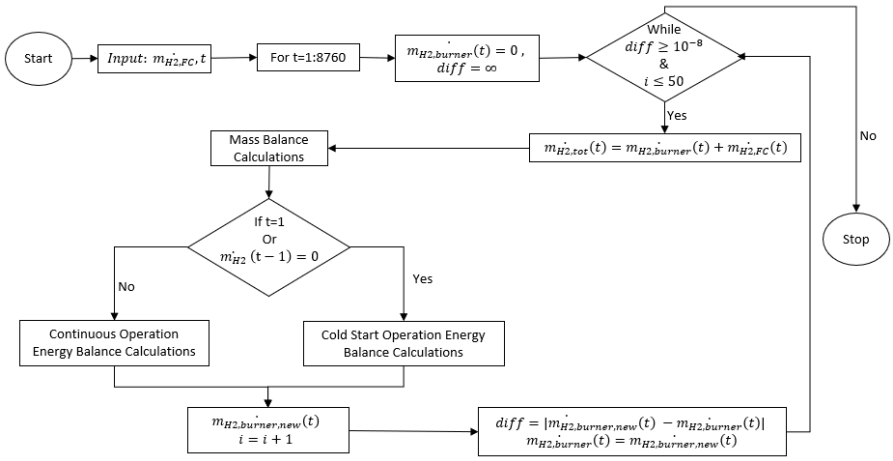

Figure 4.6: Hydrogen Burned Calculation Process Flow Diagram

4.8. Equipment Sizing

This section provides a detailed overview of the calculations conducted to size the LOHC process components.

4.8.1. Reactor sizing

To estimate the cost of the hydrogenation and dehydrogenation process, the maximum power rating of the reactor needs to be calculated. This was achieved by applying the methodology described by (Niermann, Drünert, et al., 2019), in which the maximum hydrogen input in the hydrogenation reactor symbolised as $\dot{m}_{H_2}$ and maximum hydrogen output for dehydrogenation reactor, symbolised as $\dot{m}_{H_{2,tot}}$, over the course of a year is multiplied by the lower heating value of hydrogen.

$$P_{hy} = LHV_{H_2} \max_{1 \leq t \leq 8760} \dot{m}_{H_2}(t) \qquad P_{dehy} = LHV_{H_2} \max_{1 \leq t \leq 8760} \dot{m}_{H_{2,tot}}(t) \tag{4.59}$$

Next, to estimate the reactor volume, the space time yield (STY) is required. For the dehydrogenation Equation 7 from (Niermann, Drünert, et al., 2019) and data for a reactor supported in Pd/Al_2O_3 as presented in 4.2.7 are used to define the STY_{dehy}.

$$\mathrm{STY}_{\mathrm{dehy}} = \frac{\nu \cdot \eta_{\mathrm{dehy}} \cdot M_{\mathrm{H_2}}}{V_{0,\mathrm{dehyd}} \cdot t_R} \left[\frac{g_{H_2}}{L \cdot h}\right] \tag{4.60}$$

In this equation, v represents the maximum number of moles of hydrogen released per mole of carrier, η_{dehy} is the dehydrogenation conversion efficiency, M_{H_2} is the molar mass of hydrogen in g/mol, ($V_{0,dehyd} = M_{H_{12}NEC}/\rho_{H_{12}NEC}$) is the molar volume of the loaded liquid organic hydrogen carrier (LOHC) in L/mol, and t_R is the residence time in h.
Conversely, for the hydrogenation of NEC under Ru/Al_2O_3 catalyst, the space time STY_{hy} found by (Niermann, Drünert, et al., 2019) and introduced in 4.2.7 is used.
When both STYs are found, the desired reactor volume can be determined by dividing the maximum hydrogen output, $\dot{m}_{H_{2,tot}}$ for dehydrogenation and maximum 12H-NEC output $\dot{m}_{L^+}$ for hydrogenation, by the obtained STY.

$$V_{hy} = \frac{\max_{1\leq t\leq 8760} \dot{m}_{L^+}(t)}{\mathrm{STY}_{\mathrm{hy}}} \qquad V_{dehy} = \frac{\max_{1\leq t\leq 8760} \dot{m}_{H_{2,tot}}(t)}{\mathrm{STY}_{\mathrm{dehy}}} \tag{4.61}$$

The required mass of the active metal (m_{metal}) is calculated by multiplying the peak hourly LOHC molar flow (L^-,L^+) entering the hydrogenation/dehydrogenation with the molar catalyst loading ($x_{catalyst}$) and the molar mass of the metal (M_{metal}).

$$m_{\mathrm{metal}} = \frac{\dot{m}^{\max}_{L^-/L^+}}{M_{L^-/L^+}} x_{catalyst}\, M_{metal} \tag{4.62}$$

For hydrogenation reactor, a 5% Ru/Al_2O_3 ruthenium based catalyst is used, with catalyst loading of x_{Ru/Al_2O_3}=0.25mol Ru per mol NEC, and molar mass of M_{Ru}=0.10107(kg/mol) as introduced in 4.2.7. For the dehydrogenation, a 0.5% wt Pd/Al_2O_3 paladium based catalyst with a loading of x_{Pd/Al_2O_3}=0.1% mol of Pd per mol of 12H-NEC and a molar mass of M_{Ru}=0.10642(kg/mol).
After the active metal mass is determined, it is converted to the mass of the supported catalyst by multiplying the metal weight fraction of the catalyst as shown in equation 4.7.2 below.

$$m_{\mathrm{cat}} = \frac{m_{\mathrm{metal}}}{w_{\mathrm{metal}}} \tag{4.63}$$

4.8.2. Hydrogen Burner Sizing

The hydrogen burner for both hydrogenation and dehydrogenation is sized based on the maximum heat duty required. The maximum heat duty can be found in the cold start operation of the dehydrogenation process, as it provides both the duty for preheating the cold stream and the duty for reaction heat during the cold start operation of dehydrogenation.

$$Q_{burner,rated} = \max_{1\leq t\leq 8760} Q_{burner}(t) \tag{4.64}$$

4.8.3. Tank Sizing

To determine the tank size required to store the NEC and 12-NEC calculated in our model, the yearly total mass of unloaded and loaded hydrogen is divided by the density of the medium and a safety factor of s_f=10% is added.

$$V_{tank_{(NEC)}} = \frac{\sum_{1\leq t\leq 8760} \dot{m}_{L^-}(t)}{\rho_{NEC}} s_f \qquad V_{tank_{12H-NEC}} = \frac{\sum_{1\leq t\leq 8760} \dot{m}_{L^+}(t)}{\rho_{12H-NEC}} s_f \tag{4.65}$$

4.9. Economic Analysis

The economic analysis assesses important economic factors, including capital expenditures (CAPEX), annual operating expenditures (OPEX), avoided grid import costs, the project's internal rate of return (IRR), and the discounted levelized cost of energy (LCOE) for all system components. The estimation of these factors is based on the equipment sizes identified in each module following the determination of the optimal PV system.

4.9.1. CAPEX Estimation

To estimate the total capital expenditure for each scenario, the size/capacity identified for each component P_i or C_i is multiplied by the corresponding cost per kW or kWh, denoted as c_i where i ε (pv, batt, el, FC, compressor), as mentioned in the economic assumptions section. The estimation of each $CAPEX_i$ is then found via equation 4.66.

$$CAPEX_i = c_i\, P_i \quad or \quad CAPEX_i = c_i\, C_i \tag{4.66}$$

To estimate the cost of compressed-hydrogen tanks in the alternate scenario, the electrolyser's annual hydrogen production is multiplied by the introduced in 4.2.8.(N. Li et al., 2023):

$$CAPEX_{tank} = \sum_{t=1}^{8760} \dot{m}_{H_2,EL}(t)\, c_{comp,tank} \qquad OPEX_{tank} = CAPEX_{tank} \times \alpha_i \tag{4.67}$$

LOHC Process CAPEX The LOHC costs are estimated based ons are given as follows:

$$c_{\text{hyd}} = 2840.81\,(P_{\text{hyd}}^{\max})^{-0.375}\,\frac{\text{STY}_{\text{DBT,hyd}}}{\text{STY}_{\text{NEC,hyd}}}, \quad c_{\text{dehyd}} = 3122.83\,(P_{\text{dehyd}}^{\max})^{-0.375}\,\frac{\text{STY}_{\text{DBT,dehyd}}}{\text{STY}_{\text{NEC,dehyd}}} \quad [€/kW] \tag{4.68}$$

where $P_{\text{hyd}}/P_{\text{dehyd}}$ represents the maximum power rating of the reactor in kW. The cost of each reactor in euros is then calculated as follows:

$$C_{\text{hyd}} = c_{\text{hyd}}\, P_{\text{hyd}}^{\max}, \qquad C_{\text{dehyd}} = c_{\text{dehyd}}\, P_{\text{dehyd}}^{\max}. \tag{4.69}$$

Since these equations were derived in 2017, the costs were adjusted based on the Chemical Engineering Plant Cost Index (CEPCI) using the most recent available value from 2022:

$$C^{2022} = C^{2017} \times \frac{\text{CEPCI}_{2022}}{\text{CEPCI}_{2017}}. \tag{4.70}$$

The resulting value was then multiplied by an installed-cost multiplier ($\times 4.6$) and a total capital investment (TCI) factor for indirect costs and contingencies ($\times 1.25$):

$$\text{TCI}_{\text{hyd}} = 1.25 \times 4.6 \times C_{\text{hyd}}^{2022}, \qquad \text{TCI}_{\text{dehyd}} = 1.25 \times 4.6 \times C_{\text{dehyd}}^{2022}. \tag{4.71}$$

The capital expenditure for the total NEC required for seasonal storage is calculated by multiplying the total NEC needed to be hydrogenated in a year by the cost per kilogram of NEC $c_{\text{NEC}} = 40[€/kg]$.

$$\text{CAPEX}_{\text{NEC}} = c_{\text{NEC}} \sum_{t=1}^{8760} \dot{m}_{L^-}(t). \tag{4.72}$$

The cost of the catalyst is estimated by multiplying the mass of the catalyst by the cost per kg $c_{\text{cat}}$of the catalyst in [€/kg].

$$\text{CAPEX}_{\text{cat}} = c_{\text{cat}}\,(m_{\text{cat,hyd}} + m_{\text{cat,dehyd}}).$$

The tank size is multiplied by its purchase price $\text{tank}[€/\text{m}^3]$, resulting in the total cost.

$$\text{CAPEX}_{\text{tank}} = c_{\text{tank}}\,(V_{\text{summer}} + V_{\text{winter}}). \tag{4.73}$$

For the hydrogen burner, the total CAPEX is estimated by multiplying the rated burner capacity with the cost in €/kW as found in literature, thus

$$\text{CAPEX}_{\text{burner}} = c_{\text{burner}}\ Q_{burner,rated}. \tag{4.74}$$

To estimate the CAPEX of heat exchangers, the average cost of the heat exchangers of the costs calculated in Aspen is multiplied by the number of heat exchangers.

$$\text{CAPEX}_{\text{HXs}} = c_{\text{HX,avg}}\, N_{HXs}. \tag{4.75}$$

After the CAPEX of each LOHC process component is defined, the total capital expenditure can be estimated as:

$$\mathrm{CAPEX_{LOHC}} = \mathrm{TCI_{hyd}} + \mathrm{TCI_{dehyd}} + \mathrm{CAPEX_{NEC}} + \mathrm{CAPEX_{cat}} + \mathrm{CAPEX_{tank}} + \mathrm{CAPEX_{burner}} + \mathrm{CAPEX_{HXs}}. \tag{4.76}$$

When all the aforementioned steps are completed, the total system CAPEX for each scenario can be estimate as:

$$\begin{aligned} CAPEX_{tot,main} &= CAPEX_{PV} + CAPEX_{BAT} + CAPEX_{EL} + CAPEX_{LOHC} + CAPEX_{FC} \\ CAPEX_{tot,alt} &= CAPEX_{PV} + CAPEX_{BAT} + CAPEX_{EL} + CAPEX_{COMP} + CAPEX_{FC} + CAPEX_{tank} \end{aligned} \tag{4.77}$$

4.9.2. OPEX Estimation

The annual operational expenditure (OPEX) is estimated to include fractional operations and maintenance costs for PV, batteries, electrolysers, and fuel cells, represented as a fixed percentage a_i of their CAPEX.

$$OPEX_i = CAPEX_i\, a_i \tag{4.78}$$

The OPEX of each LOHC process component is determined using the fixed percentage α, which represents the O&M fraction per year and is multiplied by the component's CAPEX as seen below:

$$OPEX_{LOHC_{comp}} = \alpha\,(\mathrm{TCI_{hy}} + \mathrm{TCI_{dehy}} + \mathrm{CAPEX_{tank}} + \mathrm{CAPEX_{HXs}} + \mathrm{CAPEX_{burner}}) \tag{4.79}$$

To calculate the total annual OPEX for the LOHC process, we aggregate the OPEX of the individual LOHC components with the annual costs associated with NEC makeup and catalyst replacement as presented below,

$$\mathrm{OPEX_{LOHC}} = \underbrace{OPEX_{components}}_{\text{annual O\&M}} + \underbrace{\beta_{\mathrm{NEC}}\Big(\sum_{t=1}^{8760} \dot{m}_{L^-}^{\mathrm{hy}}(t)\Big) c_{\mathrm{NEC}}}_{\text{annual NEC makeup}} + \underbrace{\Big(\frac{\sum_{t=1}^{8760} \dot{m}_{L^-}^{\mathrm{hy}}(t)}{A_{\mathrm{cat}}} + \frac{\sum_t \dot{m}_{L^+}^{\mathrm{dehy}}(t)}{A_{\mathrm{cat}}}\Big) c_{\mathrm{cat}}}_{\text{catalyst activity–based replacement}} \tag{4.80}$$

where the annual NEC make-up is calculated by multiplying the annual NEC loss fraction (β_{NEC}) with the total LOHC mass of LOHC in our system and the cost per kg of NEC, while the catalyst replacement is calculated by dividing the total amount of LOHC entering each reactor in a year by the catalyst activity (A_{cat}) and multypling the result with cost of catalyst. Finally, the overall system OPEX for each scenario is calculated as:

$$\begin{aligned} OPEX_{tot,main} &= OPEX_{PV} + OPEX_{BAT} + OPEX_{EL} + OPEX_{LOHC} + OPEX_{FC} \\ OPEX_{tot,alt} &= OPEX_{PV} + OPEX_{BAT} + OPEX_{EL} + OPEX_{H_2\text{-storage}} + OPEX_{FC} \end{aligned} \tag{4.81}$$

4.9.3. Economic Indicators

If such a system is installed, the amount of energy imported from the grid will be significantly reduced, resulting in a clear benefit for TGV's utilities. To quantify the benefit of avoiding imported energy, the average electricity price (p_{el} in €/kWh for 2023 is multiplied by the difference between the annual energy demand of the buildings (E_{demand} and the annual imported energy E_{import} from the grid. The equation for the avoided cost is given by:

$$B_{\mathrm{avoid}} = (E_{\mathrm{demand}} - E_{\mathrm{import}})\, p_{\mathrm{el}} \tag{4.82}$$

To capture the financial advantage of reducing electricity purchases in the cash flow, the benefit is classified as a constant annual inflow and is introduced in its calculation.
To estimate the cash flow $CF_{y=0}^{T}$ over the system's lifetime,it is essential to identify the capital expenditures for all subsystems for the initial year, $y = 0$, which is expressed as a negative cash flow as presented below:

$$\mathrm{CF}_0 \;=\; -\,\mathrm{CAPEX_{total}}. \tag{4.83}$$

Then, for each operating year $y = 1, \ldots, T$, the net operating cash flow is considered constant and is equal to the avoided cost B_{avoid} minus the annual OPEX:

$$\mathrm{CF}_y \;=\; B_{avoid} \;-\; OPEX_{total}, \qquad y = 1, \ldots, T, \tag{4.84}$$

To incorporate the replacement cost for the components with a lower lifespan, the replacement cost (CAPEX of the component) is subtracted from the cash flow in the year of replacement. Finally, the cash flows over the lifetime can be estimated as follows:

$$\mathtt{CF} = \left[-\mathrm{CAPEX}_{\mathrm{total}}, \underbrace{(B_{avoid} - \mathrm{OPEX}), \ldots, (B_{avoid} - \mathrm{OPEX})}_{T \text{ entries}} \right]^{\mathrm{T}}, \tag{4.85}$$

Upon completion of the calculations for the previously mentioned economic metrics, the assessment of the economic viability for each scenario will be conducted by calculating the economic KPIs of NPV, IRR, and LCOE introduced in §3.5.2 and comparing their results.

5
Results

The objective of this chapter is to present the results for each scenario, which will be subsequently compared and analysed. Additionally, it aims to provide insights into the economic assumptions that significantly influence the overall costs.

5.1. Main Scenario (LOHC storage)

The PV system size after the optimal solution is found consists of 552 PV modules with a total system capacity of 165.60 kWp.
Using the optimally sized system components, the yearly grid export was found to be 8.88% of annual PV production, while the import was 0.78% of the total building load. The mismatch of produced and consumed NEC is found at 0.41%.
This PV system was sized to meet the annual energy demand for the eight buildings covered in this study, which was found to be 60.86 MWh.The highest consumption, as expected for the demand profile, is being noticed in the winter months.

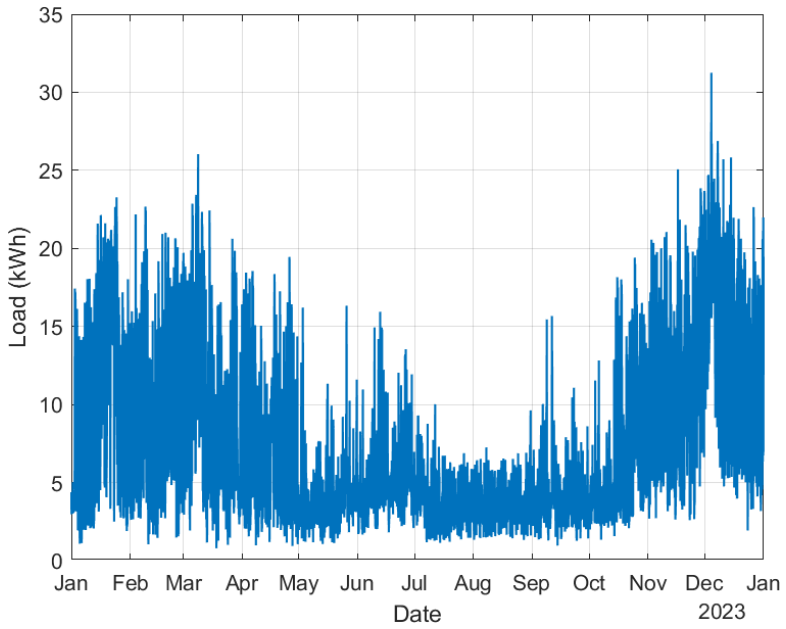

Figure 5.1: Hourly site load profile. Winter peaks align with increased PEMFC dispatch; summer minima enable LOHC charging.

Battery & EMS
For the selected system of 165.60 kWp and for the given panel conditions, the annual generation reaches 145.75 MWh. This generation peaks in the summer months, as expected, due to longer days, higher sun angle and less cloud coverage.

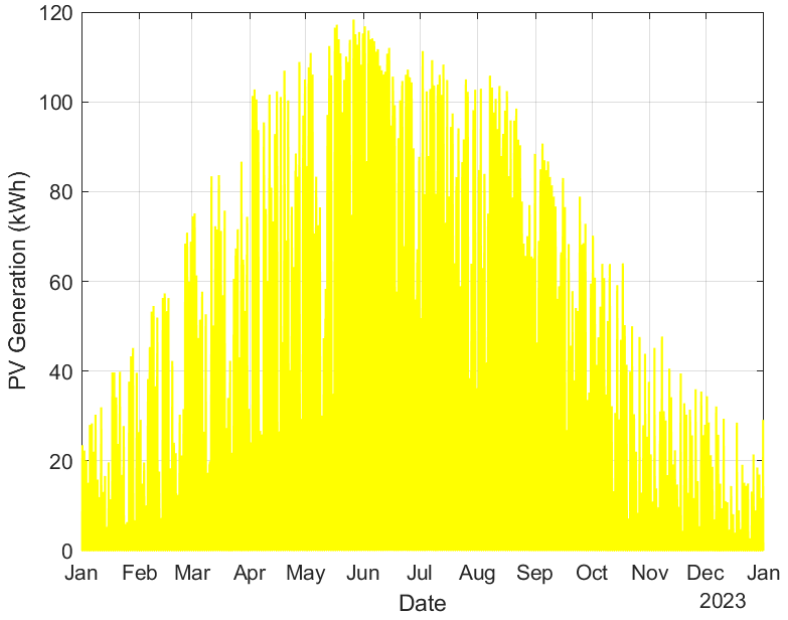

Figure 5.2: Hourly PV generation profile.

The battery was sized at 261 kWh to meet a daily demand based on the equations in §4.3, allowing for one day of self-sufficiency. After sizing the battery, the results of the energy dispatch from the battery and the EMS module align with seasonal trends, as demonstrated in figures 5.3,5.4, 5.5. The battery, is discharged at a higher level during winter, where PV production is scarce, while the SOC stays above 50% through most of the summer months.

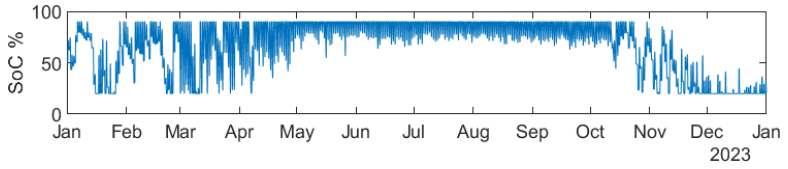

Figure 5.3: Battery Dispatch

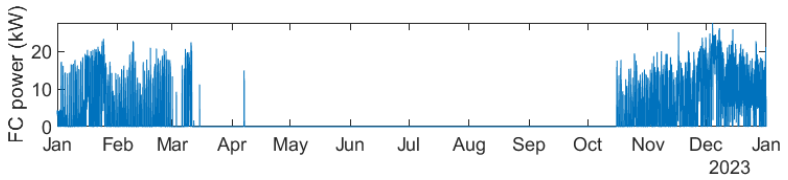

Figure 5.4: Hourly Fuel Cell Dispatch

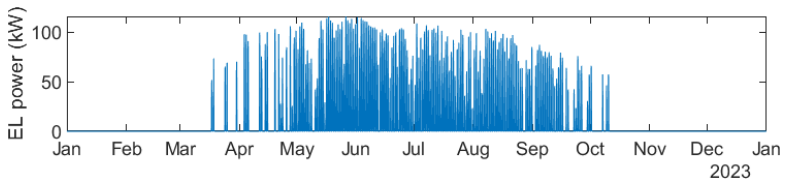

Figure 5.5: Hourly Electrolyser Dispatch

Grid imports are higher during the winter months, while exports to the grid typically occur in the summer months, when the operational conditions are not met or the power generation from the PV is too low. The hourly grid exchange can be seen in detail in figures 5.6 and 5.7 below.

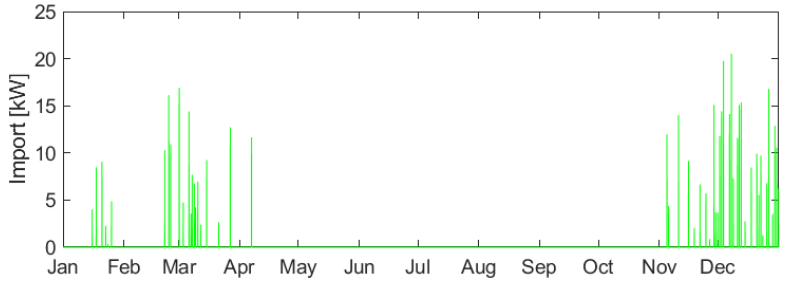

Figure 5.6: Hourly Grid Import

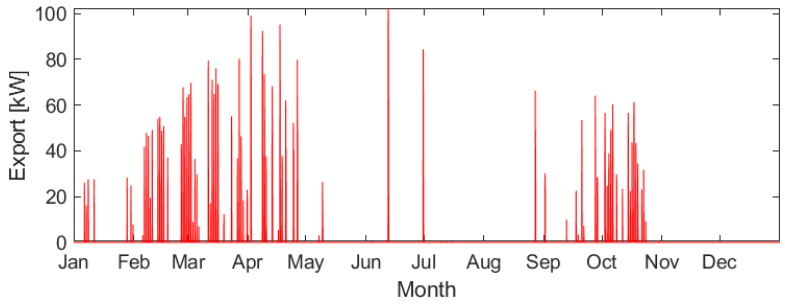

Figure 5.7: Hourly Grid Export

As can be seen from the figures above and the annual grid exchange percentages, our system achieve high levels of autonomy as the annual electricity demand is fulfilled almost entirely by on-site resources. The annual grid imports were around 471 kWh, while the exports 12,944 kWh.

Electolyser

Using the Electrolyser profile presented in 5.5, the system was sized based on the equations of section §4.4. It was concluded that 48 units were needed, totalling a capacity of 116 kW. The monthly hydrogen production from the electrolyser was calculated based on the provided power from the electrolyser profile mentioned above. This was determined using the electrolyser module described in the previous chapter, and illustrated in Figure 5.8. Over its operational period, the total hydrogen produced is approximately 1,813 kg.

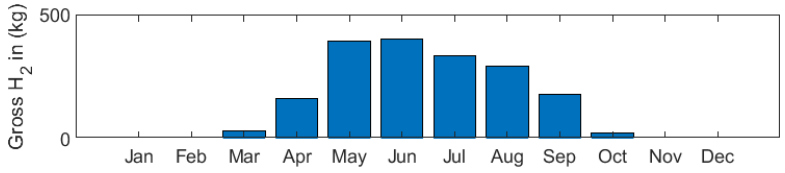

Figure 5.8: Monthly Hydrogen Production from Electrolyser

Fuel Cell

Based on the Electrolyser profile shown in 5.4, the system was sized according to the equations outlined in section §4.5. This sizing determined that five units were required, with a total capacity of 34 kW. Similarly, the hydrogen consumption of the fuel cell was computed using the fuel cell module described in the previous chapter, and the hourly consumption is as shown in Figure 5.9. The hydrogen consumption for the fuel cell is found to be 898 kg annually.

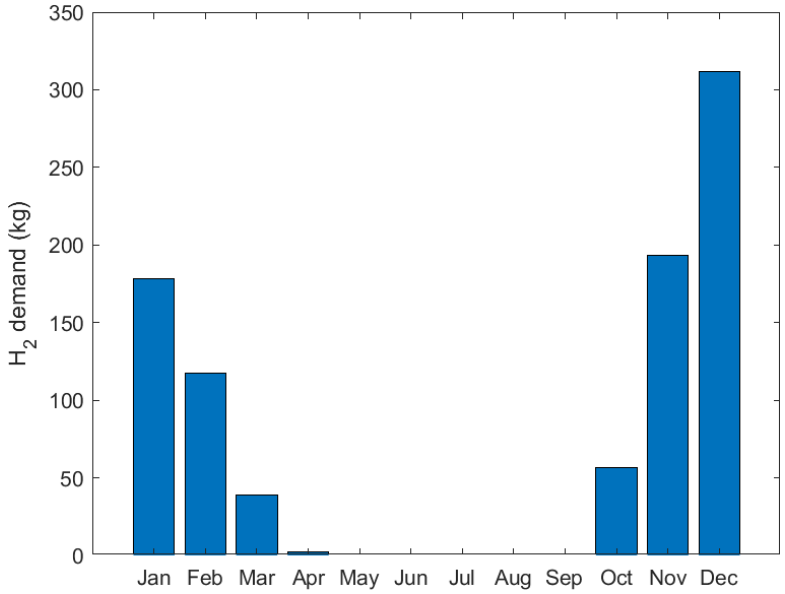

Figure 5.9: Monthly Hydrogen Consumption from Fuel Cell

In addition to hydrogen consumption, the waste heat from the fuel cell was also estimated. As can be seen in 5.10, the waste heat tracks the projectory of PEMFC dispatch in winter. It is used for stabilising reactor inlet conditions and reducing the hydrogen burner demand by preheating the inflow to the reactor.

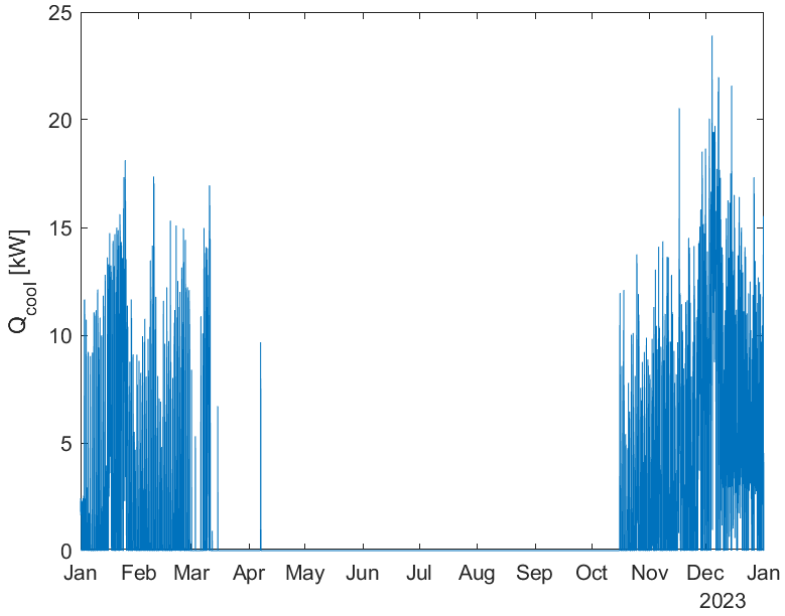

Figure 5.10: Hourly PEMFC cooling duty available for recovery

Hydrogenation

To store the hydrogen produced from the electrolyser, the total NEC that needed to be hydrogenated was 29,190 kg. From the electrolyser's hydrogen, 17 kg was used for preheating the inflow to the reactor, while the rest 1,796 kg was stored to be used during winter. The total hydrogenated 12H-NEC that is produced is calculated to 30,986 kg. The monthly hydrogenation mass flows can be found in Figure A.3 in the appendices.

By analysing hydrogen's mass flow, the peak inflow of H_2 to the hydrogenation process was determined. Based on this value, the reactor's power was estimated to be 72.29kW$_{LHV}$, which guided the

reactor cost estimation.
The energy balances & mass balances help us determine the necessary mass flows, heat duties and temperatures of heat exchangers, which were then introduced into ASPEN for sizing and costing. These mass flow rates and temperatures are based on the annual peak heat duty requirements for each heat exchanger used in hydrogenation and are:

Table 5.1: Hydrogenation side heat exchanger sizing data for $\Delta T_{min} = 10K$: inlet/outlet temperatures and mass flows.

Unit	$\dot{Q}$ [kW]	$\dot{m}_{\text{hot}}$ [kg h^{-1}]	$\dot{m}_{\text{cold}}$ [kg h^{-1}]	$T_{\text{h,in}}$ [K]	$T_{\text{h,out}}$ [K]	$T_{\text{c,in}}$ [K]	$T_{\text{c,out}}$ [K]
HX1	1.23	37.5	35.4	453.1	359.0	286.2	349.0
HX2	1.25	29.7	35.4	423.1	359.0	349.0	413.1
HX3	0.75	13.4	2.2	423.1	338.1	328.1	413.1
HX4	1.5	5.8	20.3	743.0	301.8	291.8	453.1
HX5	0.48	1.85	1.25	779.32	338.1	328.1	423.1

The heat–exchanger properties presented in Table 5.1 were transferred to the Aspen EDR to estimate the size and cost of the heat exchangers as described in §3.6. For each simulated heat exchanger, Aspen EDR returned the effective heat–transfer area and the estimated cost. Heat exchangers one and four could not be modelled in EDR as the NEC changes phase from solid to liquid, which Aspen EDR cannot simulate. Table 5.2 reports the EDR results for the hydrogenation side, while the detailed results can be found in Appendix D.

Table 5.2: Aspen EDR results — Hydrogenation side.

HX no.	**Area/Plate [m^2]**	**No. Plates**	**Total Area**	**Cost [€]**
HX1	—	—	—	—
HX2	0.075	19	1.43	810
HX3	0.097	9	0.87	676
HX4	—	—	—	—
HX5	0.057	3	0.17	548

The total heat recovered from the waste heat streams in HX1,HX2 & HX3 accounted for $\eta_{WHR_{hy}}$=88% of the total required process heat. The STY for hydrogenation used is STY_{Hy}= 388.20$g_{H12\text{-}NEC}$/ (L· h), which resulted in a reactor size of 97 L and a catalyst requirement of 0.92 kg of Ru/Al_2O_3 based on the experimental calculations of (Brückner et al., 2014).
The tanks are sized to facilitate the annual hydrogenation mass requirements. Based on the yearly demand of NEC, the tank volume is estimated to be 29 m^3, while for seasonal storing the loaded 12H–NEC, 36 m^3.

Dehydrogenation
The dehydrogenation mass flow results are obtained guided by the fuel cell's hydrogen demand. Using the mass balance equations, the total 12H-NEC that was required to produce the hydrogen for the fuel cell for the entire year, as well as the hydrogen burner to heat the process, is 30,859 $kg_{12H\text{-}NEC}$. Dehydrogenating this amount of 12H–NEC results in a production of 1,610 kg_{H_2} of which 898 kg_{H_2} are utilised for power production via the fuel cell and 712 kg_{H_2} are utilised to cover the process heat demands.
Similar to hydrogenation, the heat exchangers are sized by utilising the results of the energy and mass balances. The sizing of the dehydrogenation heat exchangers is done using the following parameters:

Table 5.3: Dehydrogenation side heat exchanger sizing data for $\Delta T_{min} = 10K$: inlet/outlet temperatures and mass flows.

Unit	$\dot{Q}$ [kW]	$\dot{m}_{hot}$ [kg h^{-1}]	$\dot{m}_{cold}$ [kg h^{-1}]	$T_{h,in}$ [K]	$T_{h,out}$ [K]	$T_{c,in}$ [K]	$T_{c,out}$ [K]
HX1	1.23	19.5	43.5	335.15	284.99	274.99	325.15
HX2	1.88	41.2	43.5	503.15	411.94	325.15	401.94
HX3	5.77	92.9	45.6	978.58	863.19	279.81	503.15

These data are then introduced in Aspen EDR, where the heat exchangers are sized and the EDR outputs for the dehydrogenation side are summarised in Table 5.4 while the detailed results can be found in Appendix D.

Table 5.4: Aspen EDR results — Dehydrogenation side.

HX no.	Area/Plate [m^2]	No. Plates	Total Area	Cost [€]
HX1	0.097	9	0.87	676
HX2	0.057	5	0.29	583
HX3	0.152	5	0.76	629

The total heat recovered from the waste heat streams in HX1 & HX2 accounted for $\eta_{WHR_{dehy}}$=11.4% of the total required process heat. The Hydrogen Burner for the system is sized based on the peak demand over the year, which is found in winter when the total thermal load that needs to be covered for both reaction heat and preheat duties is 27.4 kW, as seen in Figure A.7 in Appendices.
In December, the peak hydrogen mass flow from dehydrogenation reaches 2.38 kg_{H_2}/h. This peak outflow is used to estimate the cost of the reactor by estimating its power, which is found to be 79.3kW_{LHV}. An STY of STY_{De}=49.44$g_{H12\text{-}NEC}$/ (L· h) is estimated using the data from (Brückner et al., 2014) paper for Pd/Al_2O_3 catalyst. For this STY, the required reactor volume is estimated to be around 48 L with a catalyst mass of 4.69 kg.

Economic Analysis
After the sizing of the components, the economic analysis is conducted following the equations mentioned in §4.9. The total capital costs amount to €2,364,740, as shown in Table 5.5. A substantial portion of this total €1,654,260 refers specifically to the LOHC process cost. This significant expense includes the cost of acquisition of all the required components, such as reactors, tanks, catalysts, hydrogen burner, heat exchangers and the initial fill of NEC, as can be detailed in table 5.5 in appendices. Similar to CAPEX, operational expenditures are also dominated by the LOHC process by 46.7% of the total OPEX cost of 12,821€/year.

Table 5.5: Capital and operating expenditures

CAPEX component	Cost [€]
PV	39,744
Battery	130,560
Electrolyser	436,680
Fuel cell	103,496
LOHC process	1,654,260
Total CAPEX	€2,364,740
OPEX component	**€/yr**
PV	199
Battery	1,305
Electrolyser	4,367
Fuel cell	1,035.0
LOHC process	6,044
Total OPEX	12,950

Under the calculated costs, key economic indicators for the system have been estimated. The annual benefit from avoided energy purchases due to the system's self-sufficiency is projected to be 16,371 €/year, while the cost of energy imports is estimated at 127 €/year. Although energy purchase has been eliminated, the project's IRR is estimated at -29.48% and the NPV over the project's lifetime is -2,673,510€. Based on the assumptions mentioned earlier, the system's LCOE has been calculated at 1.686 €/kWh, which is significantly higher than the current cost of electricity.

Finally, using the definitions in Section 3.5.2, the primary scenario converts PV energy into useful on-site electricity with an overall system efficiency of 41.4%. The electrical round-trip across the hydrogen pathway is estimated at 23.4%, reflecting the conversion losses of the hydrogen pathway under the EMS profiles. The efficiency of the LOHC chain is estimated at 49.5%, meaning that roughly half of the hydrogen produced by the electrolyser is ultimately available to the fuel cell after the hydrogenation-dehydrogenation processes and their demands.

Model Validation
As mentioned in §3.7, to validate the model, the operational logic validity, thermodynamic consistency, and performance realism need to be assessed.
The results for the operational logic of the fuel cell, the hourly operation status are presented in Figure 5.11,

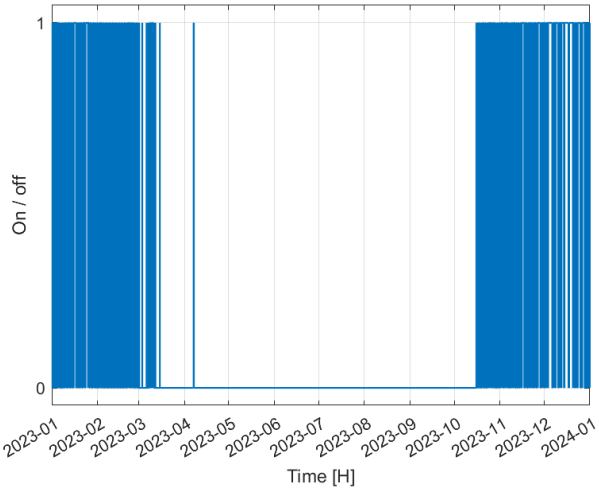

Figure 5.11: Fuel Cell Operational Status

while the figures below present the results required to validate if the electrolyser operation performed as intended under the EMS rule.

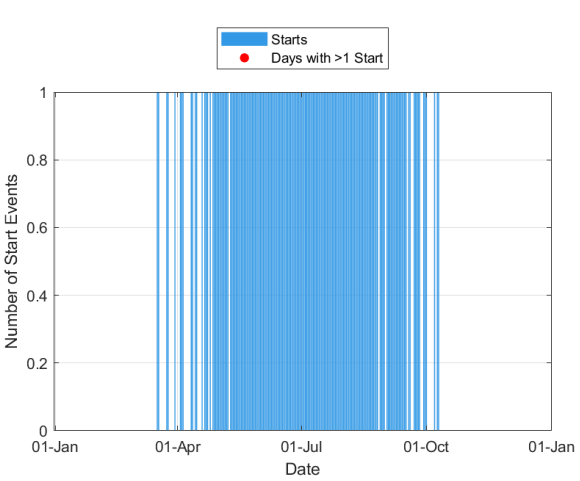

(a) Daily electrolyser start count

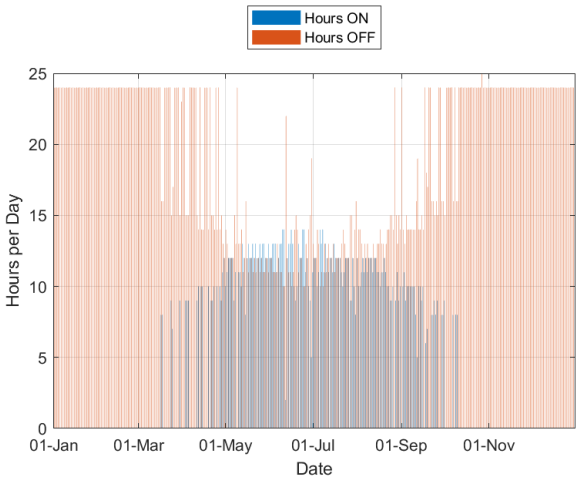

(b) Daily electrolyser ON vs OFF hours

Figure 5.12: Electrolyser operation validation.

For the thermodynamic dynamic consistency, the pinch diagrams were plotted. The pinch diagrams for the hydrogenation process can be found in Figures 5.13 and 5.14 for the LOHC stream, and in Figure 5.15 for the hydrogen stream.

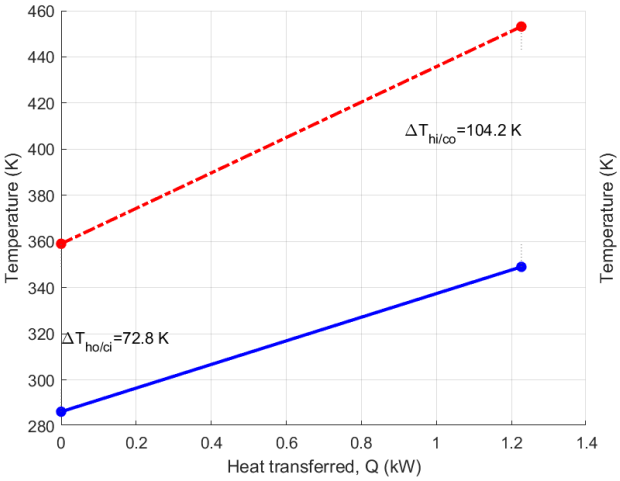

(a) Hydrogenation HX1 Pinch Diagram(12H-NEC → NEC)

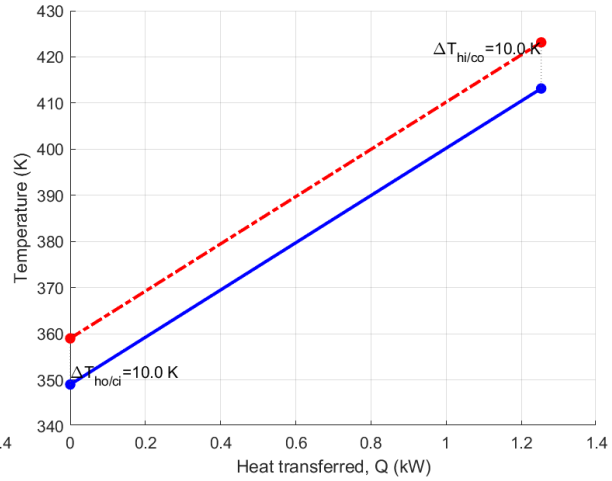

(b) Hydrogenation HX2 Pinch Diagram(Coolant → NEC)

Figure 5.13: Hydrogenation LOHC$^-$ pinch analysis focused on waste heat recovery heat exchangers

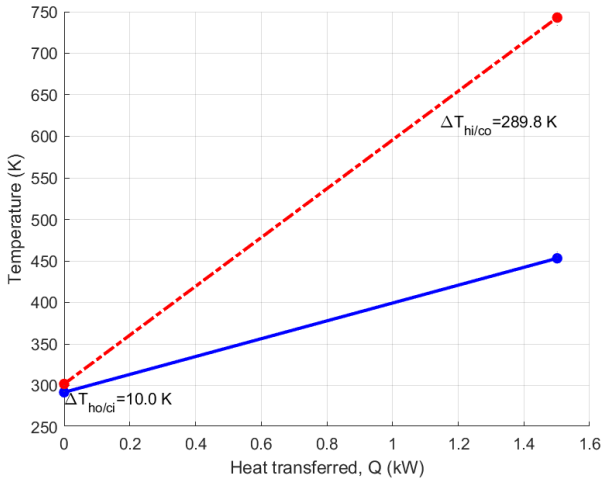

Figure 5.14: Hydrogenation HX4 Pinch Diagram (Burner Flue gas → NEC)

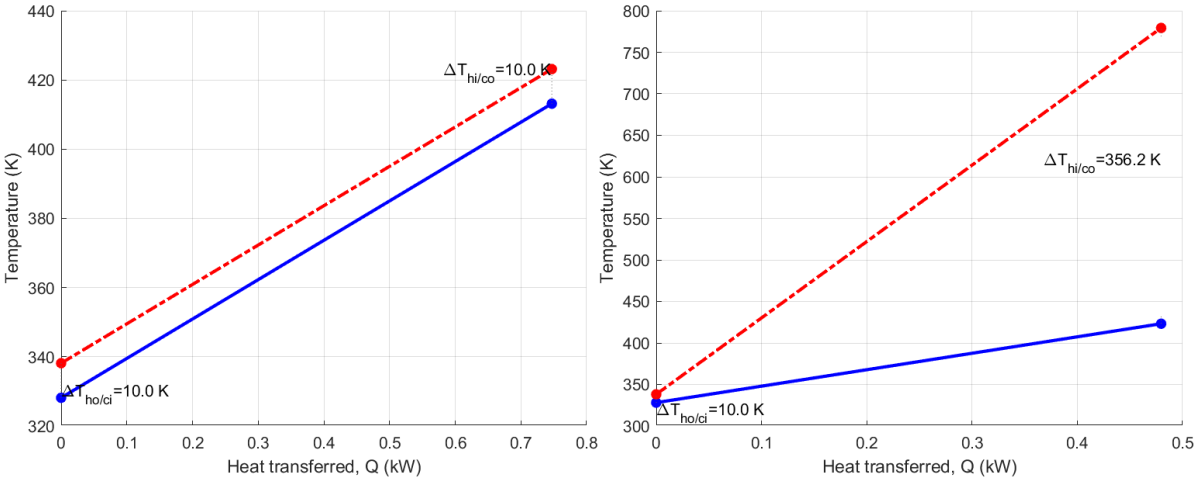

(a) Hydrogenation HX3 Pinch Diagram(Coolant → H_2)

(b) Hydrogenation HX5 Pinch Diagram(Burner Flue gas → H_2)

Figure 5.15: Hydrogenation pinch analysis of H_2 stream

For dehydrogenation, the pinch diagrams for the heat exchangers that exchange heat with the waste heat sources can be found in Figure 5.16, while the pinch diagram for the burner-heated exchanger can be found in Figure 5.17.

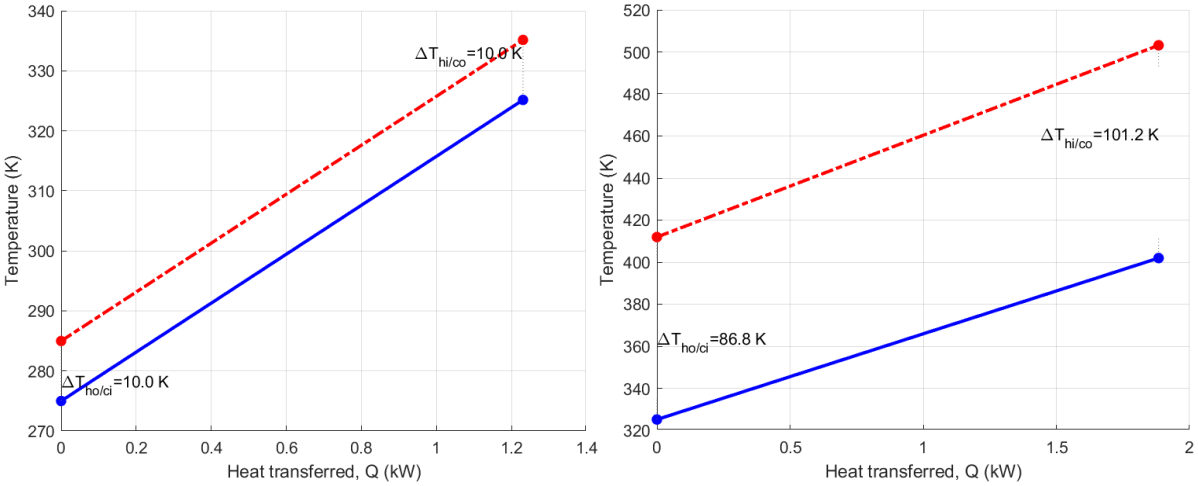

(a) Dehydrogenation HX1 Pinch Diagram(PEMFC → 12H-NEC) (b) Dehydrogenation HX2 Pinch Diagram(NEC → 12H-NEC)

Figure 5.16: Dehydrogenation pinch analysis focused on waste heat recovery heat exchangers

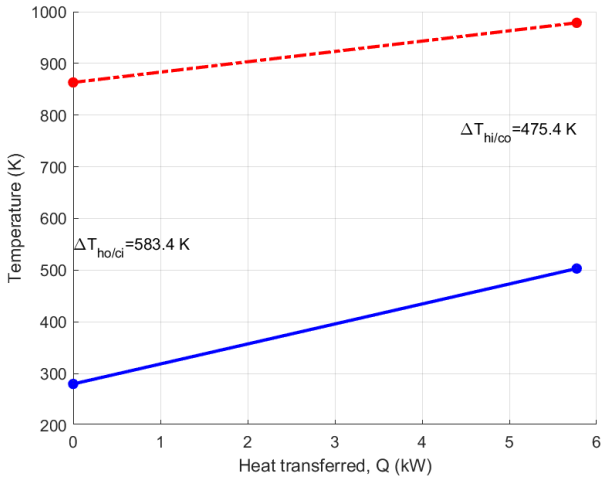

Figure 5.17: Dehydrogenation HX3 Pinch Diagram(Burner Flue gas → 12H-NEC)

For the last step of model validation, the hourly efficiencies of fuel cell and electrolyser are plotted in Figure 5.18a and 5.18b in order to be compared with literature.

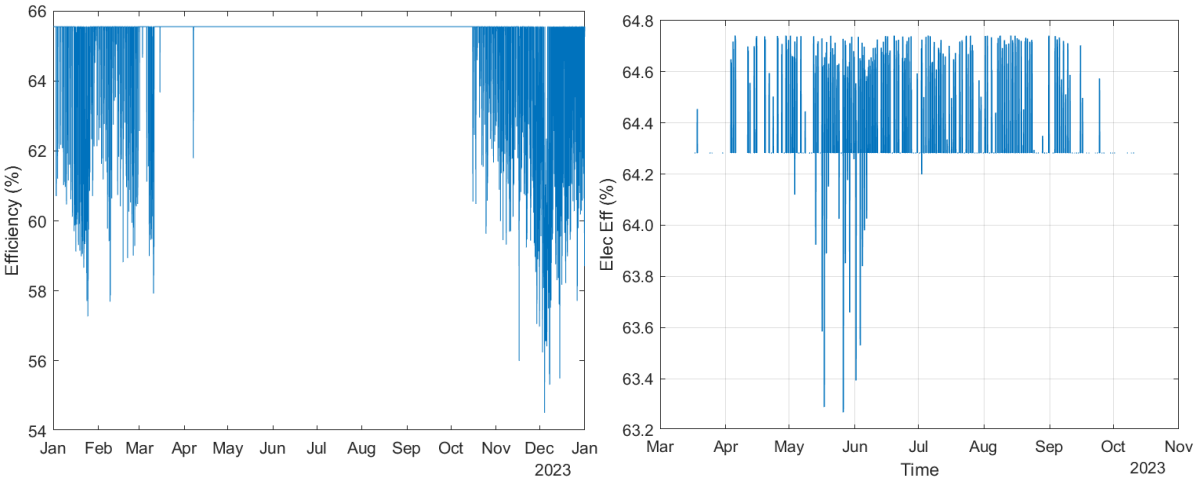

(a) Fuel Cell Hourly Electrical Efficiency) (b) Electrolyser Hourly Electrical Efficiency)

5.1.1. Space use

To estimate the space requirement that the Green Village premises should have available, the methodology described in §3.10 was used. The area required for main components is expressed m^2, while the total space requirement, expressed in m^3, includes the volume of tanks and reactors found above. This space requirement totals at 65.15 m^3 for separate loaded/unloaded LOHC tanks or 36.15m^3 if a multi-product tank is used.

Table 5.6: Space use by component (area-based) and total installed footprint.
Intensities for PV are in m^2/kW, and for Battery,Electrolyser/Fuel Cell in m^2/module

Component	Area Intensity	Capacity/No. Modules	Total Area m^2
PV system	6	165.6	993.6
Battery	0.37	17	6.3
Electrolyser	0.3	48	14.4
Fuel Cell	0.07	5	0.35
Heat Exchangers		6	4.4
		Total:	**1,019.05**

5.2. Alternate Scenario (Compressed H_2 Storage)

In the compressed H_2 scenario, the optimal PV system identified after resizing consists of 378 PV modules with a total capacity of 113.40 kWp. Here, the objective remains to minimise annual grid interaction with on-site generation and storage that satisfies the building's energy demands for the year. Using the model's sized components, the annual energy export to the grid (10,359 kWh) is found to be 10.38% of the yearly PV production, while the imported energy (622 kWh) accounts for 1.02% of the Green Village's annual load, achieving a self-sufficiency of 98.98%. The produced hydrogen from the electrolyser, with the consumed from the fuel cell, is found to have a mismatch of 2.09%.

Table 5.7: Key performance indicators for the compressed H_2 scenario.

Metric	Value
PV modules / capacity	379 / 113.7 kWp
Battery energy	261 kWh
Electrolyser power	80 kW
Fuel cell power	34 kW
Annual grid export	10,422 kWh (10.38% of PV)
Annual grid import	607 kWh ($1.\%$ of load)
H_2 produced/consumed	1,050.5 kg / 1,025 kg
Storage balance error	2.44%

The battery is sized at 261 kWh, and the energy dispatch follows the same seasonal logic.
The electrolyser is sized at 80 kW based on the profile generated from the Battery-EMS module, producing approximately 1,050 kg of H_2 per year, with the highest production during summer months.
Similarly, using the fuel cell profile, the Fuel cell capacity is estimated at 34 kW with an annual hydrogen consumption of 1,025 kg, with the operation of the fuel cell peaking during winter, following the building's demand profile. In this scenario, hydrogen is stored in a compressed form. The compressor of the system has been sized, and the calculated compression power is P_{comp} = 12.4kW.
The economic indicators are calculated using the same methodology as in §4.9. For the compressed scenario, the total CAPEX calculated is €565,306, while the annual OPEX is estimated at 6,004 €/year with the detailed cost breakdown being presented in Tables 5.8 and 5.9.

Table 5.8: CAPEX breakdown for the compressed-H_2 scenario.

CAPEX component	Cost [€]
PV	27,288
Battery	130,560
Electrolyser	300,218
Fuel cell	103,496
Compressor	3,744
Total CAPEX	565,306

Table 5.9: OPEX breakdown for the compressed-H_2 scenario.

OPEX component	€/yr
PV	136
Battery	1,306
Electrolyser	3,002
Fuel cell	1,035
Compressor	525
Total OPEX	6,004

Using the same cost of electricity as in the main scenario, the annual benefit from avoided energy purchases is 16,207 €/year, while the energy cost for the remaining grid imports is 163 €/year. Under all these calculations, the project's real IRR is -18.21% and the net present value over the project lifetime is -732,967€. The levelised cost of electricity for the alternative scenario is halved compared to the main scenario, estimated at 0.79 €/kWh.
The space utilisation results for the main components of the alternative scenario are presented in Table 5.10 below. The number of 50L compressed tanks required is estimated using the equation in section 3.10 and resulted in 1,039 tanks totalling around 52 m^3.

Table 5.10: Space use by component (area-based) and total installed footprint.
Intensities for PV are in m^2/kW, and for Battery,Electrolyser/Fuel Cell in m^2/module

Component	Area Intensity	Capacity/No. Modules	Total Area m^2
PV system	6	113.7	682.2
Battery	0.37	17	6.3
Electrolyser	0.3	33	9.9
Fuel Cell	0.07	5	0.35
		Total:	**698.75**

5.3. Sensitivity Analysis Results

A two-point sensitivity analysis was conducted in order to identify how different economic inputs affect the LCOE and NPV relative to the calculated values of the main scenario. A variance of (±20%) was implemented, with the selected inputs shown in figures 5.19a and 5.19b below:

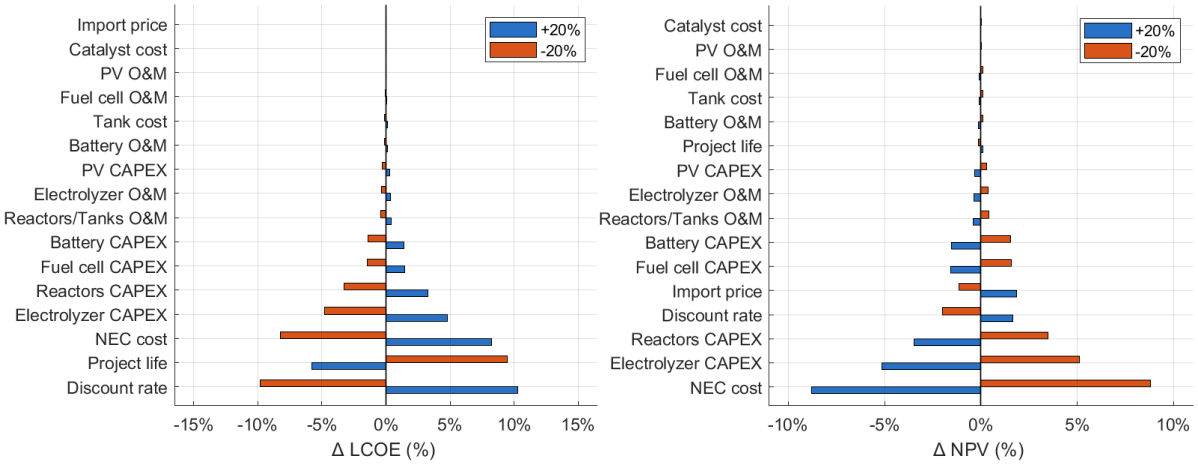

(a) LCOE Sensitivity Analysis

(b) NPV Sensitivity Analysis

Figure 5.19: Sensitivity Analysis Results

As can be seen in the figure above, the LCOE of the model is affected the most by the discount rate, which, when its value increases by 20%, the LCOE price changes by 10.3 % and when decreased, the LCOE is decreased by -9.84 %. Similarly, varying the NEC price from 40€/kg to 32 and 48 €/kg resulted in a change of ±8.22% of the LCOE value. The Electrolyser and reactor costs also have a significant influence, where with a variance of ±20% of the assumed values, the LCOE deviations varied in a percentage from ±5–8%. In contrast, the project lifetime changes increased 9.47% the LCOE value when lifetime decreased by 20%, and 5.77 % when lifetime increased by 20%.
For the NPV sensitivity analysis, the factor that influenced the NPV value the most is the NEC cost. Here, a ±20% variation of NEC's price created a swing of nearly ±9% in NPV's value, while the electrolyser and reactors variation resulted in ±3-6% variance of NPV. In contrast, factors like the PV CAPEX, tank cost, and catalyst price inflicted minor changes in NPV.

6
Discussion

In this chapter, the results presented in the previous chapter will be interpreted, and the limitations of this work will be analysed.

6.1. Interpretation of results

The results presented in the previous chapter demonstrate that a PV-battery–hydrogen system utilising an LOHC loop can achieve very high electrical autonomy for the eight-building load at Green Village while meeting the seasonal balancing objective. However, it is evident that achieving this efficiency through the proposed configuration entails both conversion and cost-related losses, ultimately affecting the project's feasibility. The optimised main scenario comprises a 165.60 kWp PV system (552 modules) with a 261 kWh battery, an electrolyser sized at 116 kW (48 units), a 34 kW PEM fuel cell (five units), and hydrogenation/dehydrogenation reactors sized according to peak mass flows. The power flows presented in the plots, shows that dispatch follows the expected seasonality where PV generation peaks during summer months (145.75 MWh/y), the battery state of charge remains high through summer and is depleting faster during winter, electrolyser production increases in high-irradiance months following the PV production, and PEMFC dispatch increases during months where the winter load peaks (Figures 5.2–5.4). On an annual basis, the model system enables near-autonomous operation for TGV, as imports from the grid are minimal, with only 0.78% of the building load (≈ 471 kWh) being imported, while grid exports are also reduced, with only 8.88% (≈ 12,944 kWh) of the overall PV generation being exported to the grid. The mass-balance closures are tight (NEC production–consumption mismatch 0.41 %), indicating the EMS and component sizing logic are internally consistent.

Despite the high autonomy achieved, the main technical finding of this study is that seasonal balancing is mainly constrained by the heat integration on the LOHC side. Hydrogenation is comparatively benign thermally compared to dehydrogenation. With the waste-heat recovery strategies implemented, an 88% recovery of the hydrogenation duty can be achieved across HX1–HX3 at the selected ΔT of 10 K, and the remaining needs are tractable with burner support during short peaks. On the contrary, for dehydrogenation, even with the implemented heat recovery strategies, only 11.4 % of the dehydrogenation duty was met by recovered heat (HX1–HX2) with the rest of the duty being provided by a hydrogen-fired burner sized to a 27.4 kW winter peak. This asymmetry explains why the electrical round-trip across the hydrogen pathway was estimated at 23.4 % and why the overall system efficiency was estimated at around 41.4 %, a roughly half of the electrolyser hydrogen produced survives the LOHC process and reaches the PEMFC (LOHC-chain efficiency 49.5 %). This inefficiency is reflected in the hydrogen calculations across the LOHC path, which shows that of the 1,813 kg_{H2} produced annually, 898 kg feed the fuel cell, while 712 kg are consumed as process fuel to heat dehydrogenation and 17 kg are spent on hydrogenation preheat. These numbers result from the lower temperature grade produced by an LT-PEMFC and the endothermic nature of dehydrogenation, both of which contribute substantially to burner demand. The pinch analyses for both processes (Figures 5.13–5.17) support this by showing a limited temperature boost for the dehydrogenation preheat process and a sufficient temperature difference on the hydrogenation side.

The economic analysis reflects this technical constraint. The increased hydrogen supply for process heat purposes increases total hydrogen demand, which in turn increases the size of the components and the required initial NEC inventory. Consequently, of the € 2.365 million CAPEX for the main scenario, € 1.654 million was attributed to the cost of LOHC process components (reactors, heat exchangers, burner, tanks, catalysts, initial NEC fill). OPEX follows the same pattern, with 46.7 % of the annual cost being attributable to LOHC operations. Although implementing such a system avoids approximately 16,371 €/year in energy purchases and reduces residual imports to 127 €/year, the project remains economically infeasible under the assumed price and finance environment, with an estimated IRR of −29.48 %, and NPV of − 2.67 million €, and an LCOE of 1.686 €/kWh. The NPV sensitivity anal-

ysis supports previous observations, revealing that the NPV is particularly susceptible to fluctuations in LOHC-related prices. Specifically, the NPV value varies by nearly ±9% in response to a ±20% change in NEC price and by approximately ±3-6% in reaction to a ±20% variation in reactor costs. Conversely, the LCOE sensitivity analysis reveals that LCOE is significantly affected by capital recovery parameters. Changes in the discount rate can vary LCOE by ±10% for a ±20% variation, while the project's lifetime influences LCOE by approximately ±5-9% under the same conditions. In other words, the cost structure is influenced by the capital invested in LOHC inventory and the thermal equipment required to release hydrogen, not by the PV system or the battery.

The compressed-hydrogen alternative helps us understand what is essential to the storage process and what relies on site management. Keeping EMS rules, price inputs, and accounting assumptions fixed, the compressed scenario reduces PV capacity to 113.40 kWp (378 modules), keeps the battery at 261 kWh, sizes the electrolyser to 80 kW and the PEMFC again to 34 kW, and introduces a 12.4 kW compressor. Overall system autonomy remains high with imports accounting for only 1.0% of load, exports were increased compared to the LOHC scenario, reaching 10.4 % of PV production, and mass-balance remained small with an error of 2–2.5 %. In this scenario, the overall CAPEX of 0.565 million € and the OPEX of 6,004 €/year significantly decreased compared to the LOHC scenario. The economics metrics were improved noticeably, with the LCOE of 0.79 €/kWh being almost half of the LOHC-based LCOE, while NPV and IRR were also decreased, accounting for − 0.733 million € and −18.21 % respectively. Even with these reduced numbers, hydrogen seasonal storage remains economically infeasible under today's economic environment. This contrast establishes two points. First, the storage choice explains much of the gap, as removing the LOHC inventory and the burner provided heat halves the LCOE and reduces the capital at risk. Second, boundary conditions beyond storage still matter, as even with a less costly compressed-H_2 pathway, storing hydrogen remains infeasible under the same prices and discounting, so the negative conclusion in the main scenario is not solely attributed to LOHC.

To ensure the model's credibility and the realism of its results, the model was validated with respect to its operational logic, thermodynamic consistency, and performance realism. The model's operational logic is validated, as it behaves as intended. The electrolyser start/stop patterns and ON/OFF hours (Figure 5.12) track surplus PV, while the fuel-cell operational status (Figure 5.11) follows winter demand, confirming that the EMS implementation enforces the dispatch rules in §4.3. The pinch analyses (Figures 5.13–**??**) confirm that our model is thermodynamically consistent, as the simulated duties do not exceed the limit and cross paths in any heat exchanger. Regarding the performance realism, hourly PEMFC and electrolyser efficiencies (Figures 5.18a, 5.18b) fall within reported ranges for the selected technologies, and the annual mass balance closes tightly (NEC mismatch 0.41%), reducing the risk of hidden bookkeeping errors. These system-level findings align with the literature reviewed in Chapter 2 in two ways. Studies for similarly scaled LOHC pathways consistently show that configurations that rely on external combustion (or only low-grade waste heat) for providing the dehydrogenation heat duty exhibit low electrical round-trip efficiency, which (Teichmann, Stark, et al., 2012) estimated to be around 20–30 % for PEMFC-based systems. The present model's 23.4 % electrical round-trip efficiency, therefore, falls close to expectations and is supported by the observed low recovery fraction on the dehydrogenation side. Likewise, techno-economic evaluations indicate that the price of the LOHC medium and the reactor size significantly affect the system's overall cost (Abdin et al., 2021; García et al., 2024). The CAPEX estimate in our model aligns with this trend under the specific constraints of Green Village, as it is dominated by NEC inventory and reactor costs.
When evaluating both scenarios, the decision becomes intricate. The thesis inquired whether LOHC-based seasonal storage could achieve techno-economic viability while still being operationally credible; Green Village focuses on safety integrated into buildings, regulatory compliance, and community acceptance within a living-lab setting. From a technical and operational standpoint, the main scenario meets the necessary criteria: it demonstrates high autonomy, maintains a tight mass balance, exhibits validated EMS performance, and shows thermodynamically consistent heat-recovery patterns. However, from an economic perspective, it was found infeasible as the combination of low-grade dehydrogenation heat, combined with capital investments required for NEC and the process components, resulted in a high LCOE and a negative NPV under base-case conditions. Regarding the safety of the system, storing hydrogen in NEC is preferable to compressed hydrogen, as it is stored in low-vapour-

pressure liquid at near-atmospheric pressure. This minimises the impact of high-pressure hazards and hydrogen concentration risks at the dehydrogenation/PEMFC boundary, allowing for focused ventilation, gas detection, and compact ATEX zoning, rather than extensive site-wide high-pressure zoning required for CHG_2. In terms of space requirements, the LOHC scenario requires a total area of 1,019 m^2 for the main components, 46% higher than the area required for the CHG_2 scenario, which totalled at 698 m^2. For reactor and tank space requirements of the LOHC scenario, approximately 65.15 m^3 are required if separate loaded/unloaded tanks are used, or 36.15 m^3 if a multi-product tank is used. For the compressed hydrogen (H_2) option, approximately 1,039 50-litre cylinders, corresponding to a cumulative vessel volume of around 52 m^3, are required for hydrogen storage. Given the associated safety concerns, this requirement is likely to lead to expanded hazardous zoning, an increased overall system footprint, and higher operational costs. For a site that receives visitors, hosts experiments, and co-locates offices and labs, an LOHC-based hydrogen storage is considered safer, requires fewer safety measures and will be easier to permit, despite its increased losses and cost.
In conclusion, the LOHC configuration successfully achieves seasonal balancing with a very high level of self-sufficiency, thanks to a validated control strategy. From a safety perspective, it aligns with Green Village's constraints and permitting requirements, despite the large installation footprint. However, economic feasibility is limited by the cost of the NEC and the process components. These components are significantly affected by the low-grade heat available for dehydrogenation, leading to increased hydrogen demand from auxiliaries and, consequently, larger component sizing. The compressed-hydrogen alternative, even though it halves the LCOE, remains infeasible under the same price and financing assumptions. Additionally, using compressed tanks for hydrogen storage may require a larger footprint due to safety concerns that require higher hazard zoning in a built environment. In this context, although the main scenario is not currently economically viable, it is expected to become so as the infiltration of renewable energy sources increases, grid congestion becomes more apparent, and demand for long-term energy storage solutions grows. This could increase the value of these systems. In this context, running a trial at Green Village could become a worthwhile opportunity to test new designs and improve heat usage while keeping an eye on market trends and potential policy changes.

6.2. Limitations & Uncertainties

The model developed for this thesis provides a comprehensive framework for assessing the feasibility of storing hydrogen in an LOHC-based seasonal storage for the Green Village. However, it inevitably relies on simplifications and assumptions that introduce limitations and uncertainties. These simplifications and assumptions affect both the quantitative values reported and the extent to which the results can be generalised beyond the specific case of The Green Village.
A first source of uncertainty comes from the model's operational logic, which is governed by a rule-based EMS. This EMS operates on a seasonal logic that deliberately prioritises self-consumption, daily battery cycling, long electrolyser runs in summer, and fuel-cell dispatch in winter while enforcing constraints on when the components will operate. This representation follows the Green Village EMS logic, yet it does not optimise hour-to-hour decisions against a cost or efficiency objective. Different thresholds for state of charge or start permissions could change cycling patterns and result in slightly different imports, exports, and hydrogen flows. Transient behaviour is also simplified, as start-up lags, ramp limits, and minimum up and down times are not simulated. Degradation of the components is treated implicitly through fixed replacement ages rather than degradation that depends on cycling history.In practice, batteries fade with cycle depth and temperature, electrolysers and PEMFC stacks lose efficiency with operating hours and starts/stops, and LOHC catalysts deactivate with time and temperature. Using this assumption, will assume a steady performance, which may lead to an overestimation of mid-life efficiency and an underestimation of OPEX.
The solar irradiance and ambient temperature data used in this study were retrieved from PVGIS for the Delft location. These datasets are representative of a typical meteorological year but do not explicitly capture local effects such as shading from nearby trees, buildings, or other obstacles on site, resulting in an overestimation of PV generation. Such an assumption could affect overall system performance during a "dunkelflaute". In such an event, solar PV generation decreases while heating demand increases. This prompts the Energy Management System (EMS) to prioritise the PEMFC to address the shortfall and enhance dehydrogenation. As a result, overall hydrogen production increases, and the LOHC inventory depletes faster, leading to increased grid imports. To address this uncertainty, the

system could be sized using a multi-year simulation and safety factors applied to component sizes.
Another factor that may have affected the overall result of the main scenario is the simplification used for the reactor modelling. The reactor was represented as a batch reactor, sized and costed using steady-state correlations updated to current indices, rather than a continuous-flow fixed-bed reactor, which is established in the literature as the preferred configuration for such installations. This simplification creates uncertainty, as a batch reactor during cycles requires loading and unloading the LOHC, which, when sized for peak duty, can lead to increased reactor space use and overall cost compared to a continuous-flow fixed-bed reactor. However, this simplification does not alter the conclusion that dehydrogenation is the thermal bottleneck and that the inventory of LOHC, along with its components, significantly impacts the (CAPEX). Implementing a continuous-flow model is likely to reduce spatial requirements and CAPEX, thereby narrowing, although not necessarily eliminating, the feasibility gap. Catalyst inventories and annual replacements follow simple activity assumptions. The long-term effects, such as gradual deactivation, selectivity drift, fouling, and pressure drop, are not addressed in this study. This assumption keeps reactor and HX performance artificially flat, likely overestimating round-trip efficiency and autonomy and underestimating OPEX/replacement costs and downtime—so LCOE/NPV appear optimistic. The waste heat recovery also comes with uncertainty, as the recovery strategies implemented in this thesis were designed around realistic process connections, such as using PEMFC cooling water to preheat the incoming LOHC stream and coupling hot and cold LOHC flows through internal heat exchangers. These assumptions reflect technically plausible designs, yet they do not represent a fully optimised configuration. In practice, a detailed process integration study could explore additional arrangements and identify whether greater recovery is achievable. Additionally, for the heat exchangers, the area and costs were calculated using ASPEN EDR. However, as previously mentioned, this software cannot model solid-liquid heat exchangers. In the hydrogenation process, heat exchangers HX1 and HX4 require this type of exchange. Therefore, the study assigned an average cost of €600 for each exchanger. This assumption is reasonable in maintaining consistent capital costs, though it introduces some uncertainty due to fluctuations in construction materials and allowable pressure drops. However, since heat exchanger costs are minor relative to total system expenses, their variability is unlikely to substantially impact the overall outcome. To eliminate this uncertainty, however, the HX size could be estimated from UA curves existing in literature and then the cost via vendor quotation .
Similarly, tank sizes are based on production and use in a reference year, without accounting for variability across years. The model was simulated using meteorological data and the Green Village load profile for 2023; however, this analysis does not evaluate the design's robustness under varying conditions of solar irradiance or demand in different years.
For the economic analysis model, all prices are treated as constants and expressed in euros of the base year. Inflation, taxes, financing structure, contingency, EPC overheads, permitting, and owners' costs are not included. Capital costs are estimated using cost coefficients (€/kW, €/kWh, €/kg) for the calculated sizes based on literature, resulting in realistic estimated values, but not site-specific quotations. The avoided cost is determined using a fixed electricity price for imports, while exports are regarded as an exchange constraint rather than a revenue stream, without accounting for remuneration associated with exports. Replacement of the battery, electrolyser, and fuel cell is imposed deterministically, and O&M is represented as fixed fractions of CAPEX of each system component. The discount rate, project duration, NEC unit pricing, and unit capital expenditure (CAPEX) for critical equipment are associated with inherent uncertainties. The sensitivity analysis assesses variations of ±20%; however, it is important to note that more extensive fluctuations may be feasible, particularly concerning NEC procurement at the required scale and future advancements in the learning rates of electrolysers and fuel cells. As a result, the reported CAPEX, OPEX, LCOE and NPV represent an idealised project case rather than a comprehensive investment analysis. The model does not account for explicit costs associated with permitting and safety measures, such as blast panels, ventilation, and gas detection, which can significantly influence installed costs and operational practices in a real-world project, as to estimate these cost would require a detailed risk assessment and hazarard and operability studies for which can significantly influence installed costs and operational practices in a real-world project.
Despite these uncertainties, the model performs as intended. The electrolyser adheres to the "one start per day" rule during the production season and aligns with the PV profile as expected. The PEMFC dispatch respects module limits and follows the winter demand profile, while both the electrolyser and fuel cell demonstrate efficiencies within accepted ranges. Furthermore, the annual imports/exports

and the LOHC mass balance KPIs remain within established bounds, and the estimated efficiencies are reasonable and consistent with existing literature.
Taken together, these limitations do not overturn the main message. At the scale studied, the LOHC system can deliver the required seasonal shift with the control logic used here, but it does so with modest round-trip electrical efficiency and high capital intensity. The exact values of LCOE, NPV, and optimal sizes should be read as decision-grade for this site and methodology rather than as universal benchmarks. Considering the identified limitations, it is essential to note that they do not invalidate the main finding that an LOHC system can be technically feasible for seasonal storage while achieving a high level of self-sufficiency. Nonetheless, the execution of such a project may present challenges due to its capital intensity under current cost conditions. These limitations do, however, place bounds on the precision of the absolute figures presented.

7
Conclusion

7.1. Answers to the Research Questions

How does a PV-battery-electrolyser-fuel-cell system with LOHC storage compare to compressed hydrogen under identical operating conditions in terms of component sizing, performance,safety, and cost?

Under the same conditions, both the LOHC-based and compressed-hydrogen storage systems can achieve near-complete annual self-sufficiency for the Green Village with minimal grid use. However, the LOHC-based scenario requires 5% more PV capacity and a significantly larger electrolyser system than compressed H_2 for the same energy demand, to compensate for its lower round-trip efficiency and internal hydrogen consumption for process heat. This results in significantly higher capital expenditure, with the LOHC scenario costing over four times more than the compressed hydrogen alternative. These results were in line with the literature, which identified that LOHC technologies, despite being innovative, face challenges due to high heat requirements and expensive carrier material, which undermines their economic viability. Additionally, the LOHC system exhibits a considerably larger spatial footprint, primarily due to the increased size of components, while the tanks' volumes are relative to the tank of choice. For compressed hydrogen, system components occupy less overall area, while the greater number of pressurised tanks required increases safety risks, necessitating extra safety measures and expanded safety zones that can increase the overall footprint. In contrast, the LOHC approach offers inherent safety advantages by storing hydrogen in a stable liquid at ambient conditions, making it easier to permit in the built environment with fewer special safety provisions despite its added complexity.
In summary, while both systems are technically capable of enabling long-term renewable energy storage and while neither option is economically viable under present cost assumptions, the

Which techno-economic factors most significantly influence the economic feasibility of the project?

The main findings indicate that the project's economic feasibility is most sensitive to the cost of capital, project lifespan, and costs associated with the LOHC chain. Specifically, a 20% increase in the discount rate can raise the LCOE by over 10%, while shortening the project lifetime by five years increases LCOE by approximately 9.5%. Conversely, extending the lifespan yields moderate cost reductions. Among capital expenses, the NEC is identified as a key factor, as it accounts for nearly 50% of the LOHC system's capital cost. A 20% reduction in NEC price can significantly improve net present value and lower LCOE by about 8%. Additionally, the electrolyser and dehydrogenation/hydrogenation reactors are key cost drivers, with ±20% variations in their prices impacting the LCOE by roughly 3–5%. Operationally, reducing the thermal energy demand of the dehydrogenation process, which currently requires burning up to 44% of the stored hydrogen, could substantially improve round-trip efficiency and reduce operating losses. Overall, the system's feasibility depends on optimising financial conditions and achieving targeted cost reductions in LOHC-specific components.

What percentage of the required process heat for hydrogenation and dehydrogenation can be recovered through waste-heat recovery, and how does this affect round-trip efficiency and hydrogen consumption?

In the main scenario, heat recovery strategies were applied to both hydrogenation and dehydrogenation to reduce thermal demand. The exothermic hydrogenation process enabled 88% of the required heat duty to be recovered via a heat exchanger network using the reactor coolant and outflow. In contrast, dehydrogenation, which requires high-temperature heat, was more constrained, with only 12.3% of its thermal demand being met through waste heat recovery from the reactor outflow and a PEM fuel

cell, which primarily produces low-grade heat. The remaining heat was supplied by burning hydrogen, with 712 kg of the 1,610 kg released annually diverted to the burner, and only 898 kg used in the fuel cell. This internal consumption significantly reduced efficiency, resulting in a hydrogen storage round-trip efficiency of 23.4% and an overall LOHC chain efficiency of 49.5%. To improve performance, high-grade heat from a solid oxide fuel cell (SOFC) would be needed to cover a greater share of the dehydrogenation duty, thereby reducing hydrogen losses and improving system efficiency.

How feasible is a LOHC-based system for seasonal energy storage in The Green Village, considering its technical, economic, and operational aspects?

TThe LOHC-based seasonal energy storage system developed in this thesis for The Green Village is technically and operationally feasible but economically infeasible under current market conditions. The proposed hybrid configuration comprises a PV system, battery, electrolyser, LOHC storage, and a fuel cell that will supply the community's energy demands with minimal reliance on the grid. The system prioritises immediate solar consumption and battery charging, converts surplus energy into hydrogen for chemical storage in N-ethylcarbazole during summer, and releases it in winter via dehydrogenation and fuel cell generation. This approach achieves a nearly closed annual hydrogen loop, with only 0.41From an economic perspective, the system faces significant challenges, with capital expenditures totaling around €2.36 million. The LOHC infrastructure, particularly the reactors and NEC, accounts for over €1.6 million of this amount, with the upfront cost of N-ethylcarbazole alone exceeding €1.1 million. In contrast, the annual operations and maintenance costs are relatively modest, estimated at approximately €12,950. Consequently, the resulting levelized cost of energy is approximately €1.69 per kilowatt-hour, which is several times higher than that of grid electricity. This results in a poor financial performance for the project, with a negative net present value (–€2.66 million) and an internal rate of return of –29.5

The results of the study collectively demonstrate that a seasonal storage system utilising N-ethylcarbazole as a seasonal storage medium at The Green Village is *technically* feasible and *operationally* coherent throughout the year, achieving near self-sufficiency. However, from an economic standpoint, and considering the aforementioned assumptions and the current market prices, the project is deemed *economically* unfeasible. The sensitivity analysis results indicate that costs associated with the carrier and the components of the process have the most significant influence on the project's viability. This finding aligns with earlier techno-economic studies, which have identified that LOHC systems at the building scale are typically cost-intensive unless notable improvements occur in carrier expenses, capital intensity, or heat integration.

7.2. Recommendations for Further Research

Future research should focus on developing a cost-aware optimisation model that sizes the system to minimise the cost while maximising self-sufficiency. Additionally, a multi-year simulation that incorporates site-specific factors and explicit "dunkelflaute" stress tests could strengthen the credibility of the results by demonstrating that the selected sizes remain adequate across inter-annual variability.

Another aspect that could be explored is the introduction of dynamic electricity pricing in the model, including export remuneration, which will adjust system operation in response to prices, thereby increasing cost efficiency. Furthermore, the modelling of component degradation factors such as battery capacity fade, electrolyser stack efficiency loss, PEMFC voltage decay, and catalyst deactivation will yield a more precise model for estimating system reliability and long-term costs. At the process level, the system should be modelled in Aspen Plus, preferably using continuous fixed-bed reactors rather than a batch model, to provide a reliable estimate of the required size and cost. Additionally, the economic framework should move beyond coefficients to installed costs, including EPC, contingency, permitting and safety measures (blast relief, ventilation, gas detection), owner's costs, taxes, financing, and inflation to provide a more accurate estimate of the system's initial and operational costs

Lastly, this research could be extended to include an evaluation of alternative LOHCs based on the same assumptions, assessing their performance, cost and identifying the most promising carrier for this application and a site-specific validation pathway (pilot metering and a lightweight digital twin) to calibrate the model and verify KPI ranges.

Bibliography

Abdin, Z., Tang, C., Liu, Y., & Catchpole, K. (2021). Large-scale stationary hydrogen storage via liquid organic hydrogen carriers. https://doi.org/10.1016/j.isci

Abe, J., Popoola, A., Ajenifuja, E., & Popoola, O. (2019). Hydrogen energy, economy and storage: Review and recommendation. *International Journal of Hydrogen Energy*, *44*(29), 15072–15086. https://doi.org/https://doi.org/10.1016/j.ijhydene.2019.04.068

Ali, M. S., Hossain Khan, M. S., Tuhin, R. A., Kabir, M. A., Azad, A. K., & Farrok, O. (2024). Chapter 9 - hydrogen energy storage and transportation challenges: A review of recent advances. In M. M. K. Khan, A. K. Azad, & A. M. T. Oo (Eds.), *Hydrogen energy conversion and management* (pp. 255–287). Elsevier. https://doi.org/https://doi.org/10.1016/B978-0-443-15329-7.00001-6

Ali, M. S., Khan, M. S. H., Tuhin, R. A., Kabir, M. A., Azad, A. K., & Farrok, O. (2023). Hydrogen energy storage and transportation challenges: A review of recent advances. *Hydrogen Energy Conversion and Management*, 255–287. https://doi.org/10.1016/B978-0-443-15329-7.00001-6

ANSI/AIAA. (2017). Guide to safety of hydrogen and hydrogen systems (ansi/aiaa g-095a-2017). *Guide to Safety of Hydrogen and Hydrogen Systems (ANSI/AIAA G-095A-2017)*. https://doi.org/10.2514/4.105197

Authayanun, S., Mamlouk, M., Scott, K., & Arpornwichanop, A. (2013). Comparison of high-temperature and low-temperature polymer electrolyte membrane fuel cell systems with glycerol reforming process for stationary applications. *Applied Energy*, *109*, 192–201. https://doi.org/10.1016/J.APENERGY.2013.04.009

Aziz, M. (2021). Liquid hydrogen: A review on liquefaction, storage, transportation, and safety. *Energies 2021, Vol. 14, Page 5917*, *14*, 5917. https://doi.org/10.3390/EN14185917

Brigljević, B., Byun, M., & Lim, H. (2020). Design, economic evaluation, and market uncertainty analysis of lohc-based, co2 free, hydrogen delivery systems. *Applied Energy*, *274*. https://doi.org/10.1016/j.apenergy.2020.115314

Brückner, N., Obesser, K., Bösmann, A., Teichmann, D., Arlt, W., Dungs, J., & Wasserscheid, P. (2014). Evaluation of industrially applied heat-transfer fluids as liquid organic hydrogen carrier systems. *ChemSusChem*, *7*, 229–235. https://doi.org/10.1002/cssc.201300426

Buonomano, A., Calise, F., d'Accadia, M. D., Palombo, A., & Vicidomini, M. (2015). Hybrid solid oxide fuel cells–gas turbine systems for combined heat and power: A review. *Applied Energy*, *156*, 32–85. https://doi.org/10.1016/J.APENERGY.2015.06.027

Büthker, E., Elliott, A., & te Ronde, I. (2015). *Internal safety distances for pgs 35* (Background report). Publicatiereeks Gevaarlijke Stoffen (PGS Programme Council). Retrieved October 10, 2025, from https://publicatiereeksgevaarlijkestoffen.nl/documents/81474/1664358056-pgs_35_wg_2015_032_pgs35_definitief-20achtergronddocument.pdf

B.V., V. (2025). *Energy density* [Part of the series "Things to consider when planning your zero-emission future."]. Voyex B.V. Retrieved October 20, 2025, from https://www.voyex.nl/energy-density/

BYD Company Limited. (2025). *Battery-box premium lvl: Datasheet (lvl15.4)* (Datasheet) (Technical parameters page footer shows version V1.0). BYD Company Limited. Retrieved October 13, 2025, from https://bydbatterybox.com/uploads/downloads/Premium_Datasheet_LVL%20V1.1%20EN-5ebcbeddb3624.pdf

Cartaxo, S. J., & Fernandes, F. A. (2011). Counterflow logarithmic mean temperature difference is actually the upper bound: A demonstration. *Applied Thermal Engineering*, *31*(6), 1172–1175. https://doi.org/https://doi.org/10.1016/j.applthermaleng.2010.12.015

Cigolotti, V., Genovese, M., & Fragiacomo, P. (2021, August). Comprehensive review on fuel cell technology for stationary applications as sustainable and efficient poly-generation energy systems. https://doi.org/10.3390/en14164963

Collignon. (2019). What is the major accidents (risk) decree 2015 and to which companies. https://www.stibbe.com/publications-and-insights/what-is-the-major-accidents-risk-decree-2015-and-to-which-companies-does

Copernicus Climate Change Service. (2025). 2024 is the first year to exceed 1.5^oc above pre-industrial level [Retrieved 9 October 2025]. https://climate.copernicus.eu/copernicus-2024-first-year-exceed-15degc-above-pre-industrial-level

Ding, Y., Dong, Y., Zhang, H., Zhao, Y., Yang, M., & Cheng, H. (2021). A highly adaptable ni catalyst for liquid organic hydrogen carriers hydrogenation. *International Journal of Hydrogen Energy*, *46*(53), 27026–27036. https://doi.org/https://doi.org/10.1016/j.ijhydene.2021.05.196

Eblagon, K. M., Tam, K., & Tsang, S. C. E. (2012). Comparison of catalytic performance of supported ruthenium and rhodium for hydrogenation of 9-ethylcarbazole for hydrogen storage applications. *Energy Environmental Science*, *5*, 8621–8630. https://doi.org/10.1039/C2EE22066K

El-Shafie, M. (2023). Hydrogen production by water electrolysis technologies: A review. *Results in Engineering*, *20*. https://doi.org/10.1016/j.rineng.2023.101426

Enapter. (n.d.). *Aem technology by enapter*. Enapter. Retrieved October 20, 2025, from https://enapter.com/en/aem-by-enapter-electrolysis/

Enapter. (2025). *Electrolyser el 2.1: Datasheet* (Datasheet). Enapter. Retrieved October 13, 2025, from https://handbook.enapter.com/electrolyser/el21/downloads/Enapter_Datasheet_EL21_EN.pdf

Esposito, A. M., Peterson, H. D., Miller, H. E., Stanford, H. J., Rodezno, E., Roizen, F. J., McMurtry, B., Satyapal, O. S., Rinaldi, H. K., Vickers, H. J., Pomeroy, H. E., Green, H. T., Hahn, H. M., Farmer, H. R., Ulsh, H. M., Badgett, A., Pivovar, N. B., Murphy, N. C., Casteel, N. M., & Prosser, J. (2024). Hydrogen shot: Water electrolysis technology assessment.

European Commission. (2014a). Directive - 2014/34 - en - atex directive - eur-lex. https://eur-lex.europa.eu/eli/dir/2014/34/oj/eng

European Commission. (2014b). Electromagnetic compatibility (emc) directive - european commission. https://single-market-economy.ec.europa.eu/sectors/electrical-and-electronic-engineering-industries-eei/electromagnetic-compatibility-emc-directive_en

European Commission. (2014c). Low voltage directive (lvd) - european commission. https://single-market-economy.ec.europa.eu/sectors/electrical-and-electronic-engineering-industries-eei/low-voltage-directive-lvd_en

European Commission. (2014d). Pressure equipment directive - european commission. https://single-market-economy.ec.europa.eu/sectors/pressure-equipment-and-gas-appliances/pressure-equipment-sector/pressure-equipment-directive_en

Eypasch, M., Schimpe, M., Kanwar, A., Hartmann, T., Herzog, S., Frank, T., & Hamacher, T. (2017). Model-based techno-economic evaluation of an electricity storage system based on liquid organic hydrogen carriers. *Applied Energy*, *185*, 320–330. https://doi.org/10.1016/j.apenergy.2016.10.068

Fan, Y., Wang, P., Zhang, J., Zhang, J., et al. (2024). Continuous hydrogenation of *N*-ethylcarbazole in a micro-packed bed reactor for hydrogen storage. *Chemical Engineering Journal*, *484*, 149404. https://doi.org/10.1016/j.cej.2024.149404

Fan, Y., Wang, P., Zhang, J., Zhang, J., et al. (2025). Continuous dehydrogenation of dodecahydro-*N*-ethylcarbazole for hydrogen production in a micro-packed bed reactor [In press]. *International Journal of Hydrogen Energy*. https://www.researchgate.net/publication/388606677

García, A., Marín, P., & Ordóñez, S. (2024). Hydrogenation of liquid organic hydrogen carriers: Process scale-up, economic analysis and optimization. *International Journal of Hydrogen Energy*, *52*, 1113–1123. https://doi.org/10.1016/J.IJHYDENE.2023.06.273

Harrison, K. W., Remick, R., Martin, G. D., & Hoskin, A. (2010). *Hydrogen production: Fundamentals and cas study summaries e preprint*. http://www.osti.gov/bridge

Hoecke, L. V., Laffineur, L., Campe, R., Perreault, P., Verbruggen, S. W., & Lenaerts, S. (2021, February). Challenges in the use of hydrogen for maritime applications. https://doi.org/10.1039/d0ee01545h

Hydrogen Safety Innovation Programme (WVIP). (2020, June). *Permitting process on hydrogen refuelling stations: Summary of the practical guide for operators and local residents* (tech. rep.) (Retrieved 10 October 2025). Dutch H2 Platform. https://nlhydrogen.nl/wp-content/uploads/2020/06/Summary_Guide-permitting_process_hydrogen_refuelling_stations.pdf

Hydrogen Tools. (2025). Hydrogen compressibility at different temperatures and pressures [Hydrogen Analysis Resource Center (HyARC), Pacific Northwest National Laboratory]. Retrieved Oc-

tober 21, 2025, from https://h2tools.org/hyarc/hydrogen-data/hydrogen-compressibility-different-temperatures-and-pressures

HyETHydrogen. (2025). Products | hyet hydrogen. https://hyethydrogen.com/products/

ICM. (2023). Atex zone determination (2025) | icm projects. https://icmprojects.nl/en/atex-zones/determination/

IEA. (2024). *Renewables 2024 report: Global energy trends*. IEA. https://www.iea.org/reports/renewables-2024

International Energy Agency. (2024a). *Co2 emissions in 2023: A new record high, but is there light at the end of the tunnel?* International Energy Agency. Retrieved October 9, 2025, from https://www.iea.org/reports/co2-emissions-in-2023

International Energy Agency. (2024b). Global electricity generation by renewable energy technology, main case, 2023 and 2030 [Retrieved 9 October 2025]. https://www.iea.org/data-and-statistics/charts/global-electricity-generation-by-renewable-energy-technology-main-case-2023-and-2030

International Energy Agency. (2025). Climate change [Retrieved 9 October 2025]. https://www.iea.org/topics/climate-change

IRENA. (2025). Hydrogen [Retrieved 9 October 2025]. https://www.irena.org/Energy-Transition/Technology/Hydrogen

Jiang, Z., Gong, X., Wang, B., Wu, Z., & Fang, T. (2019). A experimental study on the dehydrogenation performance of dodecahydro-n-ethylcarbazole on m/tio2 catalysts. *International Journal of Hydrogen Energy*, *44*(5), 2951–2959. https://doi.org/https://doi.org/10.1016/j.ijhydene.2018.11.236

Knosala, K., Kotzur, L., Röben, F. T., Stenzel, P., Blum, L., Robinius, M., & Stolten, D. (2021). Hybrid hydrogen home storage for decentralized energy autonomy. *International Journal of Hydrogen Energy*, *46*, 21748–21763. https://doi.org/10.1016/j.ijhydene.2021.04.036

Krieger, C., Müller, K., & Arlt, W. (2016). Coupling of a liquid organic hydrogen carrier system with industrial heat. *Chemical Engineering and Technology*, *39*, 1570–1574. https://doi.org/10.1002/ceat.201600180

Kumar, S. S., & Himabindu, V. (2019). Hydrogen production by pem water electrolysis – a review. *Materials Science for Energy Technologies*, *2*, 442–454. https://doi.org/10.1016/J.MSET.2019.03.002

Lang, C., Jia, Y., & Yao, X. (2020). Recent advances in liquid-phase chemical hydrogen storage. *Energy Storage Materials*, *26*, 290–312. https://doi.org/10.1016/j.ensm.2020.01.010

Li, L., Aravind, P. V., Woudstra, T., & van den Broek, M. (2023). Assessing the waste heat recovery potential of liquid organic hydrogen carrier chains. *Energy Conversion and Management*, *276*. https://doi.org/10.1016/j.enconman.2022.116555

Li, N., Lukszo, Z., & Schmitz, J. (2023). An approach for sizing a pv–battery–electrolyzer–fuel cell energy system: A case study at a field lab. *Renewable and Sustainable Energy Reviews*, *181*. https://doi.org/10.1016/j.rser.2023.113308

Lin, A., & Bagnato, G. (2024, April). Revolutionising energy storage: The latest breakthrough in liquid organic hydrogen carriers. https://doi.org/10.1016/j.ijhydene.2024.03.146

Magliano, A., Carrera, C. P., Pappalardo, C. M., Guida, D., & Berardi, V. P. (2024). A comprehensive literature review on hydrogen tanks: Storage, safety, and structural integrity. *Applied Sciences 2024, Vol. 14, Page 9348*, *14*, 9348. https://doi.org/10.3390/APP14209348

Makaryan, I. A., & Sedov, I. V. (2021). Catalytic reactors for dehydrogenation of liquid organic hydrogen carriers. *Russian Journal of Applied Chemistry*, *94*(8), 1011–1021. https://doi.org/10.1134/S1070427221080012

March, L. (1998). Introduction to pinch technology. www.linnhoffmarch.com

Marcy, C. (2017, May 3). *Power plants' costs and value to the grid are not easily reflected using simple metrics*. U.S. Energy Information Administration (EIA) — Today in Energy. Retrieved October 11, 2025, from https://www.eia.gov/todayinenergy/detail.php?id=31052

Modisha, P. M., Ouma, C. N. M., Garidzirai, R., Wasserscheid, P., & Bessarabov, D. (2019). The prospect of hydrogen storage using liquid organic hydrogen carriers (lohcs). *Energy & Fuels*, *33*(4), 2778–2796. https://doi.org/10.1021/acs.energyfuels.9b00296

Müller, K., Thiele, S., & Wasserscheid, P. (2019). Evaluations of concepts for the integration of fuel cells in liquid organic hydrogen carrier systems. *Energy and Fuels*, *33*, 10324–10330. https://doi.org/10.1021/acs.energyfuels.9b01939

National Center for Biotechnology Information. (2025). *N-ethylcarbazole* [PubChem Compound Summary for CID 6836]. PubChem. Retrieved October 18, 2025, from https://pubchem.ncbi.nlm.nih.gov/compound/N-ethyl-carbazole

Nedstack Fuel Cell Technology B.V. (2019, November). *Product data sheet — nedstack fcs 7-xxl: Pem fuel cell stack* (Product data sheet) (Version: November 2019). Nedstack Fuel Cell Technology B.V. Retrieved October 13, 2025, from https://nedstack.com/sites/default/files/2019-11/20191105_nedstack_fcs_7-xxl.pdf

Niermann, M., Drünert, S., Kaltschmitt, M., & Bonhoff, K. (2019). Liquid organic hydrogen carriers (lohcs)-techno-economic analysis of lohcs in a defined process chain. *Energy and Environmental Science*, *12*, 290–307. https://doi.org/10.1039/c8ee02700e

Niermann, M., Timmerberg, S., Drünert, S., & Kaltschmitt, M. (2021). Liquid organic hydrogen carriers and alternatives for international transport of renewable hydrogen. *Renewable and Sustainable Energy Reviews*, *135*, 110171. https://doi.org/https://doi.org/10.1016/j.rser.2020.110171

Niermann, M., Beckendorff, A., Kaltschmitt, M., & Bonhoff, K. (2019, March). Liquid organic hydrogen carrier (lohc) – assessment based on chemical and economic properties. https://doi.org/10.1016/j.ijhydene.2019.01.199

Papapetrou, M., Cipollina, A., La Commare, U., Micale, G., Zaragoza, G., & Kosmadakis, G. (2017). Assessment of methodologies and data used to calculate desalination costs. *Desalination*, *419*, 8–19. https://doi.org/10.1016/j.desal.2017.05.038

Peters, W., Seidel, A., Herzog, S., Bösmann, A., Schwieger, W., & Wasserscheid, P. (2015). Macrokinetic effects in perhydro-*N*-ethylcarbazole dehydrogenation and h_2 productivity optimization by using egg-shell catalysts. *Energy & Environmental Science*, *8*, 3013–3021. https://doi.org/10.1039/C5EE02024G

PGS. (2021). Pgs 35:2021 versie 1.0 (augustus 2021). https://publicatiereeksgevaarlijkestoffen.nl/publicaties/online/pgs-35/2021/1-0-augustus-2021/#top

PGS. (2023). Brandbare vloeistoffen – opslag. https://publicatiereeksgevaarlijkestoffen.nl/publicaties/pgs29/

PVGIS. (2025). Jrc photovoltaic geographical information system (pvgis) - european commission. https://re.jrc.ec.europa.eu/pvg_tools/en/

Qasem, N. A., & Abdulrahman, G. A. (2024). A recent comprehensive review of fuel cells: History, types, and applications. https://doi.org/10.1155/2024/7271748

Richardson, J. (2025, August 25). *Ground mounted solar panel systems uk* [Reviewed by Richard Burdett-Gardiner]. The Renewable Energy Hub. Retrieved October 20, 2025, from https://www.renewableenergyhub.co.uk/main/solar-panels/ground-mounted-solar-panels

Schat, D. (2025, January). *H2 integration into residential energy hub: Report on the green village electrolyser and compressor data analysis* (Thesis) (SET3091). Delft University of Technology.

Schleifer, A. H., Cohen, S. M., Cole, W., Denholm, P., & Blair, N. (2025). Exploring the future energy value of long-duration energy storage. *Energies*, *18*, 1751. https://doi.org/10.3390/EN18071751/S1

Seveso-Omgevingsdiensten. (2024, March). *De veiligheid van waterstof(dragers): Een handreiking voor de vergunningverlening van grootschalige industriële waterstofprojecten* (Projectleiders: Wim Derksen (ODNZKG) en Yolanda Waas (DCMR); Programmamanager: Axel Pel (DCMR).). Omgevingsdienst.nl. Nederland. Retrieved October 10, 2025, from https://www.omgevingsdienst.nl/wp-content/uploads/2024/10/De-veiligheid-van-waterstofdragers.pdf

Shah, R. K., & Sekulic, D. P. (2003). Fundamentals of heat exchanger design.

Sharaf, O. Z., & Orhan, M. F. (2014). An overview of fuel cell technology: Fundamentals and applications. *Renewable and Sustainable Energy Reviews*, *32*, 810–853. https://doi.org/10.1016/J.RSER.2014.01.012

Shukla, A., Karmakar, S., & Biniwale, R. B. (2012). Hydrogen delivery through liquid organic hydrides: Considerations for a potential technology. *International Journal of Hydrogen Energy*, *37*, 3719–3726. https://doi.org/10.1016/J.IJHYDENE.2011.04.107

Sotoodeh, F., & Smith, K. J. (2011). Structure sensitivity of dodecahydro-n-ethylcarbazole dehydrogenation over pd catalysts. *Journal of Catalysis*, *279*(1), 36–47. https://doi.org/https://doi.org/10.1016/j.jcat.2010.12.022

Spoelstra, M. B. (2025). *Kennisbundel waterstof in de gebouwde omgeving* (tech. rep.) (Published 24 March 2025; Met medewerking van F. van de Ven; Retrieved 10 October 2025). Nederlands Instituut Publieke Veiligheid (NIPV). https://nipv.nl/wp-content/uploads/2025/03/20250324-NIPV-Kennisbundel-waterstof-in-de-gebouwde-omgeving.pdf

Stark, K., Emelyanenko, V. N., Zhabina, A. A., Varfolomeev, M. A., Verevkin, S. P., Müller, K., & Arlt, W. (2015). Liquid organic hydrogen carriers: Thermophysical and thermochemical studies of carbazole partly and fully hydrogenated derivatives. *Industrial and Engineering Chemistry Research*, *54*, 7953–7966. https://doi.org/10.1021/acs.iecr.5b01841

StatLine. (2025). Statline - average energy prices for consumers. https://opendata.cbs.nl/#/CBS/en/dataset/85592ENG/table?searchKeywords=energy%20prices%20for%20consumers

Teichmann, D., Arlt, W., & Wasserscheid, P. (2012). Liquid organic hydrogen carriers as an efficient vector for the transport and storage of renewable energy. *International Journal of Hydrogen Energy*, *37*, 18118–18132. https://doi.org/10.1016/J.IJHYDENE.2012.08.066

Teichmann, D., Stark, K., Müller, K., Zöttl, G., Wasserscheid, P., & Arlt, W. (2012). Energy storage in residential and commercial buildings via liquid organic hydrogen carriers (lohc). *Energy and Environmental Science*, *5*, 9044–9054. https://doi.org/10.1039/c2ee22070a

The University of Manchester. (2025). *Cepci (chemical engineering plant cost index)* [GCED training resource.]. The University of Manchester. Retrieved October 10, 2025, from https://www.training.itservices.manchester.ac.uk/public/gced/CEPCI.html?reactors/CEPCI/index.html

Thornton, G. (2019). *Renewable energy discount rate survey results-2018*. https://www.grantthornton.co.uk/insights/renewable-energy-discount-rate-survey/

TNO. (2024). *H2 industrial boiler technology factsheet* (tech. rep.). TNO. https://energy.nl/wp-content/uploads/h2industrialboiler_28092020_upd-7.pdf

Tsogt, N., Gbadago, D. Q., & Hwang, S. (2024). Exploring the potential of liquid organic hydrogen carrier (lohc) system for efficient hydrogen storage and transport: A techno-economic and energy analysis perspective. *Energy Conversion and Management*, *299*. https://doi.org/10.1016/j.enconman.2023.117856

United Nations Framework Convention on Climate Change. (2015). The paris agreement [Retrieved October 9, 2025]. https://unfccc.int/process-and-meetings/the-paris-agreement

U.S. Department of Energy, Hydrogen and Fuel Cell Technologies Office. (2017). Hydrogen safety fact sheet [Accessed 20 Oct 2025]. https://www1.eere.energy.gov/hydrogenandfuelcells/pdfs/h2_safety_fsheet.pdf

U.S.DOE. (2022, June). *Liquid hydrogen technologies workshop – summary report* (tech. rep. No. DOE/EE-2608) (Workshop held February 22–23, 2022; prepared in coordination with NASA). U.S. Department of Energy, Office of Energy Efficiency, Renewable Energy, Hydrogen, and Fuel Cell Technologies Office. Washington, DC. https://www.energy.gov/eere/fuelcells/liquid-hydrogen-technologies-workshop

van Trigt, L., & van Praag, R. (n.d.). *The green village seasonal storage system* (tech. rep.). The Green Village.

Village, T. G. (2025). *The green village website* [Accessed 2025-10-20]. The Green Village. https://www.thegreenvillage.org/

Wei, X., Sharma, S., Waeber, A., Wen, D., Sampathkumar, S. N., Margni, M., Maréchal, F., & herle, J. V. (2024). Comparative life cycle analysis of electrolyzer technologies for hydrogen production: Manufacturing and operations. *Joule*. https://doi.org/10.1016/j.joule.2024.09.007

Wu, Y., Yu, H., Guo, Y., Jiang, X., Qi, Y., Sun, B., Li, H., Zheng, J., & Li, X. (2019). A rare earth hydride supported ruthenium catalyst for the hydrogenation of n-heterocycles: Boosting the activity via a new hydrogen transfer path and controlling the stereoselectivity. *Chemical Science*, *10*, 10459–10465. https://doi.org/10.1039/C9SC04365A

WVIP. (2021). Waterstoftankstations en de omgevingswet. https://www.nen.nl/media/wysiwyg/WVIP_vergunningverlening_Waterstoftankstations_en_de_omgevingswet_sept21-1.pdf

Xue, J., et al. (2024). Experimental investigation on product and temperature distribution in a continuous flow packed-bed reactor for dodecahydro-*N*-ethylcarbazole dehydrogenation [In press;

PII: S138589472408313X]. *Chemical Engineering Journal*. https://www.sciencedirect.com/science/article/abs/pii/S138589472408313X

Yang, M., Dong, Y., Fei, S., Ke, H., & Cheng, H. (2014a). A comparative study of catalytic dehydrogenation of perhydro-n-ethylcarbazole over noble metal catalysts. *International Journal of Hydrogen Energy*, *39*(33), 18976–18983. https://doi.org/https://doi.org/10.1016/j.ijhydene.2014.09.123

Yang, M., Dong, Y., Fei, S., Ke, H., & Cheng, H. (2014b). A comparative study of catalytic dehydrogenation of perhydro-n-ethylcarbazole over noble metal catalysts. *International Journal of Hydrogen Energy*, *39*, 18976–18983. https://doi.org/10.1016/J.IJHYDENE.2014.09.123

Yu, S., Fan, Y., Shi, Z., Zhang, J., Zhao, X., Zhang, J., & Zhang, Y. (2024). The pemfc-mhp-chp system for independent energy supply and peak shaving: Performance analysis under load fluctuations. *International Journal of Hydrogen Energy*, *67*, 863–874. https://doi.org/10.1016/j.ijhydene.2023.12.163

Yue, M., Lambert, H., Pahon, E., Roche, R., Jemei, S., & Hissel, D. (2021). Hydrogen energy systems: A critical review of technologies, applications, trends and challenges. *Renewable and Sustainable Energy Reviews*, *146*, 111180. https://doi.org/10.1016/J.RSER.2021.111180

Zhang, J., Yang, F., Wang, B., Li, D., Wei, M., Fang, T., & Zhang, Z. (2023, May). Heterogeneous catalysts in n-heterocycles and aromatics as liquid organic hydrogen carriers (lohcs): History, present status and future. https://doi.org/10.3390/ma16103735

Zhou, Y. (2022, February). Pv scan for tgv [Presentation slides]. *TU Delft Urban Energy platform*.

A Additional Figures

This section includes additional figures that were created during the modelling of the main scenario.

A.1. Fuel Cell hourly projections

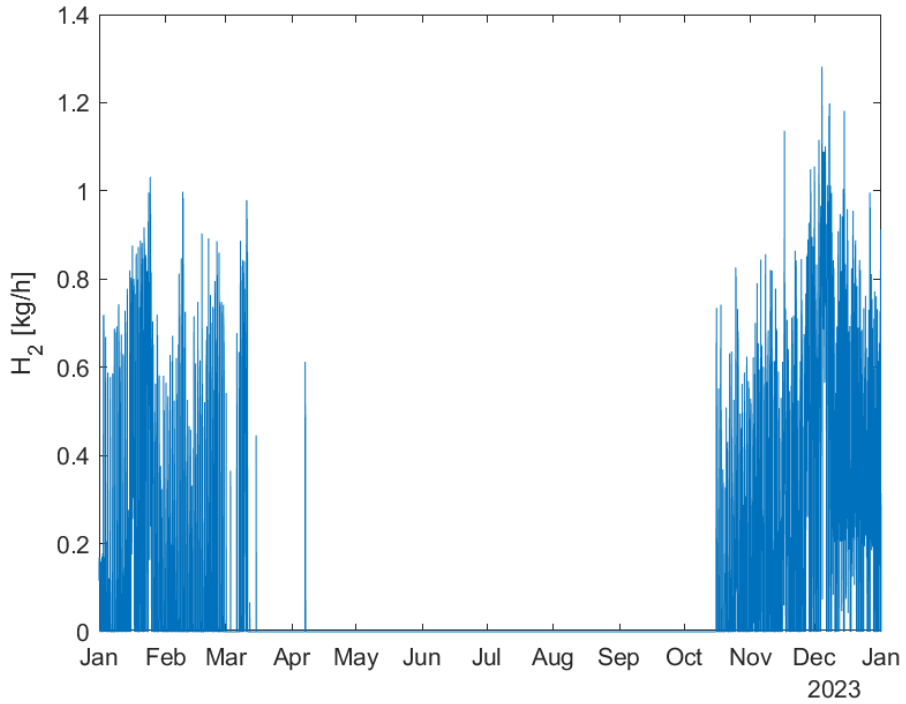

Figure A.1: Hourly Hydrogen Consumption

A.2. Electolyser hourly projections

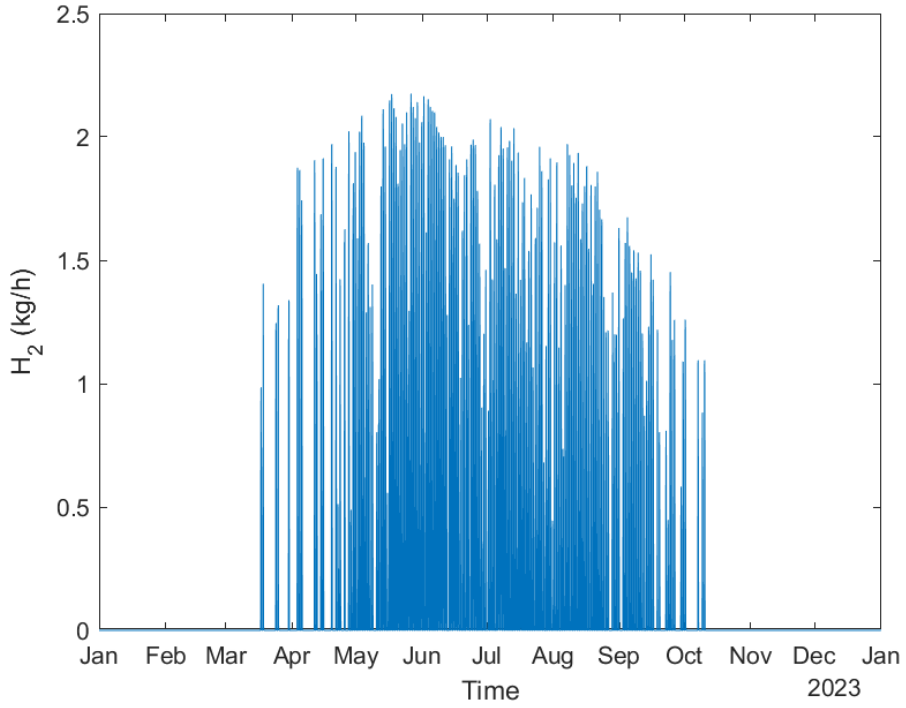

Figure A.2: Electrolyser Hourly Hydrogen Production

A.3. LOHC Process Mass Flow Projections

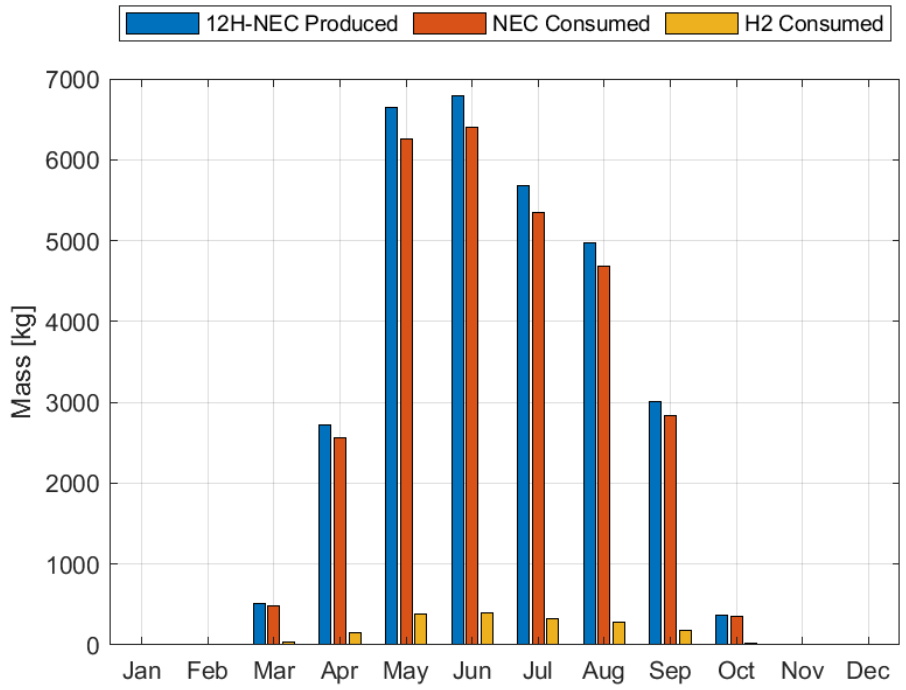

Figure A.3: Monthly Hydrogenation Mass Flows

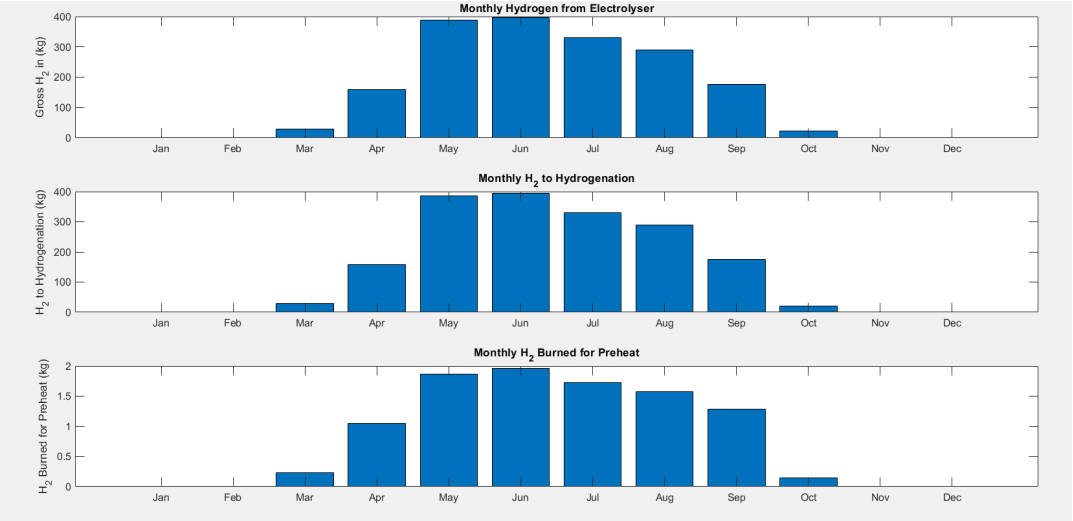

Figure A.4: Monthly Hydrogenation Hydrogen Flows

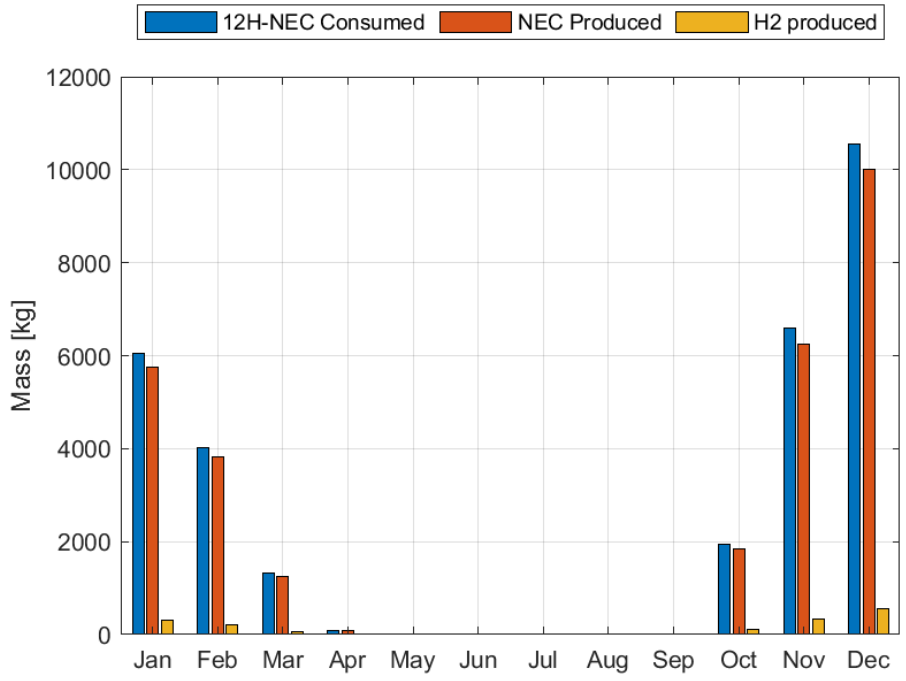

Figure A.5: Monthly Dehydrogenation Mass Flows

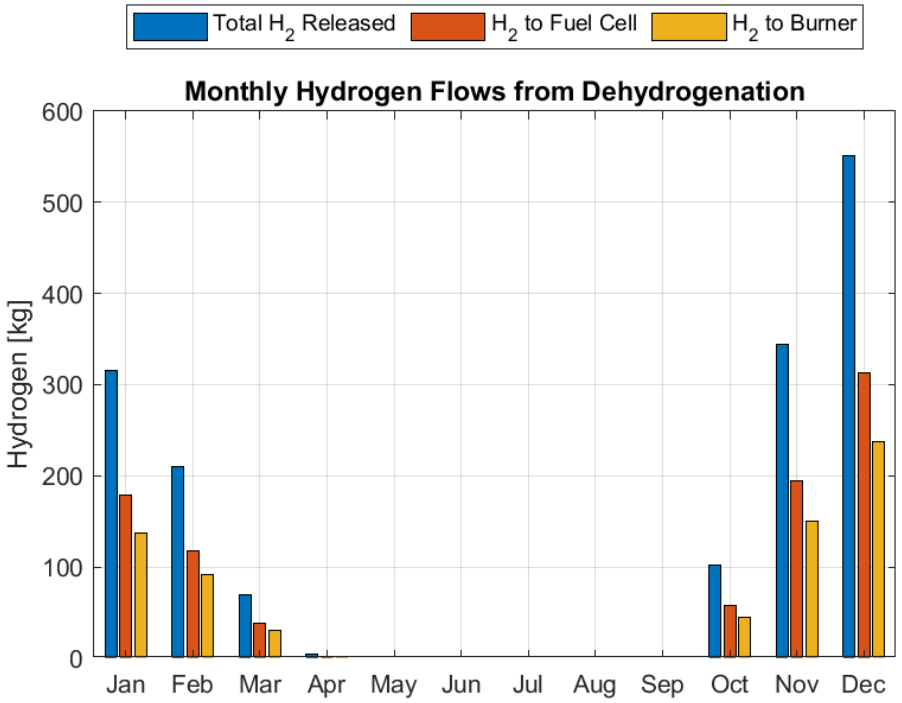

Figure A.6: Monthly Dehydrogenation Hydrogen Flows

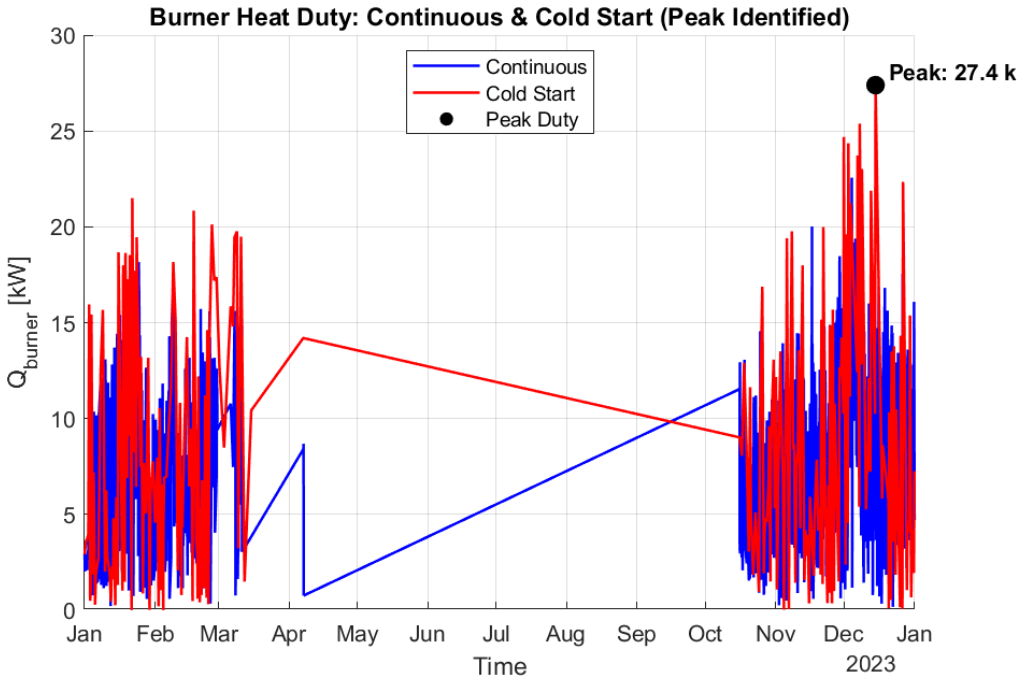

Figure A.7: Dehydrogenation Hourly Burner Heat Duty

A.4. Battery-EMS Module Process Flow Diagram

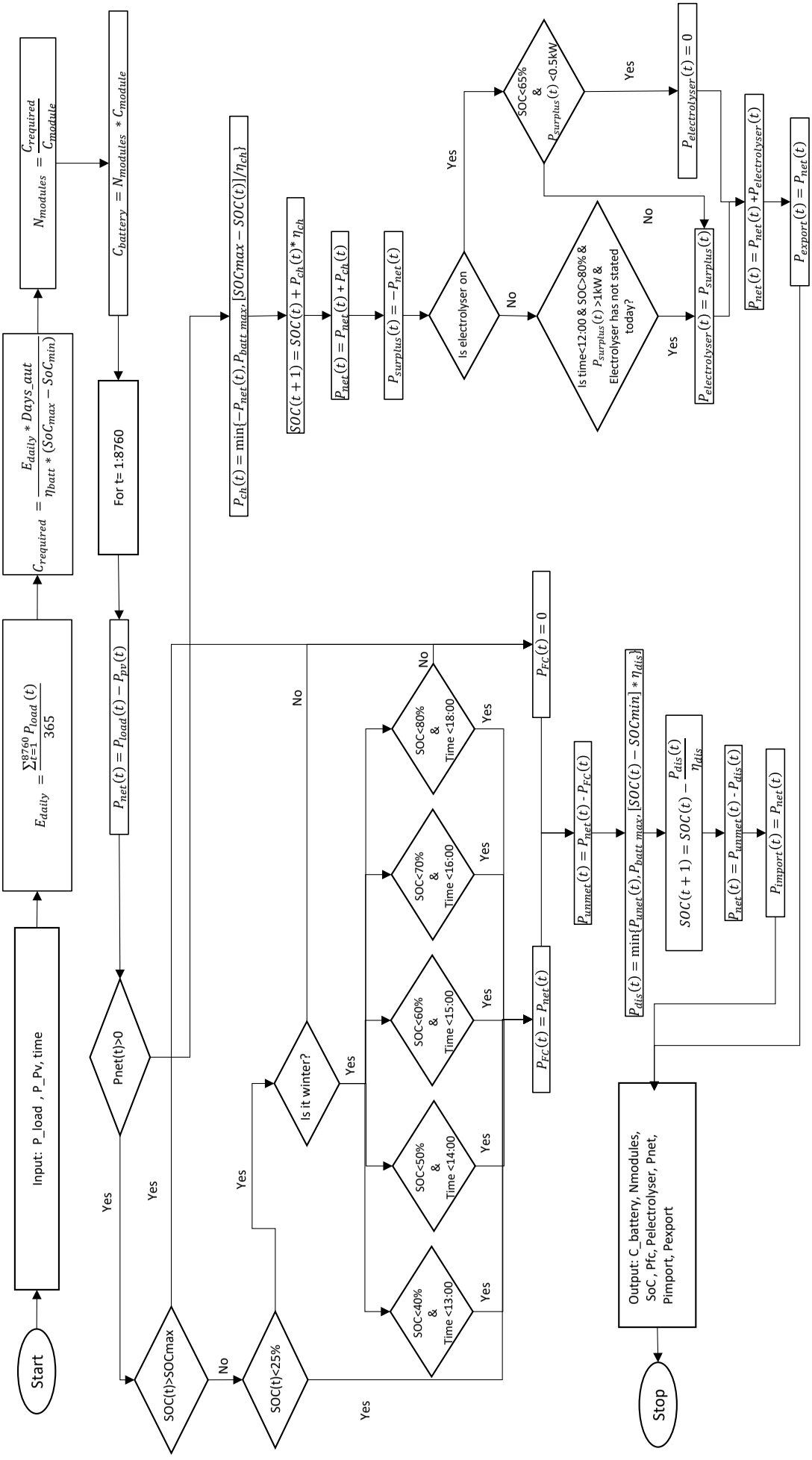

B

Specific Heat Capacity Calculation

(Stark et al., 2015) on their research described that the molar heat capacity of N-ethylcarbazole exhibits a temperature dependence and can be expressed in a linear form as C_p= A+BT. Based on their experimental results, a solid/liquid phase change occurred at 342.4 K for NEC, thus specific heat capacity is calculated based on equation B.1, where for the solid phase A_s=−36.316 & B_s=0.8654 and for the liquid phase A_l=202.58 & B_l=0.3326.

$$C_{p,m}^{\text{solid}}(T) = A_s + B_s T, \qquad C_{p,m}^{\text{liquid}}(T) = A_\ell + B_\ell T. \tag{B.1}$$

To calculate the average mass heat capacity of the unloaded LOHC over the temperature range from T_{amb} to T_{hy}, equation A-6 by (L. Li et al., 2023) is utilised. First, the specific heat capacity ($C_{p,m}$) at T_{amb} for both the solid and liquid phases is computed, as shown in B.2. Next, the specific heat capacity at T_{hy} is estimated, as detailed in B.3. Finally, the average is calculated by incorporating the phase change enthalpy (from solid to liquid) of $\Delta H_{s\to l}$ = 15.1 [kJ/mol], as indicated in B.4.

$$C_{p,m,0} = \begin{cases} A_s + B_s T_{amb}, & T_{amb} < 342.4\ \text{K}, \\ A_\ell + B_\ell T_{amb}, & T_{amb} \geq 342.4\ \text{K}, \end{cases} \tag{B.2}$$

$$C_{p,m,\text{hy}} = A_\ell + B_\ell T_{\text{hy}}, \tag{B.3}$$

$$c_{p,L^-} = \frac{\dfrac{C_{p,m,0} + C_{p,m,\text{hy}}}{2} + \dfrac{\Delta H_{s\to\ell} + \Delta H_{\ell\to g}}{T_{\text{hy}} - T_{amb}}}{M_{L^-}} \quad \left[\frac{\text{J}}{\text{kg K}}\right]. \tag{B.4}$$

Loaded NEC remains in a liquid phase, thus its specific heat capacity is computed at T_{hy} where A_l=127.16 & B_l=0.7543 is used (Stark et al., 2015).

$$c_{p,L^+} = \frac{A_{L^+} + B_{L^+} T_{\text{hy}}}{M_{L^+}}.$$

C
Detailed LOHC Costs

This section provides a detailed breakdown of the LOHC process capital costs.

Table C.1: CAPEX (LOHC)

CAPEX component	**Cost [€]**
Reactor TCI (Hydrogenation)	244,640
Reactor TCI (Dehydrogenation)	220,087
NEC Purchase (one-time)	1,167,590
Catalyst Purchase (initial)	841
Tanks CAPEX	12,578
Heat Exchangers CAPEX	5,224
Burner CAPEX	3,330
Total LOHC Process CAPEX	**1,654,260**

D
Aspen EDR Results

This appendix includes the results for heat exchangers that were obtained using ASPEN EDR.

D.1. Dehydrogenation Heat Exchanger Results

Aspen Exchanger Design and Rating HX1 Dehydrogenation

Setting Plan

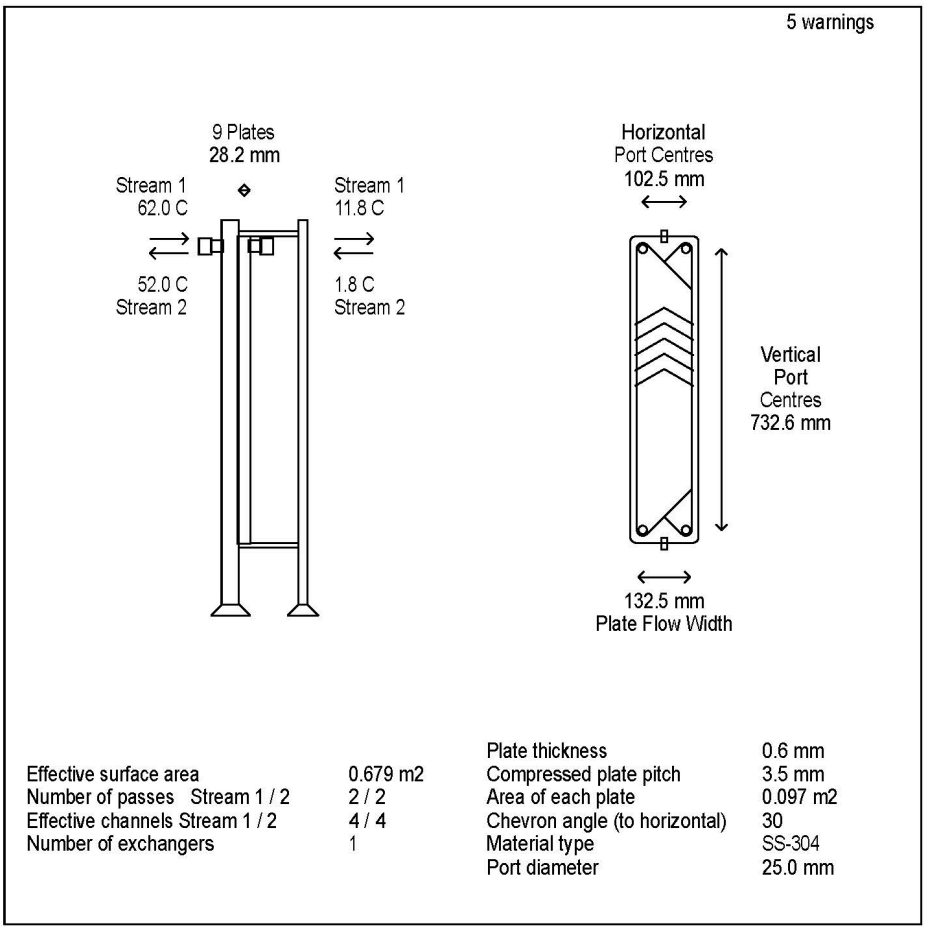

Effective surface area	0.679 m2	Plate thickness	0.6 mm
Number of passes Stream 1 / 2	2 / 2	Compressed plate pitch	3.5 mm
Effective channels Stream 1 / 2	4 / 4	Area of each plate	0.097 m2
Number of exchangers	1	Chevron angle (to horizontal)	30
		Material type	SS-304
		Port diameter	25.0 mm

Costs/Weights

Weights	kg	Cost	Euro(EU)
Plate pack weight - empty (1 PHE)	5.9	Total cost (1 PHE)	676
Plate pack weight - with water (1 PHE)	8.1	Total cost (all PHEs)	676

Figure D.1: Heat Exchanger 1 size and cost

Aspen Exchanger Design and Rating HX2 Dehydrogenation

Setting Plan

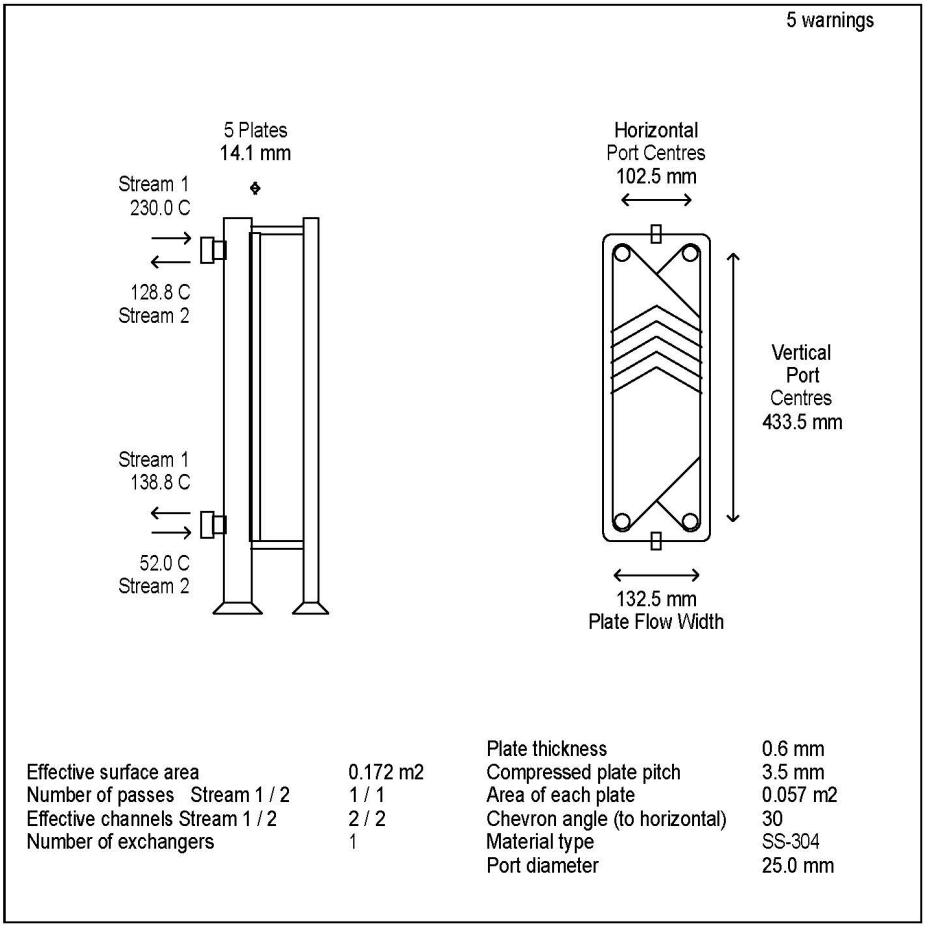

Effective surface area	0.172 m2	Plate thickness	0.6 mm
Number of passes Stream 1 / 2	1 / 1	Compressed plate pitch	3.5 mm
Effective channels Stream 1 / 2	2 / 2	Area of each plate	0.057 m2
Number of exchangers	1	Chevron angle (to horizontal)	30
		Material type	SS-304
		Port diameter	25.0 mm

Costs/Weights

Weights	kg	Cost	Euro(EU)
Plate pack weight - empty (1 PHE)	2.1	Total cost (1 PHE)	583
Plate pack weight - with water (1 PHE)	2.7	Total cost (all PHEs)	583

Figure D.2: Heat Exchanger 2 size and cost

Aspen Exchanger Design and Rating HX3 Dehydrogenation

Setting Plan

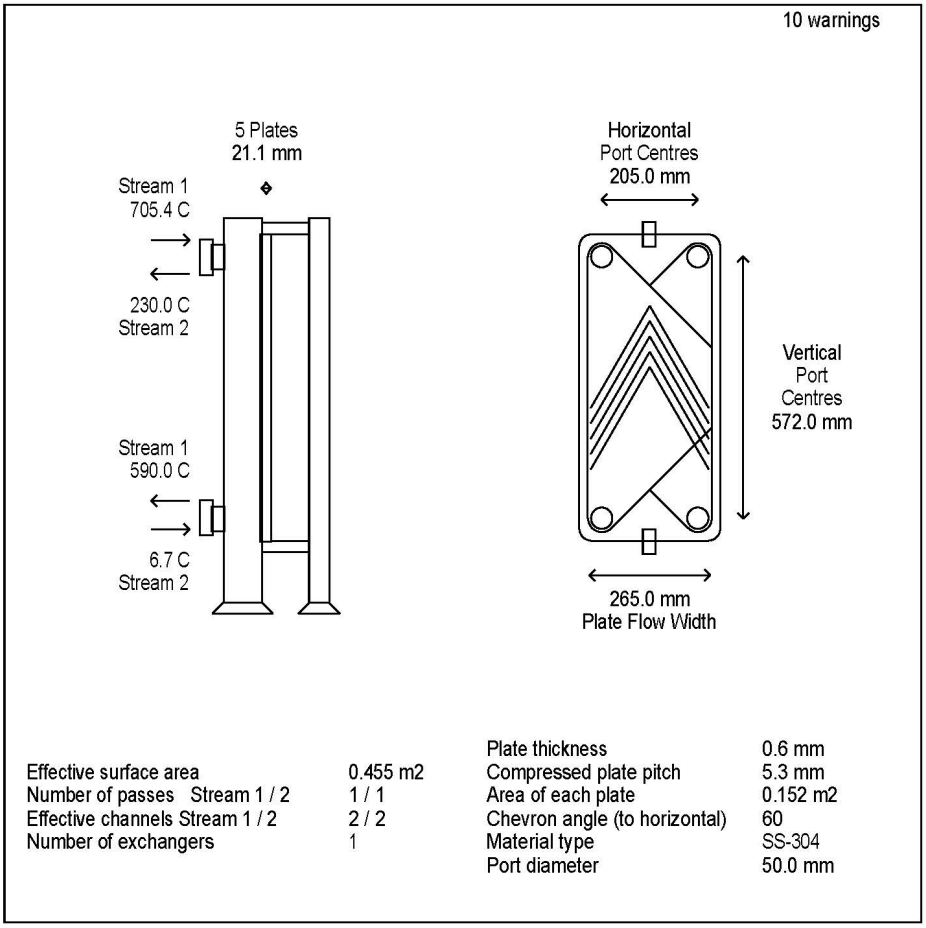

Effective surface area	0.455 m2	Plate thickness	0.6 mm
Number of passes Stream 1 / 2	1 / 1	Compressed plate pitch	5.3 mm
Effective channels Stream 1 / 2	2 / 2	Area of each plate	0.152 m2
Number of exchangers	1	Chevron angle (to horizontal)	60
		Material type	SS-304
		Port diameter	50.0 mm

Costs/Weights

Weights	kg	Cost	Euro(EU)
Plate pack weight - empty (1 PHE)	4.6	Total cost (1 PHE)	629
Plate pack weight - with water (1 PHE)	7.4	Total cost (all PHEs)	629

Figure D.3: Heat Exchanger 3 size and cost

D.2. Hydrogenation Heat Exchanger Results

Aspen Exchanger Design and Rating **HX2 Hydrogenation**

Setting Plan

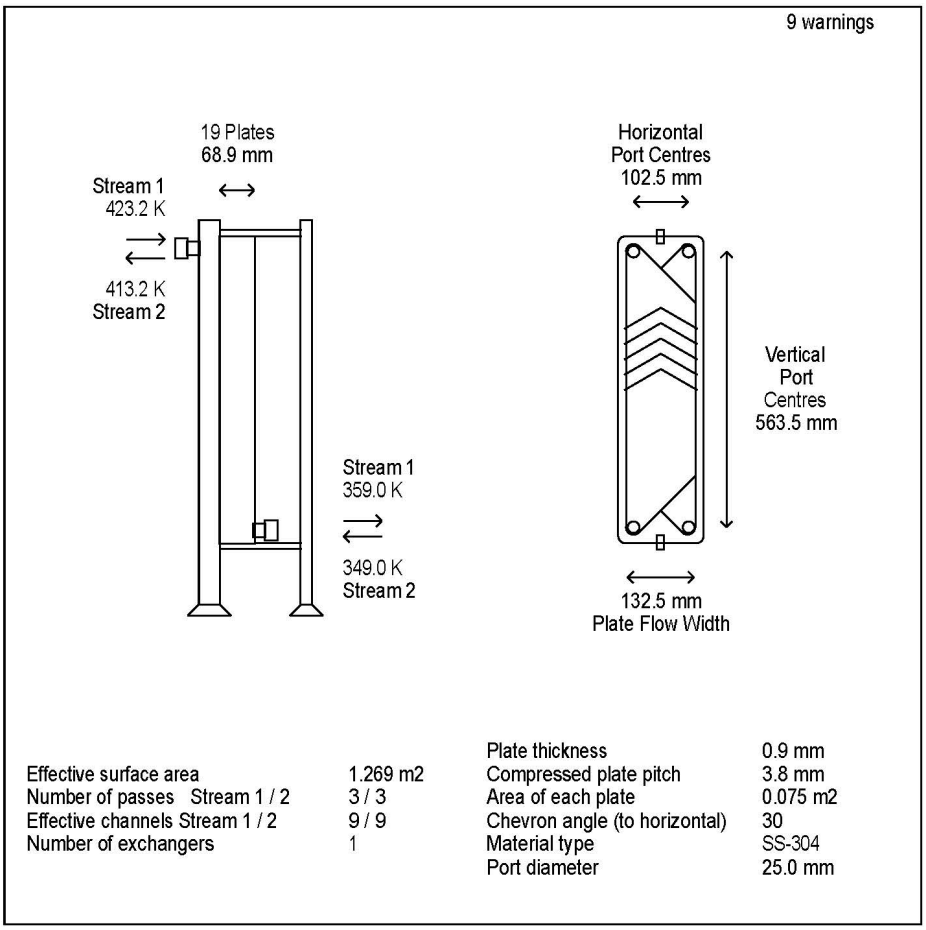

Effective surface area	1.269 m2	Plate thickness	0.9 mm
Number of passes Stream 1 / 2	3 / 3	Compressed plate pitch	3.8 mm
Effective channels Stream 1 / 2	9 / 9	Area of each plate	0.075 m2
Number of exchangers	1	Chevron angle (to horizontal)	30
		Material type	SS-304
		Port diameter	25.0 mm

Costs/Weights

Weights	kg	Cost	Euro(EU)
Plate pack weight - empty (1 PHE)	14.8	Total cost (1 PHE)	810
Plate pack weight - with water (1 PHE)	18.6	Total cost (all PHEs)	810

Figure D.4: Heat Exchanger 2 size and cost

Aspen Exchanger Design and Rating **HX3 Hydrogenation**

Setting Plan

11 warnings

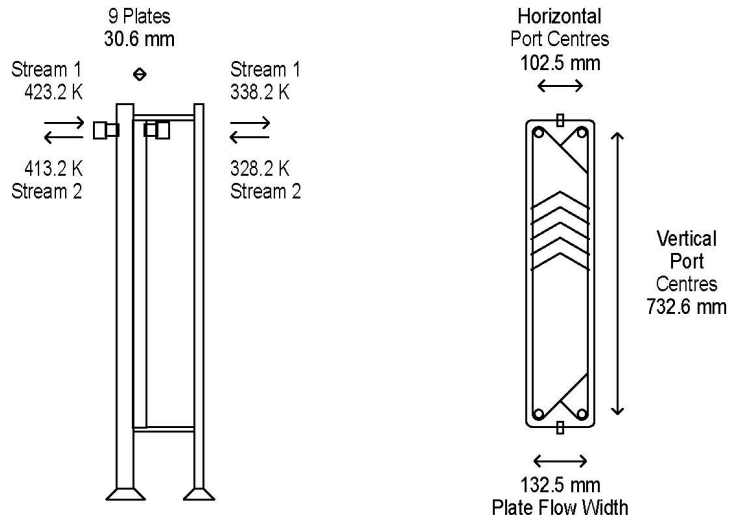

Effective surface area	0.679 m2	Plate thickness	0.9 mm
Number of passes Stream 1 / 2	2 / 2	Compressed plate pitch	3.8 mm
Effective channels Stream 1 / 2	4 / 4	Area of each plate	0.097 m2
Number of exchangers	1	Chevron angle (to horizontal)	30
		Material type	SS-304
		Port diameter	25.0 mm

Costs/Weights

Weights	kg	Cost	Euro(EU)
Plate pack weight - empty (1 PHE)	8.9	Total cost (1 PHE)	676
Plate pack weight - with water (1 PHE)	11.1	Total cost (all PHEs)	676

Figure D.5: Heat Exchanger 3 size and cost

Aspen Exchanger Design and Rating **HX5 Hydrogenation**

Setting Plan

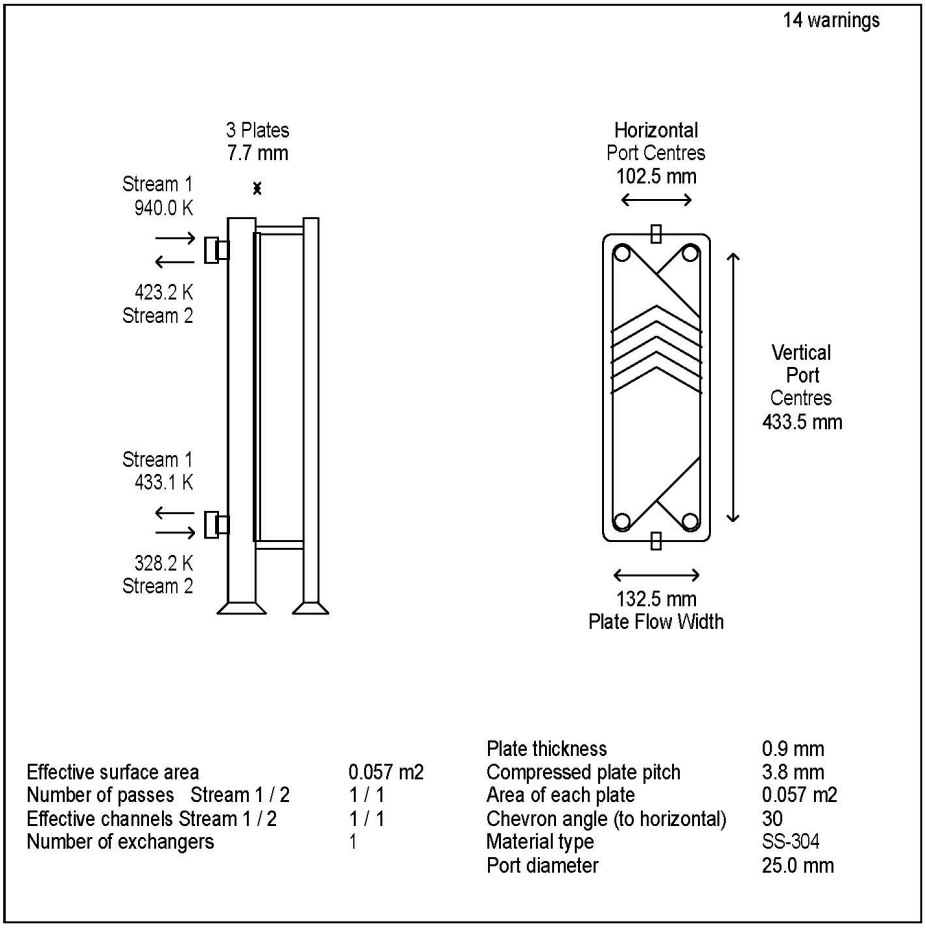

Effective surface area	0.057 m2	Plate thickness	0.9 mm
Number of passes Stream 1 / 2	1 / 1	Compressed plate pitch	3.8 mm
Effective channels Stream 1 / 2	1 / 1	Area of each plate	0.057 m2
Number of exchangers	1	Chevron angle (to horizontal)	30
		Material type	SS-304
		Port diameter	25.0 mm

Costs/Weights

Weights	kg	Cost	Euro(EU)
Plate pack weight - empty (1 PHE)	1.8	Total cost (1 PHE)	548
Plate pack weight - with water (1 PHE)	2.2	Total cost (all PHEs)	548

Figure D.6: Heat Exchanger 5 size and cost

E
Datasheets

This appendix includes the datasheet of the components used in the model.

E.1. Battery Datasheet

BATTERY-BOX PREMIUM LVL

- Scalable from 15.4 to 983 kWh
- Compatible with 1 and 3 Phase Inverters
- Cobalt Free Lithium Iron Phosphate (LFP) Battery: Maximum Safety, Life Cycle, and Power
- Capable of High-Powered Back-up and Off-Grid Function
- Space Saving via the Ability to Stack 2 Premium Batteries
- Add Additional Batteries in Parallel to Expand the System

BATTERY-BOX PREMIUM LVL

The BYD Battery-Box Premium LVL is a lithium iron phosphate (LFP) battery for use with an external inverter.

Thanks to its control and communication unit (BMU), the Battery-Box Premium LVL scales to meet the project requirements, no matter how large they may be. Start with Battery-Box Premium LVL15.4 (15.36 kWh) and extend later to 983 kWh using parallel interconnection of up to 64 batteries.

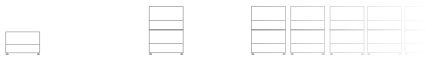

LVL15.4 | 2 x LVL15.4 | 64 x LVL15.4

FLEXIBLE, EFFICIENT, SIMPLE

Easy Installation
With Easy Transportation

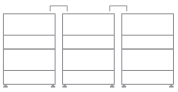

15.4 - 983 kWh
Tailored Sizing for Each Application

Extend Anytime
Easily Adapts to New Requirements

High Power
Power for Every Application

TECHNICAL PARAMETERS **PREMIUM LVL**

	LVL15.4
Number of Modules	2
Usable Energy [1]	15.36 kWh
Max Cont. Output Current [2]	250 A
Peak Output Current [2]	375 A, 5 s
Dimensions (H/W/D)	500 x 575 x 650 mm
Weight	164 kg
Nominal Voltage	51.2 V
Operating Voltage	40-59 V
Operating Temperature	-10 °C to +50°C
Battery Cell Technology	Lithium Iron Phosphate (cobalt-free)
Communication	CAN/RS485
Enclosure Protection Rating	IP20
Round-trip Efficiency	≥95%
Scalability	Max. 64 in Parallel (983 kWh)
Certification	IEC62619 / CE / CEC / UN38.3
Applications	ON Grid / ON Grid + Backup / OFF Grid
Warranty [3]	10 Years
Compatible Inverters	Refer to BYD Battery-Box Premium LVL Minimum Configuration List
Rated DC power	12.8kW
Short Circuit Current	400A

[1] DC Usable Energy, Test conditions: 100% DOD, 0.2C charge & discharge at + 25 °C. System Usable Energy may vary with different inverter brands
[2] Charge derating will occur between -10 °C and +5 °C
[3] Conditions apply. Refer to BYD Battery-Box Premium Limited Warranty Letter.

E.2. Electrolyser Datasheet

Electrolyser
EL 2.1

Enapter

Enapter's patented anion exchange membrane (AEM) electrolyser is a standardized, stackable and flexible system to produce on-site hydrogen. The modular design – paired with advanced software integration – allows set up in minutes and remote control and management. Stack this electrolyser to achieve the required hydrogen flowrate.

KEY FEATURES

- High efficiency
- Automated & remote operation with Enapter's Energy Management System
- Low requirements for input water purity
- Ideal for on-site hydrogen production
- Modules can be easily integrated in 19" racks
- Safe operation
- Scalable and modular, add as many modules as needed
- Quick and easy installation
- Low maintenance requirements
- Small footprint thanks to compact design

Specifications

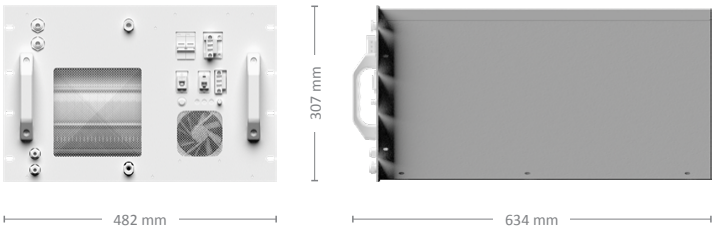

Production rate	500 NL/hr
Hydrogen output purity	35 bar: ~ 99.9% (Impurities: ~ 1000 ppm H_2O) 8 bar: > 1500 ppm H_2O
Output pressure	Up to 35 barg
Nominal power consumption per Nm^3 of H_2 produced (beginning of life)	4.8 kWh/Nm^3
Operative power consumption	2400 W
Stand-by power consumption	15 W
Power supply	200-240 V, 50/60 Hz
Ambient operative temperature range	5°C to 45°C
Ambient operative humidity range	Up to 95% humidity, non-condensing
IP rating	IP 20
Control and monitoring	Fully automatic with Enapter's EMS, Modbus TCP via Ethernet
Water consumption	~400 ml/hr
Maximum water input conductivity	20 µS/cm at 25°C
Water input pressure range	1 - 4 barg
Weight	55 kg
Dimensions (W × D × H in mm)	W:482 mm D:634 mm H:307 mm
Space inside cabinet	7 U
Conformity	CE certified according to the machine directive 2006/42/CE

E.3. Fuel Cell Datasheet

PRODUCT DATA SHEET

Version: November 2019

NEDSTACK FCS 7-XXL
PEM FUEL CELL STACK

Nedstack
PEM FUEL CELLS
To be sure.

SPECIFICATIONS

Electrical - Beginning of Life

Rated power	:	6.8 kWe @ 230 A
Power at lower current	:	see graph

Mechanical

Weight	:	27 kg (approx)
Size	:	364(l)x196(w)x288(h) mm
Cell count	:	48

Hydrogen

Humidification	:	≥ 50% RH at 62 ºC at inlet (75% recommended)
Purity (dry)	:	Grade ≥ 2.5 (max: CO 0.2ppm, CO2 0.5vol%, total sulphur 4ppb, formaldehyde 0.01ppm, formic acid 0.2ppm, ammonia 0.1ppm, total halogenated compounds 0.05ppm, particles 1µg/Nl. Hydrogen specification adapted from ISO 14687-2:2008)
Pressure drop	:	< 0.05 bar at full power
Pressure level	:	0.15 - 0.3 barg
Stoichiometry	:	1.25 - 1.50 for H_2 , minimum flow = 36 Nl/min
Max H2 consumption	:	77 Nl/min at full power

Air

Filtered

Humidification	:	75% RH at 62 ºC
Purity	:	instrument air quality (max: CO 25ppm, Sulphur 0.01ppm, nitrogen dioxide 0.3ppm, ammonia 0.1ppm, particles 1µg/Nl)
Pressure level	:	Ambient (no backpressure allowed)
Pressure drop	:	< 0.12 bar at max power
Stoichiometry	:	≥ 2.0, minimum flow = 67 Nl/min
Max air required	:	366 Nl/min at full power

MEA

Pressure difference		<0.3 bar

Emissions

Noise	:	0
Water production	:	0.5 l/kWh$_e$(approx.)
H2 respiration	:	60 ml/min (max)

Nedstack
PEM FUEL CELLS

Cooling

Nominal temperature	:	65 °C
Max temperature	:	70 °C
Capacity	:	< 10 kW_{th} at full power
Medium	:	de-mineralized water or BASF glysantine FC G20
Purity	:	conductivity < 10 $\mu S.cm^{-1}$
Pressure difference	:	< 0.15 bar (DI water) or < 0.45 bar for glysantine
Operating window	:	ΔT < 5K

Note that proper material selection in the tempering device is important to avoid release of ions into the coolant.

Connectors

Coolant	*Standard*	:	Nedstack quick coupling (male)
	Optional	:	quick coupling (female)
Hydrogen	*Standard*	:	Nedstack quick coupling (male)
	Optional	:	quick coupling (female)
Air	*Standard*	:	Nedstack quick coupling (male)
	Optional	:	quick coupling (female)
Current		:	Busbar with 10.5 mm hole (2x)
Cell voltage connector		:	M12 connector (2x)

Appearance Impression

Nedstack
fuel cell technology B.V.
Westervoortsedijk 73
6827 AV ARNHEM
P.O. Box 5167
6802 ED ARNHEM
The Netherlands
Phone +31 (0)26 319 7600
Fax +31 (0)26 319 7601
E-mail info@nedstack.com
Trade Register Arnhem
nr. 09102161
www.nedstack.com

PRODUCT DATA SHEET – NEDSTACK FCS 7-XXL

Nedstack
PEM FUEL CELLS

Electrical specifications
Beginning of Life stack performance data under standard conditions:

Stack temperature = 62 °C, Ambient pressure
Hydrogen: stoichiometry = 1.25; minimum hydrogen flow = 36 Nl/min; RH = 75%.
Air: stoichiometry = 2.0; minimum air flow = 67 Nl/min; RH = 75%

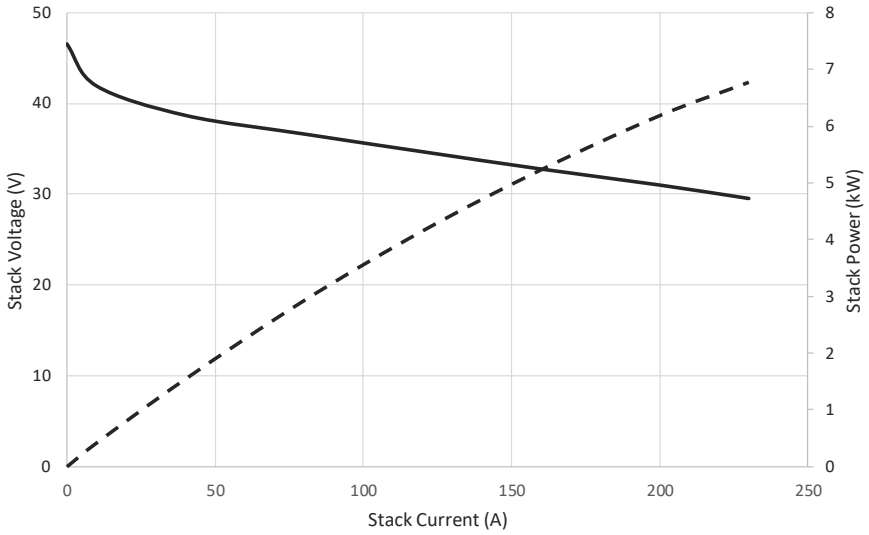

Current (A)	0	40	80	120	160	200	230
Stack Voltage (V)	46.6	38.7	36.6	34.7	32.7	31.0	29.5
Stack Power (kW)	0.0	1.5	2.9	4.2	5.2	6.2	6.8

Nedstack
fuel cell technology B.V.
Westervoortsedijk 73
6827 AV ARNHEM
P.O. Box 5167
6802 ED ARNHEM
The Netherlands
Phone +31 (0)26 319 7600
Fax +31 (0)26 319 7601
E-mail info@nedstack.com
Trade Register Arnhem
nr. 09102161
www.nedstack.com

E.4. Reactor Coolant Datasheet

THERMINOL® 55

heat transfer fluid

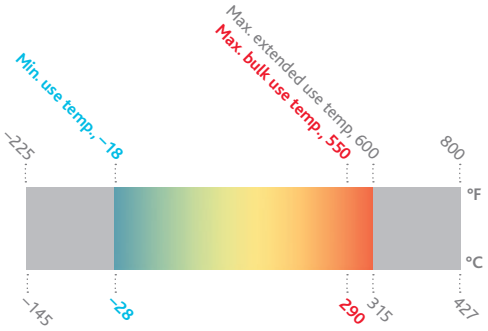

Eastman Therminol® 55 heat transfer fluid is a unique, synthetic fluid designed to provide reliable, consistent heat transfer performance over a long life at maximum bulk temperatures up to 290°C (550°F).

- Delivers excellent cost performance over the fluid life when compared to common mineral oil-based heat transfer fluids, even when operating temperatures reach a maximum extended use temperature of 315°C (600°F).
- More readily pumpable at low temperatures than the majority of other mineral oil-based heat transfer fluids.
- Savings in capital, operations, and maintenance costs are often achieved when used in applications that traditionally use steam as a heating medium.

Therminol 55 is available in the Americas and Asia-Pacific. Contact your local Eastman Therminol sales representative for more information.

Physical and chemical characteristics

Therminol 55 fluid is designed for use in nonpressurized/low-pressure, indirect heating systems. It delivers efficient, dependable, uniform process heat with no need for high pressures. The high boiling point of Therminol 55 helps reduce the volatility and fluid leakage problems associated with other fluids.

The recommended maximum bulk and film temperatures for Therminol 55 are based on industry-standard thermal studies. Operation at or below these temperature maximums can provide long service life under most operating conditions.

Actual fluid life is dependent on the total system design and operation and can vary by heat transfer fluid chemistry. As fluid ages, the formation of low- and high-boiling compounds may result. Low-boiling compounds should be vented from the system as necessary to a safe location away from personnel and sources of ignition and in compliance with applicable regulations and laws. The high-boiling compounds can be very soluble in the fluid. Significant overheating or fluid contamination will accelerate decomposition and may result in increased high-boiler and solids concentrations. Excess solids can typically be filtered for removal.

Therminol 55 has been shown to be significantly less sensitive than mineral oils to the negative consequences (sludging, fouling) of thermal oxidation. Eastman recommends that systems utilizing Therminol 55 fluid should be blanketed with an atmosphere of inert gas to protect against the effects of fluid oxidation on its performance and life expectancy. Pressure relief device(s) should be installed where required.

Therminol 55 is noncorrosive to metals commonly used in the construction of heat transfer systems.

While Therminol 55 has a relatively high flash point, it is not classified as a fire-resistant heat transfer fluid. Consequently, the use of protective devices may be required to minimize fire risk and users of Therminol 55 should check with their safety and risk management experts for specific instructions.

Typical properties[a]

Appearance	Clear, yellow liquid
Composition	Synthetic hydrocarbon mixture
Maximum bulk temperature	290°C (550°F)
Maximum extended use temperature	315°C (600°F)
Maximum film temperature	335°C (635°F)
Normal boiling point	351°C (664°F)
Pumpability, at 300 mm^2/s (cSt)	–8°C (17°F)
Pumpability, at 2000 mm^2/s (cSt)	–28°C (–18°F)
Flash point, COC (ASTM D-92)	177°C (350°F)
Autoignition temperature (ASTM E-659)	366°C (691°F)
Autoignition temperature (DIN 51794)	382°C (719°F)
Pour point (ISO 3016)	–54°C (–65°F)
Minimum liquid temperatures for fully developed turbulent flow (N_{Re} > 10000)	
10 ft/s, 1-in. tube (3.048 m/s, 2.54-cm tube)	67°C (152°F)
20 ft/s, 1-in. tube (6.096 m/s, 2.54-cm tube)	45°C (114°F)
Minimum liquid temperatures for transitional region flow (N_{Re} > 2000)	
10 ft/s, 1-in. tube (3.048 m/s, 2.54-cm tube)	24°C (75°F)
20 ft/s, 1-in. tube (6.096 m/s, 2.54-cm tube)	11°C (52°F)
Coefficient of thermal expansion @ 200°C	0.000961/°C (0.000534/°F)
Heat of vaporization at maximum use temperature	228 kJ/kg (98.1 Btu/lb)
Average molecular weight	320
Pseudocritical temperature	512°C (953°F)
Pseudocritical pressure	13.2 bar (191 psia)
Pseudocritical density	258 kg/m^3 (16.1 lb/ft^3)
Moisture content, maximum (ASTM E-203)	150 ppm
Dielectric constant @ 23°C (ASTM D-924)	2.23

[a]These data are based on samples tested in the laboratory and are not guaranteed for all samples. Contact us for complete sales specifications for Therminol 55 fluid. Does not constitute an express warranty. See disclaimer on the back page of this bulletin.

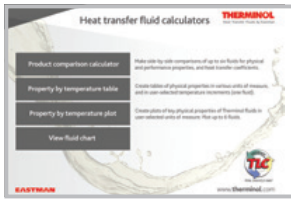

To create your own customized table
with preferred properties, units of measure,
and temperature intervals, visit
www.therminol.com/resources
and download the Therminol heat transfer fluid calculator.

**For the technical service contact in your region,
visit the CONTACT US page on our website, www.therminol.com.**

Liquid properties of Therminol® 55 heat transfer fluid by temperature[a] (SI units)

Temperature		Liquid density	Liquid heat capacity	Heat of vaporization	Liquid enthalpy[b]	Liquid thermal conductivity	Liquid viscosity[c]		Vapor pressure[d]
°C	°F	kg/m³	kJ/(kg·K)	kJ/kg	kJ/kg	W/(m·K)	cP (mPa·s)	cSt (mm²/s)	kPa
–28	–18	904	1.73	418.0	–18.8	0.1340	1820	2010	—
–20	–4	899	1.76	412.0	–3.9	0.1331	756	841	—
–10	14	892	1.80	405.0	13.9	0.1319	309	346	—
0	32	885	1.83	398.1	32.0	0.1307	143	162	—
10	50	878	1.87	391.3	50.6	0.1296	73.8	84.0	—
20	68	872	1.91	384.6	69.4	0.1284	41.6	47.7	—
30	86	865	1.94	377.9	88.7	0.1273	25.2	29.2	—
40	104	858	1.98	371.4	108.3	0.1261	16.3	19.0	—
50	122	852	2.01	364.9	128.2	0.1249	11.1	13.1	—
60	140	845	2.05	358.5	148.5	0.1238	7.93	9.39	—
70	158	838	2.08	352.2	169.2	0.1226	5.89	7.02	—
80	176	831	2.12	345.9	190.2	0.1214	4.52	5.43	0.011
90	194	825	2.16	339.8	211.6	0.1203	3.56	4.32	0.019
100	212	818	2.19	333.7	233.3	0.1191	2.88	3.52	0.032
110	230	811	2.23	327.8	255.4	0.1179	2.38	2.93	0.054
120	248	804	2.26	321.8	277.9	0.1168	2.00	2.49	0.088
130	266	797	2.30	316.0	300.7	0.1156	1.71	2.14	0.140
140	284	790	2.33	310.2	323.8	0.1144	1.48	1.87	0.219
150	302	784	2.37	304.5	347.3	0.1133	1.29	1.65	0.334
160	320	777	2.40	298.8	371.2	0.1121	1.14	1.47	0.501
170	338	770	2.44	293.2	395.4	0.1109	1.02	1.32	0.738
180	356	763	2.47	287.7	420.0	0.1098	0.913	1.20	1.07
190	374	755	2.51	282.2	444.9	0.1086	0.825	1.09	1.53
200	392	748	2.54	276.7	470.1	0.1074	0.749	1.00	2.15
210	410	741	2.58	271.3	495.7	0.1062	0.683	0.921	2.98
220	428	734	2.61	265.9	521.7	0.1051	0.625	0.852	4.07
230	446	726	2.65	260.5	548.0	0.1039	0.574	0.790	5.51
240	464	719	2.68	255.1	574.7	0.1027	0.528	0.735	7.37
250	482	711	2.72	249.7	601.7	0.1015	0.488	0.686	9.76
260	500	704	2.75	244.3	629.1	0.1004	0.451	0.641	12.8
270	518	696	2.79	239.0	656.8	0.0992	0.418	0.600	16.6
280	536	688	2.83	233.5	684.9	0.0980	0.387	0.563	21.3
290	554	680	2.86	228.1	713.3	0.0968	0.360	0.529	27.2
300	572	672	2.90	222.6	742.1	0.0957	0.334	0.497	34.4
310	590	663	2.93	217.1	771.2	0.0945	0.311	0.468	43.1
320	608	655	2.97	211.5	800.7	0.0933	0.289	0.441	53.7

[a]Maximum recommended bulk temperature 290°C (550°F). These data are based on samples tested in the laboratory and are not guaranteed for all samples. Contact us for complete sales specifications for Therminol 55 fluid. [b]Liquid enthalpy basis is –17.8°C (0°F). [c]1 cSt = 1 mm²/s and 1 mPa·s = 1 cP. [d]100 kPa = 1 bar. [e]Maximum extended use temperature is 315°C (600°F).